Does ferroelectric polarization in $LiCu_2O_2$ uniquely originate from spiral spin order?

M. H. Qin, Y. J. Guo, S. Dong, K. F. Wang, and J.-M. Liu[a)]
Laboratory of Solid State Microstructures, Nanjing University, Nanjing 210093, China and International Center for Materials Physics, Chinese Academy of Sciences, Shenyang 110016, China

(Presented 12 November 2008; received 29 August 2008; accepted 25 October 2008; published online 5 February 2009)

We perform Monte Carlo simulation of the ferroelectricity induced by spiral spin order in spin-1/2 $LiCu_2O_2$ based on the Mostovoy phenomenological theory. The simulated spiral spin order parameter and ferroelectric polarization, respectively, as a function of temperature and magnetic field are compared with recent experiments. The substantial differences in several aspects of the multiferroicity between the simulation and experiments allow a reasonable argument that the spiral spin order may not be the unique origin for the ferroelectricity generation. © *2009 American Institute of Physics*. [DOI: 10.1063/1.3062823]

Multiferroics are attracting attentions due to their potentials for novel physics and applications.[1,2] Recently, multiferroicity was found in a class of transitional metal (Me) oxides known as "frustrated magnets" such as perovskite $R\mathrm{MnO}_3$ (R=Tb, Dy, and Gd),[3–5] $R\mathrm{Mn}_2\mathrm{O}_5$ (R=Y, Tb, Dy, etc.),[6–8] delafossite CuFeO_2,[9] spinel $\mathrm{CoCr}_2\mathrm{O}_4$,[10] and kagome magnet $\mathrm{Ni}_3\mathrm{V}_2\mathrm{O}_8$.[11] It is believed that the ferroelectricity in these materials is directly generated by the frustrated spin configuration with multifold interactions.[12] On one hand, the spin supercurrent model for Me–O–Me chain was proposed, in which noncollinear spin alignment between the two Me ions mediated by the O ion becomes the core ingredient of ferroelectricity generation.[13] On the other hand, the role of Dzyaloshinskii–Moriya interaction (DMI) in generating ferroelectricity in $R\mathrm{MnO}_3$ was emphasized too.[14] In our earlier work,[15] this DMI model was used to study the ferroelectric (FE) polarization and the simulated results agree well with reported experiments on $\mathrm{Tb(Dy)MnO}_3$. Based on the two microscopic models and symmetry consideration, a phenomenological theory for ferroelectricity in noncollinear spin systems was developed by Mostovoy,[16] in which the ME coupling takes the following form:

$$\phi_{em}(P,M) = \gamma P[M(\nabla \cdot M) - (M \cdot \nabla)M], \tag{1}$$

where P is the electric polarization, M is the magnetization, and γ scales the magnitude of the DMI or the spin supercurrent effect.

The simplest noncollinear spin order is the spiral spin structure. The ferroelectricity in such structures was demonstrated in $R\mathrm{MnO}_3$,[4] $\mathrm{Ni}_3\mathrm{V}_2\mathrm{O}_8$,[10] $\mathrm{CoCr}_2\mathrm{O}_4$,[11] etc. It thus becomes reasonable that the ferroelectricity in $LiCu_2O_2$ has the same origin because the exchange interaction goes beyond the first neighbors and the structure has a triangular motif susceptible to frustration.[17–20] This material contains an equal number of Cu^{1+} and Cu^{2+}, the latter of which carries spin $S=1/2$. Each Cu^{2+} ion is on the center of oxygen square with the Cu–O–Cu bond angle of 94° and forms edge-shared chains with zigzag "ladders" along the b-axis, as illustrated in Fig. 1. The measured spin spiral modulation along the chain direction is 0.174, corresponding to a pitching angle of 62.6°.[21,22]

Fortunately, the ferroelectricity of $LiCu_2O_2$ and its response to magnetic field (H) were investigated in details,[19,20] allowing us to check the origin of ferroelectricity. Experimentally, polarization P emerges along the c-axis below the spiral spin ordering point, while the spin spiral axis is along the b-axis. For a field applying along the b-axis, H_b, P was observed to transit its direction from the c-axis to the a-axis. More interesting, it was observed that the c-axis component of P, P_c, initiates upon a field along the c-axis. Most recently, starting from the Mostovoy theory, Fang *et al.*[24] constructed a multiorder parameter phenomenological model for the zigzag spin chain system based on a group theory analysis.[23] Our aim in this work is to start from this theory and calculate in details by Monte Carlo (MC) technique the FE response to temperature and magnetic field in $LiCu_2O_2$.

The MC simulation is performed on an $L \times L'$ lattice with periodic boundary conditions. The lattice configuration with multifold spin interactions is schematically shown in Fig. 1. Here $L=100$ is the length of a double chain and L'

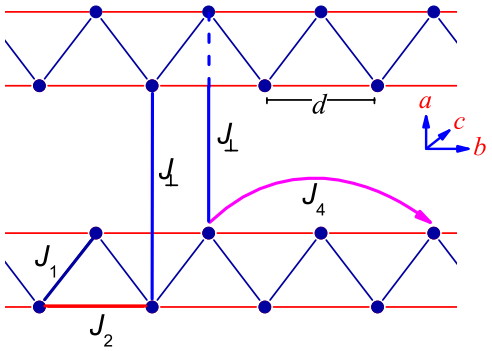

FIG. 1. (Color online) A schematic of exchange interactions between magnetic Cu^{2+} ions in $LiCu_2O_2$.

[a)]Author to whom correspondence should be addressed. Electronic mail: liujm@nju.edu.cn.

=10 is the number of the double chains. For such a lattice, the Hamiltonian is

$$H = \sum_{i,j} J_1 S_{i,j} S_{i+1,j} + J_2 S_{i,j} S_{i+2,j} + J_4 S_{i,j} S_{i+4,j} + J_\perp S_{i,j} S_{i,j+1} - g\mu_B H S_{i,j} - E P_{i,j} + \frac{P_{i,j}^2}{2\varepsilon\varepsilon_0} + \phi_{em}, \quad (2)$$

where the indices i and j run along and perpendicular to the double chains, spin moment $S_{i,j}=(S_{i,j}^x, S_{i,j}^y, S_{i,j}^z)$ are the three-component classical vectors of 1/2 length $(S=1/2)$ at site (i,j), μ_B is the Bohr magnon, g is the Lande factor, E is a small electric field, $P_{i,j}=2er_{i,j}$, e is the charge of electron, $r_{i,j}$ is the average displacement of O ions which mediate the Cu^{2+} ions at site (i,j) and site $(i+2,j)$, ε is the dielectric constant, and ϕ_{em} is the ME coupling Hamiltonian which can be expressed as[24,25]

$$\phi_{em} = \gamma_c \sum_{i,j} P_{i,j}^c (S_{i,j} \times \partial_y S_{i,j})_a + \gamma_a \sum_{i,j} P_{i,j}^a (S_{i,j} \times \partial_y S_{i+1,j} + S_{i+1,j} \times \partial_y S_{i,j})_b, \quad (3)$$

$$\partial_y S_{i,j} = \frac{S_{i,j} - S_{i-2,j}}{d}, \quad (4)$$

where $d=2.856$ Å is the separation between the nearest neighbor spins along the chain.

To quantitatively reveal the spiral order along the chains, the spin structure factor $C(k)$ for the chains is defined as[26,27]

$$C(k) = \frac{4}{L^2} \sum_{i,j=1}^{L/2} S_i \cdot S_j e^{ik(R_i - R_j)}, \quad (5)$$

where S_i and R_i, respectively, denote the spin and coordinate at site i in a single chain. For a well-defined spatial periodicity $\lambda=2\pi/k$, $C(k)$ reaches its acme at wave vector k.

We line out the parameters taken for our simulation: $J_1=6.4$ meV, $J_2=-11.9$ meV, $J_4=7.6$ meV, $J_\perp=1.8$ meV, $g_L=2.3$, and $\varepsilon=10$. These parameters are chosen according to reported values.[17,19] The Curie temperature $T_c \approx 23$ K and the value of P ranges from 3 to 10 $\mu C/m^2$, giving the displacement of O between $10^{-4} \sim 10^{-3}$ Å with $\gamma_z e/k_B=5\times10^5$ K and $\gamma_x e/k_B=2.5\times10^5$ K.

A typical snapshot showing the spin configuration at the lowest T is presented in Fig. 2(a), indicating the spiral spin order along the chain direction. In Fig. 2(b), $C(k)$ as a function of k at various T under $H=0$ is presented. At lower T (=5, 10 K), the sharp characteristic peaks at $k \sim 0.32\pi$ are observed, confirming the stability of the incommensurate magnetic (ICM) phase. However, the peak height decreases with increasing T, demonstrating the gradual suppression of the ICM phase. Figure 2(c) depicts a typical T-dependence of $C(k=0.32\pi)$ and P_c at $H=0$. The two order parameters have the same ordering point within the simulation errors, indicating the strong mutual influence of ferroelectricity and magnetic order. The simulated P_c below $T=10$ K is ~ 6 $\mu C/m^2$ and the FE transition occurs at $T=T_C \sim 15$ K, both comparable to experimental values.

The problems come out when one looks at the response of P to H. We summarize the simulated results in Fig. 3

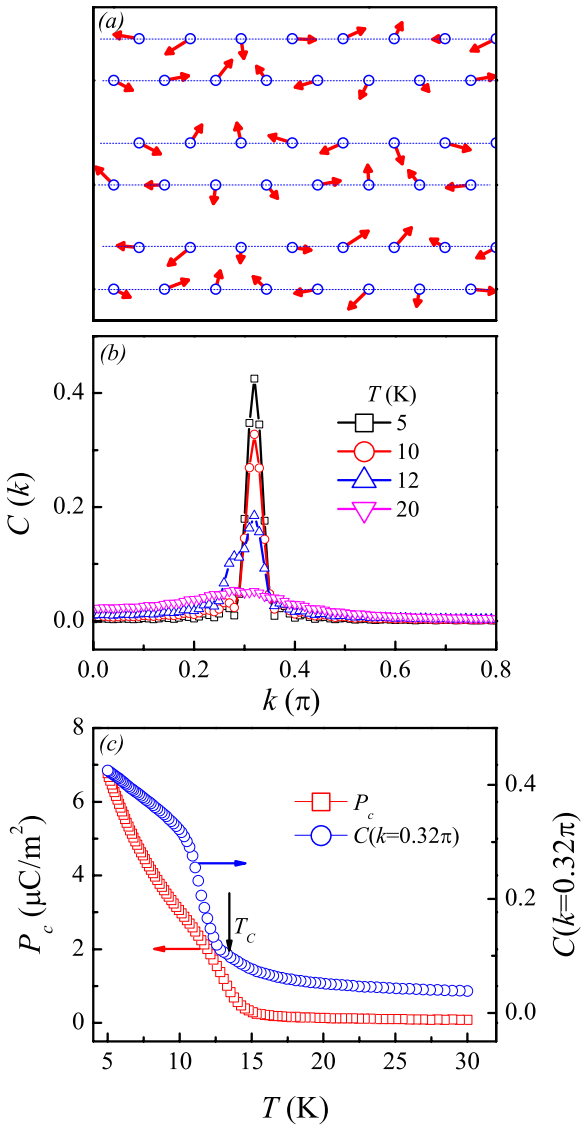

FIG. 2. (Color online) (a) Typical MC snapshot of the spiral spin structure at $T=5$ K. (b) Spin structure factor at various temperatures. (c) Polarization P_c and C (0.32π) as a function of T at zero H.

where the simulated P_a and P_c as a function of T at various H (H_a:$H\|a$, H_b:$H\|b$, H_c:$H\|c$) are plotted in order to compare with experimental data. There are several substantial differences between the simulated results and experiments.

(i) Experimentally, the measured $P_c(T)$ reflects the first-order FE transition by which P_c appears at $T \sim T_c$ and then rapidly approaches a saturated value. However, in our simulation this transition is gradual and of second-order characters, ascribed to the fact that the spiral spin ordering itself is of second order. With decreasing T, this spiral spin ordering is gradually enhanced, leading to gradually increasing polarization.

(ii) Experimentally, P_c is suppressed and P_a is generated for increasing H_b, i.e., the polarization flops from the c-axis to the a-axis. The spins should flip to the ac plane when the field applies along the b-axis. By such a mechanism, nonzero P_a would be observable due to the ME coupling. This is confirmed by our simulation. However, the behavior of P_c under various H_b, char-

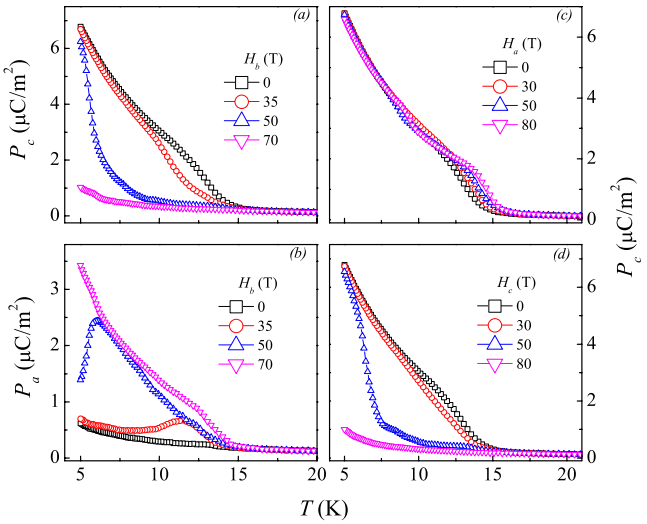

FIG. 3. (Color online) (a) Polarization P_c and (b) polarization P_a as a function of T at various H_b. P_c as a function of T at (c) various H_a and (d) various H_c.

acterized by a shifting of T_C toward the low-T side, as shown in Fig. 3(a), is different from the experimentally observed one where no shifting is observed. At the same time, the simulated P_a under various H_b also indicates that the change in P in real $LiCu_2O_2$ may be from other unrevealed origin. Furthermore, at low T, the spiral spin order is very robust. Its melting requires a field H_b as high as 35 T. A complete suppression of P_c cannot be achieved unless H_b is as high as 70 T, which is far higher than the experimental value of ~10 T. Such a big difference may be due to the fact that in real $LiCu_2O_2$, a suppression of P_c at H_b ~10 T does not mean a broken spiral spin order but a flop to P_a. However, in the present model, no mechanism other than breaking the spiral spin order is responsible for the polarization suppression. On the other hand, the ME coupling term helps to stabilize the long-range spiral spin order and act against the effect of H. Therefore, extra magnetic field is necessary to destroy the spiral spin order and suppress the polarization.

(iii) The above results are of generality if one looks at the ferroelectricity upon application of H along the a-axis, c-axis, H_a, and H_c, respectively. The simulated data are presented in Figs. 3(c) and 3(d). Since the spiral spins at $H=0$ lie in the bc plane and are perpendicular to H_a, the spiral order remains metastable against H_a because increasing H_a does not destabilize any of these spiral spins, while the response of these spins to H_c is much more sensitive. This is the reason why P_c behaves more robust against H_a than H_c. The stable P_c is observed even when H_a is as high as 80 T. Furthermore, the appearance of P_a with increasing H_a, observed experimentally, cannot be produced by the simulation. On the other hand, it is expected that H_c may flip the spiral plane from the bc to ab plane so that P_c may be suppressed with increasing H_c. This is confirmed by our simulation. Therefore, it is reasonable to argue that experimentally observed enhancement of P_c with increasing H_c must be due to some other origin.

Anyway, so far available experiments on the ferroelectricity of $LiCu_2O_2$ and its response to magnetic field cannot be satisfactorily explained by the Mostovoy theory alone, even in the qualitative sense.

The present work allows us to argue that the spiral spin order may not be the unique origin for the ferroelectricity generation in $LiCu_2O_2$.

The authors would like to acknowledge the financial support from the National Natural Science Foundation of China (Grant No. 50832002) and the National Key Projects for Basic Researches of China (Grant Nos. 2006CB921802 and 2009CB929501).

[1] M. Fiebig, J. Phys. D **38**, R123 (2005).
[2] S.-W. Cheong and M. Mostovoy, Nature Mater. **6**, 13 (2007).
[3] T. Kimura, T. Goto, H. Shintani, K. Ishizaka, T. Arima, and Y. Tokura, Nature (London) **426**, 55 (2003).
[4] T. Goto, T. Kimura, G. Lawes, A. P. Ramirez, and Y. Tokura, Phys. Rev. Lett. **92**, 257201 (2004).
[5] T. Arima, T. Goto, Y. Yamasaki, S. Miyasaka, K. Ishii, M. Tsubota, T. Inami, Y. Murakami, and Y. Tokura, Phys. Rev. B **72**, 100102 (2005).
[6] N. Hur, S. Park, P. A. Sharma, J. S. Ahn, S. Guha, and S. W. Cheong, Nature (London) **429**, 392 (2004).
[7] L. C. Chapon, P. G. Radaelli, G. R. Blake, S. Park, and S. W. Cheong, Phys. Rev. Lett. **96**, 097601 (2006).
[8] D. Higashiyama, S. Miyasaka, and Y. Tokura, Phys. Rev. B **72**, 064421 (2005).
[9] T. Kimura, G. Lawes, and A. P. Ramirez, Phys. Rev. B **73**, 220401 (2006).
[10] Y. Yamasaki, S. Miyasaka, Y. Kaneko, J. P. He, T. Arima, and Y. Tokura, Phys. Rev. Lett. **96**, 207204 (2006).
[11] K. Taniguchi, N. Abe, T. Takenobu, Y. Iwasa, and T. Arima, Phys. Rev. Lett. **97**, 097203 (2006).
[12] Y. Tokura, Science **312**, 1481 (2006).
[13] H. Katsura, N. Nagaosa, and A. V. Balatsky, Phys. Rev. Lett. **95**, 057205 (2005).
[14] I. A. Sergienko and E. Dagotto, Phys. Rev. B **73**, 094434 (2006).
[15] Q. Li, S. Dong, and J.-M. Liu, Phys. Rev. B **77**, 054442 (2008).
[16] M. Mostovoy, Phys. Rev. Lett. **96**, 067601 (2006).
[17] T. Masuda, A. Zheludev, A. Bush, M. Markina, and A. Vasiliev, Phys. Rev. Lett. **92**, 177201 (2004).
[18] S.-L. Drechsler, J. Malek, J. Richter, A. S. Moskvin, A. A. Gippius, and H. Rosner, Phys. Rev. Lett. **94**, 039705 (2005).
[19] S. Park, Y. J. Choi, C. L. Zhang, and S.-W. Cheong, Phys. Rev. Lett. **98**, 057601 (2007).
[20] S. Seki, Y. Yamasaki, M. Soda, M. Matsuura, K. Hirota, and Y. Tokura, Phys. Rev. Lett. **100**, 127201 (2008).
[21] T. Masuda, A. Zheludev, B. Roessli, A. Bush, M. Markina, and A. Vasiliev, Phys. Rev. B **72**, 014405 (2005).
[22] L. Mihaly, B. Dora, A. Vanyolos, H. Berger, and L. Forro, Phys. Rev. Lett. **97**, 067206 (2006).
[23] S. W. Huang, D. J. Huang, J. Okamoto, C. Y. Mou, W. B. Wu, K. W. Yeh, C. L. Chen, M. K. Wu, H. C. Hsu, F. C. Chou, and C. T. Chen, Phys. Rev. Lett. **101**, 077205 (2008).
[24] C. Fang, T. Datta, and J. Hu, Phys. Rev. B **79**, 014107 (2009).
[25] A. B. Harris, Phys. Rev. B **76**, 054447 (2007).
[26] S. Dong, R. Yu, S. Yunoki, J.-M. Liu, and E. Dagotto, Phys. Rev. B **78**, 064414 (2008).
[27] S. Dong, R. Yu, S. Yunoki, J.-M. Liu, and E. Dagotto, Phys. Rev. B **78**, 155121 (2008).

Two-step magnetization in a spin-chain system on the triangular lattice: Wang-Landau simulation

M. H. Qin and K. F. Wang
Laboratory of Solid State Microstructures, Nanjing University, Nanjing 210093, China

J. M. Liu*
Laboratory of Solid State Microstructures, Nanjing University, Nanjing 210093, China;
School of Physics, South China Normal University, Guangzhou 510006, China;
and International Center for Materials Physics, Chinese Academy of Science, Shenyang 110016, China
(Received 7 March 2009; published 13 May 2009)

The Wang-Landau algorithm is used to study the thermodynamic and magnetic properties of triangular spin-chain system based on two-dimensional Ising model in order to understand the magnetic-order dynamics in $Ca_3Co_2O_6$ compound. The calculated results demonstrate that the equilibrium state of the rigid spins produces the two-step magnetization curve at low temperature even when the random-exchange term is considered. This work indicates that the four-step magnetization behavior observed experimentally must be due to the nonequilibrium magnetization.

DOI: 10.1103/PhysRevB.79.172405 PACS number(s): 75.40.Mg, 02.70.Uu, 05.50.+q

During the past few years, spin-chain system $Ca_3Co_2O_6$ has drawn considerable attention from both experimental and theoretical points of view due to their unique magnetic behaviors.[1–17] As revealed experimentally, $Ca_3Co_2O_6$ has a rhombohedral structure composed of Co_2O_6 chains running along the c axis of the corresponding hexagonal cell. The Ca ions are situated between them and are not involved in magnetic interactions.[1] These chains are built by alternating, face-sharing CoO_6 trigonal prisms and CoO_6 octahedral. Each chain is surrounded by six equally spaced chains, forming a triangular lattice on the ab plane that is perpendicular to the chains along the c axis.

The most intriguing feature for such a spin-chain system is a steplike magnetization (M) as a function of external magnetic field (B) applied along the chains. Experimentally, two steps are observed in the temperature (T) range of 10–25 K. Close to $B=0$, M reaches the first plateau at $M=M_0/3$ (where M_0 is the saturated magnetization). Then the plateau stretches up to $B=3.6$ T where M springs up to M_0. Experimentally, when $T<10$ K, the first step at $M_0/3$ splits into three equidistant steps at a slow magnetic-field sweep rate, thus constituting a four-step magnetization pattern. The origin of such four-steplike magnetization behavior has been extensively studied most recently, and it is still a matter of debate.[7–9]

For $Ca_3Co_2O_6$, because the intrachain-ferromagnetic (FM) interaction is much stronger than the interchain-antiferromagnetic (AFM) coupling, the chains can be assumed to be in two ordered states (spin-up or spin-down) at low T. Based on this basic assumption, Kudasov developed a two-dimensional (2D) Ising model to investigate the steplike magnetization by an analytical method regarding a spin chain as a large rigid spin and assuming a quench at $T=0$.[9] By this theory at the fourth approximations, four equidistant steps can be produced in accordance with experimental curves. Similar model was proposed and employed for exploring the static magnetization behavior of $Ca_3Co_2O_6$ using Monte Carlo simulation,[15,16] and the four-step behavior, consistent with experimental observation, was confirmed when a random-exchange term was taken into account.

Nevertheless, recent experiments seemed to question this four-step magnetization once more. It was observed that the number of the steps in the magnetization curve strongly depends on the sweep rate of magnetic field B. As the sweep rate is decreased, some of the magnetization steps disappear. This phenomenon shows that the four-step magnetization curve may be due to the nonequilibrium magnetization dynamics. Most recently, Kudasov *et al.*[11] performed the simulation of the nonequilibrium evolution by means of a Glauber-type form of the spin-flip probability and investigated the dependence of the magnetization curves on the magnetic-field sweep rate in good agreement with the experimental data. In addition, the influence of metastable states on the magnetic behavior in $Ca_3Co_2O_6$ compound has been studied in detail using the same model.[14] As the relaxation time increases, the first three plateaus observed at low T tend to merge into one step, likely generating eventually a two-step pattern. These works seem to indicate that the spin-chain system of triangular lattice under B at low T is easily trapped into metastable states from equilibrium and probably the equilibrium state of the magnetization dynamics is not of four-step pattern.

Therefore, it is still an unsolved issue to demonstrate this equilibrium pattern in order to understand the magnetic behavior of the system. However, conventional Metropolis algorithm of Monte Carlo simulation based on local spin flip often fails to relax into the equilibrium state because the model we studied here contains the frustration in the exchange interaction due to the triangular lattice geometry. To overcome this difficulty, one can appeal to the Wang-Landau (WL) algorithm which enables the system to avoid trapping to a metastable state because this algorithm is very powerful to reach the ground state (equilibrium state). Since it was proposed in 2001,[18,19] the WL algorithm has been successfully applied to various problems, such as complex spin models,[20–22] quantum systems,[23,24] fluids,[25,26] and proteins.[27,28] However, as far as we know, there has been no work on the magnetic properties of $Ca_3Co_2O_6$ approached by the WL algorithm in any quantitative sense. In this article, we shall use the standard WL algorithm to calculate the ther-

TABLE I. Parameters chosen for the simulation.

Parameter	Value	Parameter	Value
$k_B(J/K)$	1.3807×10^{-23}	$J(J)$	3.592×10^{-25}
$\mu_B(J/T)$	9.274×10^{-24}	S	32
g	2		

modynamic and magnetic properties of $Ca_3Co_2O_6$ in order to understand the complex magnetic order at the equilibrium state.

Based on the rigid-chain model,[9] the three-dimensional issue of $Ca_3Co_2O_6$ is reduced to the 2D AFM triangular Ising model[29]

$$H = J\sum_{[m,n]} S_m S_n - B\mu_B g\sum_m S_m, \tag{1}$$

where $J>0$ is the AFM-interchain coupling, S_m is the effective spin moment of a spin chain at the site m with the value S, B is an external magnetic field applied along the direction of up-spin chains ($+c$ axis), g is the Lande factor, and μ_B is the Bohr magneton; $[m,n]$ denotes the summation over all the nearest-neighbor pairs.

For investigating the magnetic properties of a system with the WL algorithm, one has to calculate the density of state (DOS) $g(E,M)$ in energy and magnetization space where E denotes the energy of a given spin configuration of the Hamiltonian without external field. Following the pathbreaking work of Wang and Landau,[18,19] we choose the simulation procedure stated in Refs. 18 and 19.

At the very beginning, we set all entries to the DOS $g(E,M)=1$ and a histogram $RH(E,M)=0$ for all possible (E,M) states. Then we begin our random walk in the energy and magnetization space by flipping spins randomly. The transition probability from state (E_1,M_1) to state (E_2,M_2) is

$$p(E_1,M_1\rightarrow E_2,M_2) = \min\left[\frac{g(E_1,M_1)}{g(E_2,M_2)},1\right], \tag{2}$$

where states (E_1,M_1) and (E_2,M_2), respectively, denote energies and magnetizations before and after a spin is flipped. Each time a new state (E_i,M_i) is visited, we modify the existing DOS by a modification factor f_0; i.e., $g(E_i,M_i)=g(E_i,M_i)f_0$. In this Brief Report an initial modification factor of $f_0=\exp(1)$, which allows us to reach all possible energy levels quickly, is used. If the random walk rejects a possible move and stays at the same state (E,M), we also modify the existing DOS by the same modification factor. Each time, the histogram $RH(E_i,M_i)$ (the number of visits) in the energy and magnetization space is accumulated. When the histogram becomes "flat," we reduce the modification factor to a finer one according to the recipe $f_{i+1}=f_i^{1/2}$, reset the histogram $RH(E,M)=0$, and begin the next random walk. After finishing the initial run we perform 27 cycles, resulting in a final modification factor of 1.000 000 007 45. In our simulations, the flat histogram means that histogram $RH(E,M)$ for all possible (E,M) is not less than 80% of the average histogram. In addition, the histograms are generally checked at each 10 000 Monte Carlo sweeps.

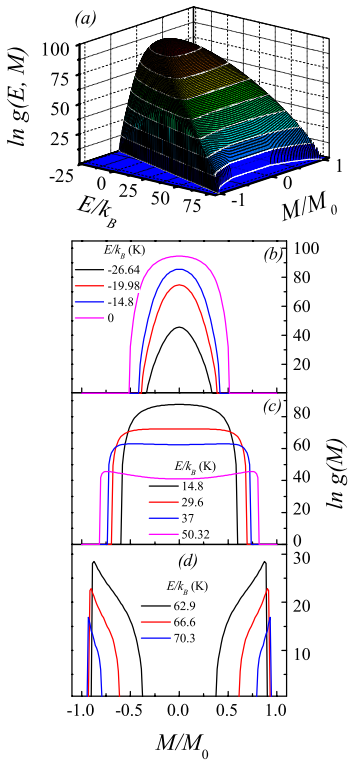

FIG. 1. (Color online) Evaluated DOS $\ln[g(E,M)]$ for $Ca_3Co_2O_6$ compound and curves in (b)–(d) represent the cross-sectioned $\ln[g(E,M)]$ at various energy values E.

After $g(E,M)$ has been obtained, we calculate the thermodynamic and magnetic quantities at any T and B. For example, the internal energy can be calculated by

$$U(T,B) = \frac{\sum_{E,M} Hg(E,M)\exp(-H/k_BT)}{\sum_{E,M} g(E,M)\exp(-H/k_BT)} \equiv \langle H\rangle_{T,B}. \tag{3}$$

The magnetization $M(T,B)$ as a function of T and B can be calculated from

$$M(T,B) = \frac{\sum_{E,M} Mg(E,M)\exp(-H/k_BT)}{\sum_{E,M} g(E,M)\exp(-H/k_BT)}. \tag{4}$$

Our simulation is performed on $L\times L$ triangular lattices with period-boundary conditions. Unless stated otherwise, $L=12$ is chosen in this Brief Report. The values of these parameters for the simulation are listed in Table I, and these parameters have been employed for a number of earlier theoretical and simulation works.[11,14–16]

The simulated DOS $g(E,M)$ for $Ca_3Co_2O_6$ compound is presented in Fig. 1(a). In the low-energy range ($E<0$), as shown in Fig. 1(b), $g(E,M)$ shows a parabolic shape for a given energy value and reaches its single maximum value at $M=0$. The calculated DOS at the lowest energy $E_{\min}(\sim-26.64)$ is quite considerable, indicating that the ground state is thus highly degenerate and can be any of a number of spin-frustrated configurations with the same en-

ergy $E_{\min}$ (within the simulation uncertainty). The similar behavior can be observed for some other systems such as $Mo_{72}Fe_{30}$.[22] In the intermediate energy range ($0<E/k_B<62.9$ K), as shown in Fig. 1(c), the single maximum of $g(M)$ at $M=0$ is replaced by a relatively flat profile. It can be observed that the profile becomes wide with increasing E and eventually concave at $E/k_B \sim 37$ K. Furthermore, the possible M range is divided into two separate subranges from $M=0$ when E exceeds 62.9 K. This behavior may stem from the fact that the model has discontinuous degrees of freedom. The two subranges shrink themselves when E further increases, as shown in Fig. 1(d). At the highest energy, only two M states ($M=1,-1$) which correspond to the ferromagnetic orders are possible. Note that the calculated DOS $g(E,M)$ covers all possible (E,M) space, so the thermodynamic and magnetic properties of the system can be accurately evaluated with the former expressions.

The calculated M as a function of T and B is shown in Fig. 2. The magnetization curves clearly show two steps at low temperature ($T<20$ K). When field B increases from zero, M rapidly reaches the first plateau ($M \sim M_0/3$) and then switches to M_0 above $B \sim 3.6$ T. As it was reported in Ref. 9, the first plateau results from the homogeneous ferrimagnetic order of the spin chains due to the AFM interaction between the chains. As temperature is raised, the steps are progressively washed out due to the thermal activation. When $T>40$ K, the first step disappears completely and the M-B relation becomes linear. Therefore, our simulation result convincingly demonstrates that the equilibrium state of the perfect triangular lattice of the rigid spins does produce the two-step magnetization curve at low temperature.

It is understood that for realistic materials significant random field as background of the lattice interactions may be available. Now we consider the effect of inhomogeneity in the system. For such a purpose, a random-exchange term $\Delta_{m,n}$ is taken into account. The Hamiltonian can be written as follows:

$$H = \sum_{[m,n]} (J + J\Delta_{m,n}) S_m S_n - B\mu_B g \sum_m S_m, \tag{5}$$

with

$$\Delta_{m,n} = \text{span} \cdot \text{RAM}_{m,n}, \tag{6}$$

where $\text{RAM}_{m,n}$ is the random number in $[-1,1]$ and span represents the magnitude of the random-exchange term. Such a strategy was extensively accepted for random fields.

In order to compare with earlier work,[15,16] a random-exchange term with its magnitude span=0.15 is considered first. Figure 3 shows the comparison of the magnetization and internal energy at various T as a function of B for the WL and Metropolis simulations. The two simulations are well coincident with each other at $T=10$ K, as clearly shown in Figs. 3(a) and 3(b), indicating that the Metropolis algorithm also allows the equilibrium state to be reached at relevant T just as the WL method does. However, there is a big discrepancy between the two simulations below $B=3.6$ T at $T=2$ K which is shown in Figs. 3(c) and 3(d). The $M_0/3$ step splits into three equidistant steps in the Metropolis simulation while it keeps invariant in the WL simulation. The relevant internal energies obtained from the Metropolis

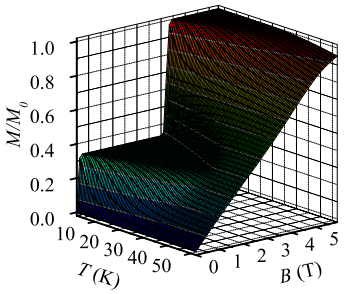

FIG. 2. (Color online) Simulated M/M_0 as a function of T and B.

simulation are higher than the corresponding WL simulation results, as clearly shown in Fig. 3(d), allowing us to argue that the four-step $M(B)$ curve must attribute to the nonequilibrium states. The equilibrium state of the rigid spins can only produce the two-step magnetization curve at $T=2$ K even when the random-exchange term is considered.

Now we can check the dependence of the steplike magnetization feature on the inhomogeneity (random-exchange term) probably available in realistic systems, and the simulated results are presented in Fig. 4(a), where M as a function of B at $T=2$ K upon various span values are plotted in order to understand the effect of the random exchange. One can find that the random-exchange term only smoothens the jumps but cannot assist in generating additional steps. The smoothness of the $M(B)$ curves may be due to the inhomogeneous states induced by the random exchange. As span arises from 0 to 0.3, the borders between the steps become more and more faint. A similar result can also be found in earlier work in which a mean-field approach is employed to study the magnetic properties of the triangular lattice.[16]

At last, we come to check the finite-lattice-size effect in our simulations in order to exclude the artificial facts due to the finite lattice size. The simulated $M(B)$ for different L at $T=2$ K upon span=0.15 are plotted in Fig. 4(b). It is demonstrated that the finite-size effect on the magnetization of the system is nearly negligible and our conclusion is reliable.

Our calculated results can be qualitatively explained by means of the spin-configuration analysis. In such a magnetic

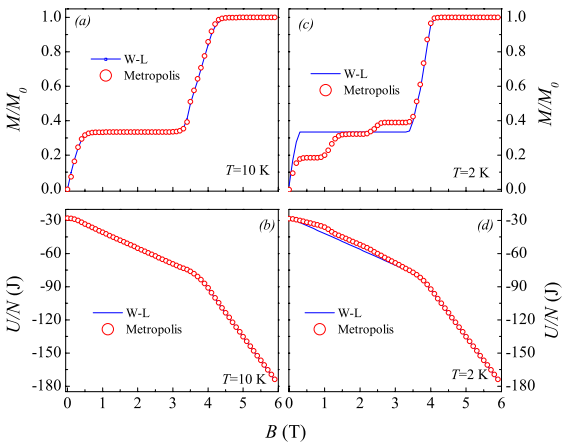

FIG. 3. (Color online) Comparison of (a),(c) M/M_0 and (b),(d) U/N as a function of B calculated from WL method with computed using the Metropolis algorithm at $T=10$ K and $T=2$ K.

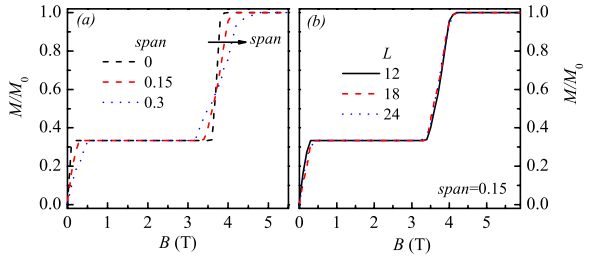

FIG. 4. (Color online) Simulated curves of M/M_0 as a function of B (a) for different spans and (b) for various lattice sizes L at $T=2$ K.

system, M is determined by the competition between the exchange interaction and applied magnetic field. When the random-exchange term is ignored, antiferromagnetic configurations, $\uparrow\uparrow\downarrow$ (spin-up, spin-up, and spin-down) and $\uparrow\downarrow\downarrow$ appear with the same probability for a triangular sublattice at $B=0$, leading to the zero M. However, a weak B breaks the infinite degeneracy, leaving the ground state $\uparrow\uparrow\downarrow$ corresponding to $M=M_0/3$.[30] Such a regular ferrimagnetic structure is formed by taking one spin-down surrounding with six chains of spin-up.[15] As the static magnetic energy increases to be comparable with the interaction energy, the central down spin may flip. The critical field can be estimated to be $6JS/(g\mu_B)\approx 3.6$ T. So when $B>3.6$ T, the ferromagnetic state $\uparrow\uparrow\uparrow$ is formed. When the random-exchange term is considered, the perfect $\uparrow\uparrow\downarrow$ state may be partially destroyed near the critical fields ($B=0$ and 3.6 T), leading to the smoothness of the $M(B)$ curve.

The present work seems to reveal once more that geometrically frustrated spin systems such as the spin-chain $Ca_3Co_2O_6$ offer very complicated spin configuration which is very sensitive to external fluctuations. Although this argument has been made repeatedly, a reliable experimental approach of the fascinating magnetic phenomena in these frustrated systems becomes extremely challenging in terms of understanding their ground state or equilibrium states. The magnetic property of $Ca_3Co_2O_6$, as an example, has attracted attention for many years, but clear knowledge of its equilibrium magnetization remained ambiguous before the present WL simulation.

In conclusion, we have calculated the magnetization of triangular spin-chain system as a function of temperature and applied magnetic field using the WL method. Our simulation demonstrates that the equilibrium state of the rigid spins produces the two-step magnetization curve at low temperature regardless of the random-exchange term being taken into account or not. The random-exchange term only smoothens the jumps but cannot result in additional steps. It is indicated that the four-step magnetization curve observed in experiments must be due to the nonequilibrium magnetization.

This work was supported by the Natural Science Foundation of China under Grants No. 50832002 and No. 10874075, the National Key Projects for Basic Researches of China under Grants No. 2006CB921802 and No. 2009CB623303, and the 111 Project of the MOE of China under Grant No. B07026.

*liujm@nju.edu.cn

[1] H. Fjellvag, E. Gulbrandsen, S. Aasland, A. Olsen, and B. Hauback, J. Solid State Chem. **124**, 190 (1996).
[2] S. Aasland, H. Fjellvag, and B. Hauback, Solid State Commun. **101**, 187 (1997).
[3] H. Kageyama, K. Yoshimura, K. Kosuge, H. Mitamura, and T. Goto, J. Phys. Soc. Jpn. **66**, 1607 (1997).
[4] H. Kageyama, K. Yoshimura, K. Kosuge, M. Azuma, M. Takano, H. Mitamura, and T. Goto, J. Phys. Soc. Jpn. **66**, 3996 (1997).
[5] A. Maignan, C. Michel, A. C. Masset, C. Martin, and B. Raveau, Eur. Phys. J. B **15**, 657 (2000).
[6] V. Hardy, D. Flahaut, M. R. Lees, and O. A. Petrenko, Phys. Rev. B **70**, 214439 (2004).
[7] V. Hardy, M. R. Lees, O. A. Petrenko, D. McK. Paul, D. Flahaut, S. Hebert, and A. Maignan, Phys. Rev. B **70**, 064424 (2004).
[8] A. Maignan, B. Hardy, S. Hebert, M. Drillon, M. R. Lees, O. Petrenko, D. M. K. Paul, and D. Khomskii, J. Mater. Chem. **14**, 1231 (2004).
[9] Y. B. Kudasov, Phys. Rev. Lett. **96**, 027212 (2006).
[10] Y. B. Kudasov, Europhys. Lett. **78**, 57005 (2007).
[11] Y. B. Kudasov, A. S. Korshunov, V. N. Pavlov, and D. A. Maslov, Phys. Rev. B **78**, 132407 (2008).
[12] S. Agrestini, C. Mazzoli, A. Bombardi, and M. R. Lees, Phys. Rev. B **77**, 140403(R) (2008).
[13] S. Agrestini, L. C. Chapon, A. Daoud-Aladine, J. Schefer, A. Gukasov, C. Mazzoli, M. R. Lees, and O. A. Petrenko, Phys. Rev. Lett. **101**, 097207 (2008).
[14] R. Soto, G. Martinez, M. N. Baibich, J. M. Florez, and P. Vargas, arXiv:0811.4772, Phys. Rev. B (to be published).
[15] X. Y. Yao, S. Dong, and J.-M. Liu, Phys. Rev. B **73**, 212415 (2006).
[16] X. Y. Yao, S. Dong, H. Yu, and J.-M. Liu, Phys. Rev. B **74**, 134421 (2006).
[17] P. L. Li, X. Y. Yao, F. Gao, C. Zhao, K. B. Yin, Y. Y. Weng, J.-M. Liu, and Z. F. Ren, Appl. Phys. Lett. **91**, 042505 (2007).
[18] F. Wang and D. P. Landau, Phys. Rev. Lett. **86**, 2050 (2001).
[19] F. Wang and D. P. Landau, Phys. Rev. E **64**, 056101 (2001).
[20] C. Zhou, T. C. Schulthess, S. Torbrugge, and D. P. Landau, Phys. Rev. Lett. **96**, 120201 (2006).
[21] C. Zhou, T. C. Schulthess, and D. P. Landau, J. Appl. Phys. **99**, 08H906 (2006).
[22] S. Torbrugge and J. Schnack, Phys. Rev. B **75**, 054403 (2007).
[23] M. Troyer, S. Wessel, and F. Alet, Phys. Rev. Lett. **90**, 120201 (2003).
[24] W. Koller, A. Prull, H. G. Evertz, and W. von der Linden, Phys. Rev. B **67**, 104432 (2003).
[25] Q. Yan and J. J. de Pablo, Phys. Rev. Lett. **90**, 035701 (2003).
[26] E. A. Mastny and J. J. de Pablo, J. Chem. Phys. **122**, 124109 (2005).
[27] N. Rathore, T. A. Knotts IV, and J. J. de Pablo, J. Chem. Phys. **118**, 4285 (2003).
[28] N. Rathore, Q. Yan, and J. J. de Pablo, J. Chem. Phys. **120**, 5781 (2004).
[29] G. H. Wannier, Phys. Rev. **79**, 357 (1950).
[30] M. Schick, J. S. Walker, and M. Wortis, Phys. Rev. B **16**, 2205 (1977).

Phase transitions in frustrated *XY* model on a square lattice

M. H. Qin and X. Chen
Laboratory of Solid State Microstructures, Nanjing University, Nanjing 210093, China

J. M. Liu
Laboratory of Solid State Microstructures, Nanjing University, Nanjing 210093, China;
School of Physics, South China Normal University, Guangzhou 510006, China;
and International Center for Materials Physics, Chinese Academy of Science, Shenyang 110016, China

(Received 4 August 2009; revised manuscript received 1 October 2009; published 14 December 2009)

We study the phase diagram of a frustrated *XY* model with a nematic coupling (Δ) on the square lattice by means of Monte Carlo simulation. Besides the conventional magnetic-chiral phase, the phase diagram shows an obvious region in which the magnetism is algebraically ordered but the chirality remains disordered. In addition, in the large Δ region, a nematic-chiral phase without magnetic order is identified, which is similar to the phase found in the frustrated *XY* model on triangular lattice [J. H. Park, S. Onoda, N. Nagaosa, and J. H. Han, Phys. Rev. Lett. **101**, 167202 (2008)]

DOI: 10.1103/PhysRevB.80.224415 PACS number(s): 61.30.Cz, 75.10.Hk, 05.10.Ln

I. INTRODUCTION

Symmetry breaking decides orders. The spontaneous breaking of continuous symmetry in magnetic systems leads to the magnetic order, such as ferromagnetic or antiferromagnetic order. However, this mechanism may not be always true and may fail in low-dimensional systems due to the thermal or quantum fluctuations.[1] For instance, the classical two-dimensional (2D) *XY* model cannot sustain long-range magnetic order even with trivial thermal fluctuations, and alternatively the so-called algebraic-magnetic (aM) order with Kosterlitz-Thouless (KT) transition may ensue.[2] On the contrary, the spontaneous breaking of discrete symmetry is still allowed.[3] The spin liquids are typical states with no conventional magnetic order, and yet can show some nontrivial orders which break some hidden discrete symmetries due to the frustrated interactions, and thus can be scaled by the topological number. For instance, spin chirality is relevant with the spontaneous breaking of discrete Z_2 symmetry.[4] The vector spin chirality (vSC) is defined as $\sim\langle \mathbf{S}_i \times \mathbf{S}_j \rangle$ with the spin $\mathbf{S}_i$ at site i, which is odd under spatial inversion and is closely related to multiferroic behavior.[5–8] Besides the vSC, there is another scalar spin chirality $\langle \mathbf{S}_i \times \mathbf{S}_j \times \mathbf{S}_k \rangle$, which breaks the time-reversal symmetry and parity, and is related to the noncoplanar spin order observed in nontrivial glass transitions.[9–11]

A typical model which contains both continuous and discrete symmetries can give rise to fertile phase transitions. The 2D fully frustrated *XY* (FF*XY*) model is a typical representative with a continuous U(1) symmetry associated with global spin rotations and a discrete Z_2 symmetry since the ground state is double degenerate.[4,12] At low temperature (T), this model has both algebraic *XY* order and long-range vSC order. As T increases, a two-stage transition will occur in which the *XY* order and chiral order will be destroyed at T_{KT} and T_χ, respectively.[13–16] In fact, the two transition temperatures are extremely close to each other, with T_χ slightly higher than T_{KT}, indicating that the chiral order is associated with the algebraic-magnetic order, although there does exist a narrow T range only with chiral order.

Based on these studies, Park *et al.* recently investigated the FF*XY* model on a triangular lattice in which an antiferronematic coupling (Δ) is included. Their calculation showed that a phase with both aM order and chiral order (magnetic-chiral phase) can transform into a phase with algebraic-nematic (aN) order and chiral order (nematic-chiral phase) with increasing Δ at low T.[17] In Fig. 1, a schematic illustration of the transition from magnetic-chiral phase to nematic-chiral phase is given. The spins within the same sublattice arrange along or against a certain direction as visually shown with red arrows (gray arrows) in Fig. 1(b), forms the nematic order. The chiral order in this novel nematic-chiral phase is induced by the broken Z_2 symmetry in the nematic phase. In fact, the transition from an algebraic-magnetic order to a nematic order in a regular *XY* model with the nematic coupling was discussed earlier in Ref. 18, where it was pointed out that the phase transition is associated with an Ising transition from an integer vortex pair excitation in the aM phase to an half-integer vortex pair excitation in the nematic phase.

One may notice that the frustration in the model studied in Ref. 17 is stemmed from the triangular lattice geometry, and may question that if there are some interesting phases in other frustrated magnetic systems in which the frustrations are induced by ingredients such as the exchange interaction other than the geometric frustration. However, as far as we know, few works on this subject have been reported. In order to make clear this question, we will study a FF*XY* model with the nematic coupling on a square lattice. The phase

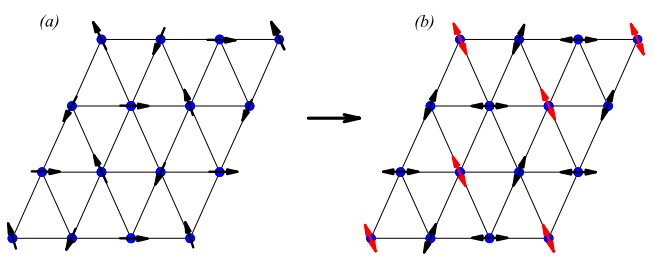

FIG. 1. (Color online) A schematic depiction of the transition from (a) magnetic-chiral phase to (b) nematic-chiral phase.

diagram obtained by means of Monte Carlo simulation shows a phase in which the magnetism is algebraically ordered but the chirality remains disordered over an extended T window. In addition, the nematic-chiral phase without magnetic order is also observed in the phase diagram, suggesting that our model as another classical spin model exhibits a vector chiral spin-liquid phase.

The remainder of this paper is organized as follows: In Sec. II the model and the simulation method will be described. Section III is attributed to the simulation results and discussion. At last, the conclusion is presented in Sec. IV.

II. MODEL AND METHOD OF SIMULATION

Here, we study a classical XY spin model on a square lattice. Different Hamiltonians for such a model were extensively investigated by rigorous and numerical approaches.[18,19] We consider the following Hamiltonian which includes the frustration ingredient

$$H = -J_1 \sum_{[i,j]} \cos(\theta_i - \theta_j - A_{ij}) - J_2 \sum_{[i,j]} \cos(2\theta_i - 2\theta_j - A_{ij}), \tag{1}$$

where $0 \le \theta_i < 2\pi$, indicates the spin orientation at site i, $[i,j]$ denotes the summation over all the nearest-neighbor spin pairs, $J_1 = 1-\Delta$ the strength of the first coupling, $J_2 = \Delta$ the nematic coupling, the bond angle $A_{ij} = \pi$ or $-\pi$ for those bonds where both y_i and y_j, the y coordination of sites i and j, are odd, and $A_{ij} = 0$ elsewhere. For definition of the energy parameters J_1 and J_2, the Boltzmann constant and also the lattice constant are set to unity. The $J_2 = 0$ limit was extensively studied due to its relevance with Josephson-junction arrays in a uniform transverse magnetic field, and it is believed to have the chirality transition at $T_\chi \approx 0.452$ and the KT transition at $T_{\mathrm{KT}} \approx 0.446$.[13–15,20–23]

Unlike the model studied in Ref. 19, which lacks the frustration ingredient, our model contains possible chiral orders induced by the frustration in the magnetic coupling. The ground state for our model is one in which the angular difference between the nearest neighbors is $\Phi_{ij} = \theta_i - \theta_j - A_{ij} = \pm \pi/4$ in the $J_2 = 0$ limit and $\Psi_{ij} = 2\theta_i - 2\theta_j - A_{ij} = \pm \pi/4$ in the $J_1 = 0$ limit. Therefore the two interactions are frustrated, and the ground state is decided by the competition between the two interactions, which is different from the model in Ref. 17 where no frustration exists between the J_1 and J_2 terms and the first term just lifts the degeneracy of the ground state of the second term.

Our simulation is performed on a 2D $L \times L$ ($L = 16, 24, 32, 40, 48, 64$) square lattice with period boundary conditions using the standard Metropolis algorithm and temperature exchange method.[24,25] Here, the temperature exchange method is utilized in order to prevent the system from trapping in metastable free-energy minima caused by the frustration, if any. The initial spin configuration is totally disordered. Typically, the initial 1.5×10^5 Monte Carlo steps are discarded for equilibrium consideration and another 2×10^5 Monte Carlo steps are retained for statistic averaging of the simulation.

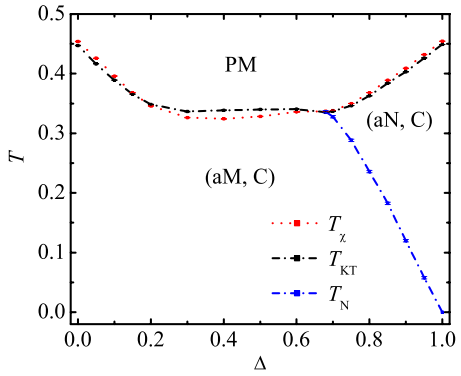

FIG. 2. (Color online) Calculated phase diagram for the model in Eq. (1). The high-temperature paramagnetic phase is denoted by PM, the phases with algebraic correlations in magnetic and nematic order by aM and aN, respectively, and the long-range correlations in the chirality order by C. The statistical errors of all the symbols are the same as their thickness in the T direction.

III. SIMULATION RESULTS AND DISCUSSION

A phase diagram in the Δ-T plane for the present model is constructed by the extensive simulation, and without any detailed analysis the simulated result is shown in Fig. 2. The three curves mark the boundaries between three different phases. The transition from the chiral (C) phase to the paramagnetic (PM) phase occurs at T_χ, and the transition from the algebraically correlated phase to the PM phase occurs at T_{KT}. As Δ increases, the transition from the aM order to the aN order occurs at T_{N}. In addition to the conventional magnetic-chiral order, our simulated result shows a obvious region in which the magnetism is algebraically ordered but the chirality remains disordered ($T_\chi < T_{\mathrm{KT}}$). In the large Δ region, a nematic-chiral phase without magnetic order is observed, same as earlier report.[17] In Sec. III A, we shall address separately these phase transitions in the phase diagram.

A. KT transition at T_{KT}

To determine T_{KT}, the point for the KT transition, we measure the helicity modulus, also called the spin-wave stiffness.[4,26] For this case, the helicity modulus can be defined by

$$\begin{aligned}\Upsilon = {} & \frac{J_1}{L^2}\left\langle \sum_{[i,j]} x_{ij}^2 \cos(\theta_i - \theta_j - A_{ij}) \right\rangle \\ & + \frac{4J_2}{L^2}\left\langle \sum_{[i,j]} x_{ij}^2 \cos(2\theta_i - 2\theta_j - A_{ij}) \right\rangle \\ & - \frac{1}{TL^2}\left\langle \left[J_1 \sum_{[i,j]} x_{ij} \sin(\theta_i - \theta_j - A_{ij}) \right.\right. \\ & \left.\left. + 2J_2 \sum_{[i,j]} x_{ij} \sin(2\theta_i - 2\theta_j - A_{ij}) \right]^2 \right\rangle, \end{aligned} \tag{2}$$

where $x_{ij} = x_i - x_j$ is the separation of the x coordinates. For a given lattice size L, the KT transition point can be estimated by the crossing between the straight line $(2/\pi)(J_1 + 4J_2)T = (2/\pi)(1+3\Delta)T$ and the helicity modulus curve $\Upsilon(T)$. The

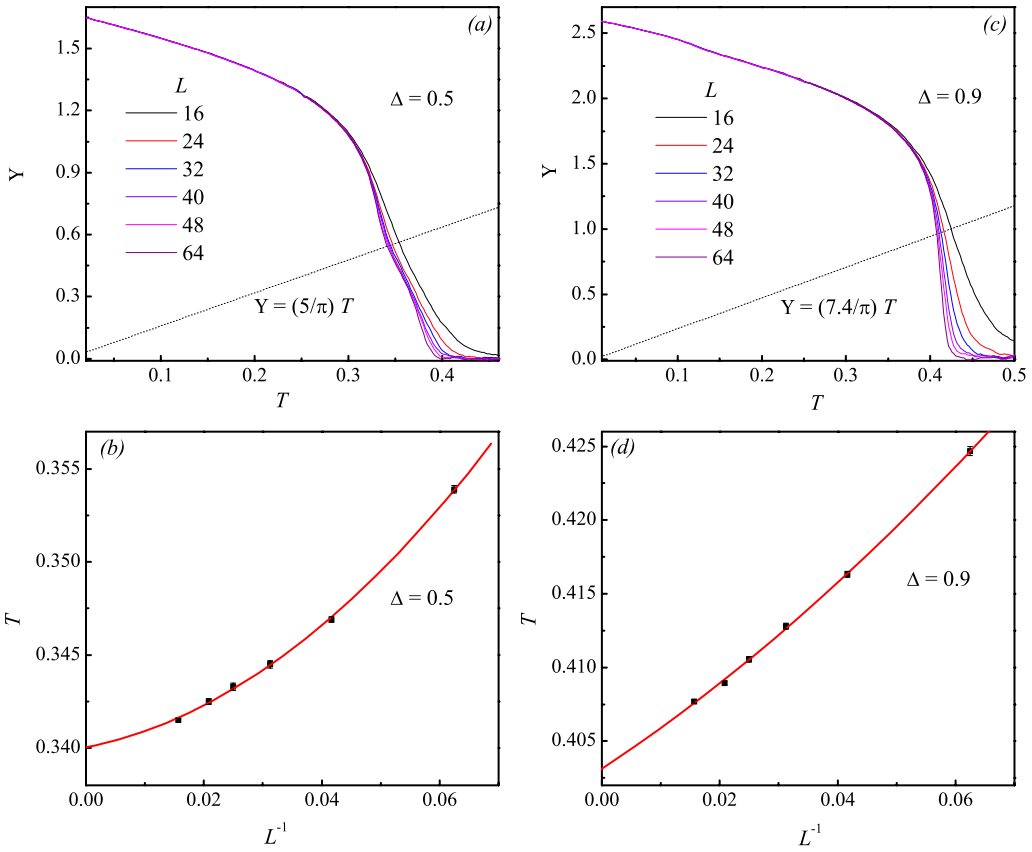

FIG. 3. (Color online) Helicity modulus Υ as a function of T for various sizes L (a) at $\Delta=0.5$ and (c) $\Delta=0.9$. The straight line is $(2/\pi)(1+3\Delta)T$. The crossing temperatures of this line and Υ for each L^{-1} are shown in (b) for $\Delta=0.5$ and (d) $\Delta=0.9$ with the extrapolation to $L^{-1}=0$.

helicity modulus for $L=16-64$ at $\Delta=0.5$ and 0.9 are plotted in Figs. 3(a) and 3(c), and the corresponding crossing points are shown in Figs. 3(b) and 3(d). In the bulk limit, the extrapolations using the polynomial fits give $T_{\mathrm{KT}}=0.340(3)$ at $\Delta=0.5$ and $T_{\mathrm{KT}}=0.403(1)$ at $\Delta=0.9$. This method has been approved to be effective in giving a good estimate of the KT transition temperature in some earlier works, and another method taking into account the logarithmic correction gives a similar result.[17,23]

B. Chirality transition at T_χ

For the chirality transition, it is customary to study the staggered magnetization[16]

$$M=\frac{J_1}{L^2}\left|\sum_i(-1)^{x_i+y_i}m1_i\right|+\frac{2J_2}{L^2}\left|\sum_i(-1)^{x_i+y_i}m2_i\right|, \quad (3)$$

where the sum is over all the plaquettes of the system, $m1=\sin\Phi_{12}+\sin\Phi_{23}+\sin\Phi_{34}+\sin\Phi_{41}$ and $m2=\sin\Psi_{12}+\sin\Psi_{23}+\sin\Psi_{34}+\sin\Psi_{41}$ are the vorticities. For determining the phase-transition temperature, it is convenient to employ the Binder's fourth-order cumulant[27]

$$U_L=1-\frac{\langle M^4\rangle}{3\langle M^2\rangle^2}, \quad (4)$$

where $\langle\ldots\rangle$ is the ensemble average. For the usual cases where finite-size scaling applies, this quantity is size independent at the critical point. So, the critical temperature T_χ can be obtained from the crossing of U_L for different L. As an example, the simulated U_L as a function of T at $\Delta=0.5$ and 0.9 for different lattice sizes are plotted in Fig. 4. From the well common defined crossing points shown in Figs. 4(a) and 4(b), we estimate $T_\chi=0.328(5)$ at $\Delta=0.5$ and $T_\chi=0.408(9)$ at $\Delta=0.9$.

As clearly shown in Fig. 2, T_χ stays slightly above T_{KT} in the small Δ range ($\Delta\leq 0.15$) and in the large Δ region ($\Delta\geq 0.7$), same as earlier report.[17] In addition, the phase diagram contains two crossings of the KT transition and the chirality transition, as well as a certain Δ range in which T_{KT} stays well above T_χ. The identification of T_{KT} well above T_χ

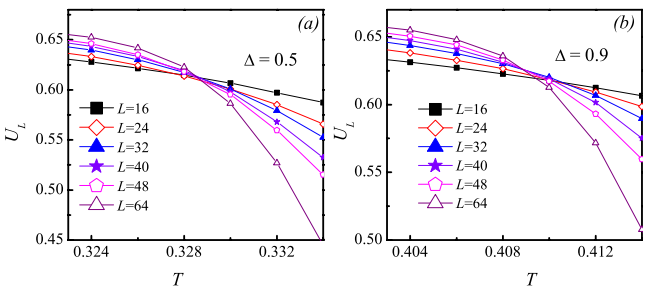

FIG. 4. (Color online) Binder's fourth-order cumulant U_L as a function of T for different lattice sizes at (a) $\Delta=0.5$ and (b) $\Delta=0.9$.

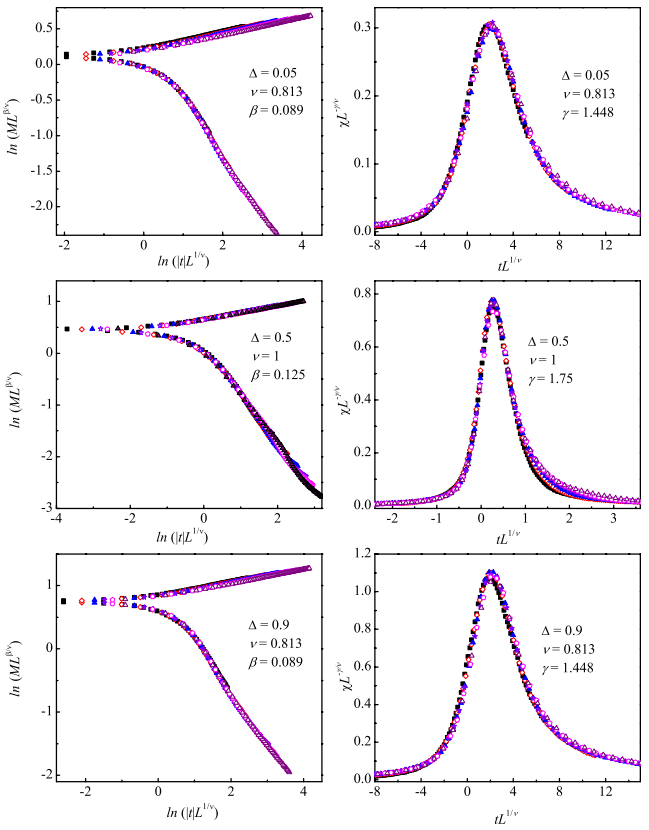

FIG. 5. (Color online) A scaling plot of M and its susceptibility χ for $\Delta=0.05$, $\Delta=0.5$, and $\Delta=0.9$.

proves the existence of the phase with only aM order in our model. In fact, the phase with only aM order has been observed in earlier work in which the phase diagram of the generalized FFXY model on square lattice is studied in details.[23] It is identified that the chirality order disappears when p, the manipulated parameter of the interaction potential, becomes larger than its critical value p_c, due to the ground state in this region has no broken chirality symmetry. This result is different from our work where the chirality order exists in the whole Δ region. As analyzed earlier, the two terms (J_1 and J_2) of our model compete with each other for the formation of the chirality orders, while both of them contribute to the KT phase transition. Therefore in the middle Δ region, the chirality order can be significantly suppressed, leading to T_χ stays well below T_{KT}.

In Fig. 5, we plot the simulated M and its susceptibility, $\chi=(L^2/T)(\langle M^2\rangle-\langle M\rangle^2)$, in the scaling form: $M=L^{-\beta/\nu}f(|t|L^{1/\nu})$, $\chi=L^{\gamma/\nu}g(tL^{1/\nu})$, with $t=(T-T_\chi)/T_\chi$, at $\Delta=0.05$, 0.5, and 0.9. It is observed that the chiral transition at these small sizes with the critical exponents $\nu=0.813(5)$, $\beta=0.089(8)$, and $\gamma=1.448(5)$ in the small Δ range ($\Delta\leq 0.15$) and in the large Δ region ($\Delta\geq 0.7$), consistent with earlier report at $\Delta=0$.[14] However, recent research at large sizes [up to $L=\mathrm{O}(10^3)$] at $\Delta=0$ has demonstrated that the chiral critical exponents are those of the 2D Ising model, i.e., $\nu=1$, $\beta=1/8$, and $\gamma=7/4$ which can be observed only after a preasymptotic regime.[21,22] The non-Ising exponents obtained earlier have been thought of as an enhanced finite-size scaling effect at small sizes due to the screening length associated

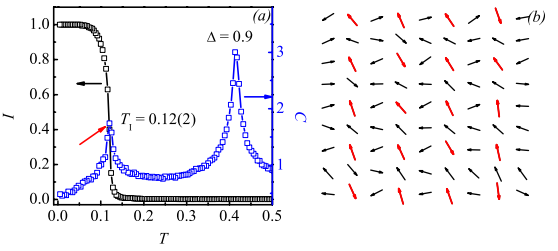

FIG. 6. (Color online) (a) Simulated curves of I and special heat C as a function of T at $\Delta=0.9$. (b) A snapshot of the nematic-chiral state at $T=0.2$ for $\Delta=0.9$. The spins in the same sublattice are shown with red arrows (gray arrows) for clarity.

with the nearby KT transition.[15] On the other hand, in the middle Δ region ($0.2<\Delta<0.6$) where T_{KT} stays well away from T_χ, the finite-size scaling effect can be significantly weakened leading to the chirality transition with the exponents of 2D Ising model even at small sizes. So, it is likely that the non-Ising exponents obtained in this work are also effective ones and the true universality class of the chirality transition in the whole Δ region is that of 2D Ising transition.

C. Nematic transition at T_{N}

For $\Delta>0.68$, a further transition from the aN phase to the aM one, which is associated with the transition from the integer vortex pair to the half-integer vortex pair, occurs at T_{N}. Following earlier work,[17] the order parameter can be defined by

$$I=(4/L^2)\sum_{i\in B}\mathrm{sgn}(\cos[\theta_i-\theta_{i_0}]), \tag{5}$$

where θ_{i0} is the spin angle at some reference site i_0 of the sublattice B. Here, the site i in the sublattice B is selected with both odd x_i and y_i. In the nematic phase, θ_i and $\theta_i+\pi$ occur with equal probabilities, leading to a zero-order parameter I. In Fig. 6(a), parameter I and specific heat C as a function of T at $\Delta=0.9$ for $L=48$ are plotted. The sudden flop of I and the lower-temperature specific-heat peak at $T_{\mathrm{N}}=0.12(2)$ clearly mark the nematic transition. However, the nematic transition cannot be scaled with the 2D Ising critical exponents, which may due to the frustrations in our system. As clearly shown in Fig. 2, this nematic transition occurs at a much lower temperature than either the chiral or the KT transition, leading to the existence of a nematic-chiral phase in which the chirality is ordered but the magnetism remains disordered. The chiral phase is induced by the breaking of Z_2 symmetry in the nematic transition as reported earlier. To some extent, our work proves that the same mechanism may hold true in some other similar frustrated systems. In Fig. 6(b), we show a snapshot of the nematic-chiral order at $T=0.2$ for $\Delta=0.9$. The spins within the same sublattice generally parallel or antiparallel with each other, as clearly shown with the red arrows. Therefore, apart from the FFXY model on the triangular lattice, our model is another classical spin model which exhibits a vector chiral spin-liquid phase.

IV. CONCLUSION

In summary, we have studied the phase diagram of a frustrated *XY* model with a nematic coupling (Δ) on the square lattice using Monte Carlo simulation. The phase diagram for middle Δ exhibits a phase in which the magnetism is ordered but the chirality remains disordered, which is ascribed to the competition between the two couplings in the formation of the chirality order. For large Δ, the simulated result shows the existence of the nematic-chiral phase without any magnetic order, which qualifies our model as another classical spin model that exhibits a vector chiral spin-liquid phase, in addition to the FF*XY* model on the triangular lattice.

ACKNOWLEDGMENTS

This work was supported by the National Natural Science Foundation of China (Grants No. 50832002, No. 50601013, and No. 50528203) and the National Key Projects for Basic Researches of China (Grants No. 2009CB929501 and No. 2006CB921802).

[1] N. D. Mermin and H. Wagner, Phys. Rev. Lett. **17**, 1133 (1966).
[2] J. M. Kosterlitz and D. J. Thouless, J. Phys. C **6**, 1181 (1973).
[3] R. B. Griffiths, Phys. Rev. **136**, A437 (1964).
[4] D. H. Lee, J. D. Joannopoulos, J. W. Negele, and D. P. Landau, Phys. Rev. B **33**, 450 (1986).
[5] K. F. Wang, J.-M. Liu, and Z. F. Ren, Adv. Phys. **58**, 321 (2009).
[6] H. Katsura, N. Nagaosa, and A. V. Balatsky, Phys. Rev. Lett. **95**, 057205 (2005).
[7] M. Mostovoy, Phys. Rev. Lett. **96**, 067601 (2006).
[8] D. Khomskii, Phys. **2**, 20 (2009).
[9] H. Kawamura and D. Imagawa, Phys. Rev. Lett. **87**, 207203 (2001).
[10] L. W. Lee and A. P. Young, Phys. Rev. Lett. **90**, 227203 (2003).
[11] D. X. Viet and H. Kawamura, Phys. Rev. Lett. **102**, 027202 (2009).
[12] J. Villain, J. Phys. C **10**, 1717 (1977).
[13] S. Teitel and C. Jayaprakash, Phys. Rev. B **27**, 598 (1983).
[14] S. Lee and K. C. Lee, Phys. Rev. B **49**, 15184 (1994).
[15] P. Olsson, Phys. Rev. Lett. **75**, 2758 (1995).
[16] S. Lee and K. C. Lee, Phys. Rev. B **57**, 8472 (1998).
[17] J. H. Park, S. Onoda, N. Nagaosa, and J. H. Han, Phys. Rev. Lett. **101**, 167202 (2008).
[18] D. H. Lee and G. Grinstein, Phys. Rev. Lett. **55**, 541 (1985).
[19] D. B. Carpenter and J. T. Chalker, J. Phys.: Condens. Matter **1**, 4907 (1989).
[20] S. E. Korshunov, Phys. Rev. Lett. **88**, 167007 (2002).
[21] M. Hasenbusch, A. Pelissetto, and E. Vicari, Phys. Rev. B **72**, 184502 (2005).
[22] M. Hasenbusch, A. Pelissetto, and E. Vicari, J. Stat. Mech.: Theory Exp. (2005) P12002.
[23] P. Minnhagen, B. J. Kim, S. Bernhardsson, and G. Cristofano, Phys. Rev. B **76**, 224403 (2007).
[24] D. P. Landau and K. Binder, *A Guide to Monte Carlo Simulations in Statistical Physics* (Cambridge University Press, Cambridge, England, 2005).
[25] K. Hukushima and K. Nemoto, J. Phys. Soc. Jpn. **65**, 1604 (1996).
[26] M. E. Fisher, M. N. Barber, and D. Jasnow, Phys. Rev. A **8**, 1111 (1973).
[27] K. Binder, Phys. Rev. Lett. **47**, 693 (1981).

Multiferroic response to magnetic field in orthorhombic manganites

M. H. Qin,[1] Y. M. Tao,[2] S. Dong,[3] H. B. Zhao,[1] X. S. Gao,[1] and J.-M. Liu[1,2,4,a)]
[1]*School of Physics, South China Normal University, Guangzhou 510006, People's Republic of China*
[2]*Laboratory of Solid State Microstructures, Nanjing University, Nanjing 210093, People's Republic of China*
[3]*Department of Physics, Southeast University, Nanjing 211189, People's Republic of China*
[4]*International Center for Materials Physics, Chinese Academy of Science, Shenyang 110016, People's Republic of China*

(Received 5 January 2011; accepted 18 February 2011; published online 10 March 2011)

The magnetoelectric coupling in $Eu_{0.55}Y_{0.45}MnO_3$ is studied based on a microscopic spin model which includes the superexchange interaction, the single-ion anisotropy, the Dzyaloshinskii–Moriya interaction, and the cubic anisotropy. Our Monte Carlo simulation reproduces the experimentally observed multiferroic response to magnetic field B. It is demonstrated that the magnetic field can control the multiferroic behaviors by modulating the spin arrangements, leading to various flops of electric polarization. In addition, an interesting state in which both the electric polarizations along the a-axis and c-axis are activated under high B is predicted and discussed. © *2011 American Institute of Physics*. [doi:10.1063/1.3565241]

Multiferroics are attracting continuous attentions due to the interesting physics and potential applications.[1] In the past few years, multiferroicity has been found in a number of systems, such as spiral magnets, orthorhombically distorted perovskite manganites $RMnO_3$ [R=Tb, Dy, $Eu_{1-x}Y_x$, etc., crystal structure on the ab-plane is shown in Fig. 1(a)],[2] $Ni_3V_2O_8$,[3] $MnWO_4$,[4] and a conical magnet $CoCr_2O_4$.[5] The ferroelectricity in these materials is induced by spiral spin order through the inverse Dzyaloshinskii–Moriya (DM) mechanism (alternatively the spin current model).[6] In the spin current scenario, adjacent two spins (S_i,S_j) can generate a local polarization $P_{ij} \propto -e_{ij} \times (S_i \times S_j)$ with e_{ij} the unit vector connecting the two neighboring sites. Thus, polarization P in the ab-plane cycloidal spin (ab-CS) phase with propagation vector along the b-axis is induced along the a-axis while in the bc-plane cycloidal spin (bc-CS) phase it is induced along the c-axis, as illustrated in Figs. 1(b) and 1(c). $RMnO_3$ offers the capability for magnetic control of ferroelectricity via the strong magnetoelectric (ME) coupling. For $TbMnO_3$ and $DyMnO_3$, application of a magnetic field B along the b-axis (field B_b) flops P from the c-axis (polarization P_c) to the a-axis (polarization P_a).[7] Several theoretical works in order to understand the origin for such multiferroic response and the ME coupling in $RMnO_3$ are available.[8,9]

Most recently, a microscopic spin model (Mochizuki–Furukawa model) which includes the superexchange interaction, the single-ion anisotropy (SIA), the DM interaction, and the cubic anisotropy, was proposed and reproduced the phase diagrams of $RMnO_3$ in the plane of temperature (T) versus R-site ionic radius.[9] It was demonstrated that the orthorhombic lattice distortion mainly controlled by the R-ionic radius tunes the SIA and the DM interaction energies and in turn determines the competition between the ab-CS phase and bc-CS phase. This leads to the flop of P from the a-axis to the c-axis with reduced R-ionic radius. Subsequently, several other phenomena have been well explained based on the same or similar models.[10–14] For example, the phase diagrams of $TbMnO_3$ and $DyMnO_3$ under magnetic field B have been reproduced.[11]

On the other hand, several multiferroic states and strong ME effects were revealed in $RMnO_3$ (R=$Eu_{1-x}Y_x$) by tuning the R site ionic size.[15–17] In $Eu_{0.55}Y_{0.45}MnO_3$, polarization P flops from P_a to P_c when B is applied along the a-axis (B_a) while it flops from P_c to P_a with B along the c-axis (B_c) [see Figs. 1(d)–1(f)].[16] These ME phenomena may help us to understand the origin of the multiferroic response to B, due to the fact that this system is free from the influence of magnetic moments of R ions. Furthermore, a multiferroic state in which P is induced via the spin exchange striction mechanism was observed in $EuMnO_3$ under a field up to 30 Tesla (T).[10] It is thus reserved to question some unrevealed phases in $Eu_{0.55}Y_{0.45}MnO_3$ in the high B range.

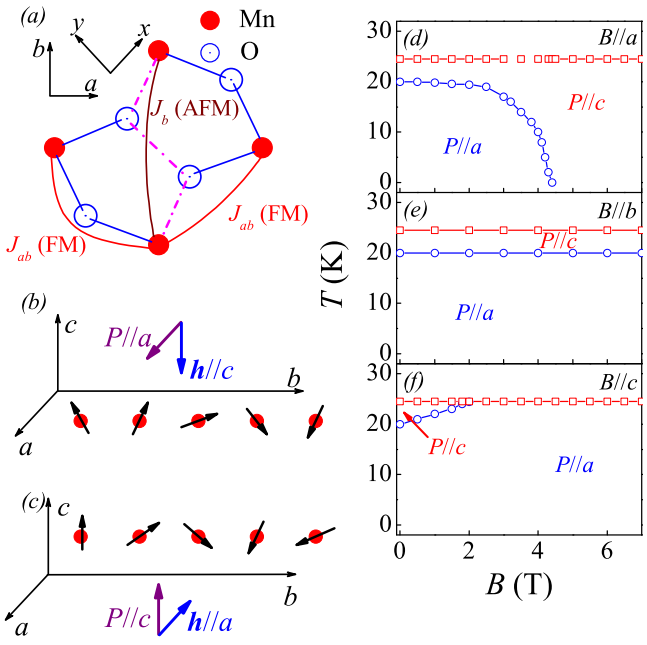

FIG. 1. (Color online) (a) Crystal structure (ab-plane) of $RMnO_3$. The induced P and spin-helicity vector $\boldsymbol{h}=\Sigma_{ij}S_i \times S_j$ in the ab-CS (b) and bc-CS (c) states. Experimentally obtained B-T phase diagrams for (d) $B \| a$, (e) $B \| b$, and (f) $B \| c$ are reproduced from Ref. 16.

a)Electronic mail: liujm@nju.edu.cn.

In this work, we study the Mochizuki–Furukawa model with Mn spin $S=2$ on a cubic lattice.[9] The Hamiltonian can be written as $H=H_{ex}+H_{\mathrm{SIA}}+H_{\mathrm{DM}}+H_{cub}+H_{\mathrm{Zeeman}}$. The first term $H_{ex}=\Sigma_{\langle i,j\rangle}J_{ij}\times(S_i\cdot S_j)$ denotes the spin exchange interactions, where $J_{ab}=-0.8$ and $J_b=0.8$ are the coupling constants in the Mn–Mn bonds on the *ab* plane [Fig. 1(a)], $J_c=1.25$ is the antiferromagnetic (AFM) exchange in the Mn–Mn bonds along the *c*-axis. Here the energy unit is millielectron volt. The second term is the SIA, which consists of two parts as $H_{\mathrm{SIA}}=D\cdot\Sigma_i S^i_{\zeta i}+E\cdot\Sigma_i(-1)^{i_x+i_y}\cdot(S^i_{\xi i}-S^i_{\eta i})$ with $D=0.25$, $E=0.30$. Here, ξ_i, η_i, ζ_i are the tilted local axes attached to the *i*th MnO_6 octahedron, as clearly given in Ref. 9. For their direction vectors, we use the experimental data of $EuMnO_3$.[18] The third term H_{DM} represents the DM interactions expressed by $H_{\mathrm{DM}}=\Sigma_{\langle i,j\rangle}d_{i,j}\times(S_i\times S_j)$. Here the DM vectors $d_{i,j}$ are determined by five DM parameters, $(\alpha_{ab},\beta_{ab},\gamma_{ab})=(0.10,0.10,0.14)$ and $(\alpha_c,\beta_c)=(0.30,0.30)$. The fourth term $H_{cub}=A\cdot\Sigma_i(S^4_{\mathrm{xi}}+S^4_{\mathrm{yi}}+S^4_{\mathrm{zi}})/S(S+1)$ represents the cubic anisotropy with coupling constant $A=0.0162$. The last term $H_{\mathrm{Zeeman}}=-B\mu_B g\Sigma_i S_i$ stands for the Zeeman coupling. Here $g=2$ is the Lande factor, and μ_B is the Bohr magneton.

Our Monte Carlo simulation is performed on a $36\times36\times6$ cubic lattice with periodic boundary conditions using the standard Metropolis algorithm and temperature exchange method.[19–21] The selected parameters reproduce well the magnetic states of $Eu_{0.55}Y_{0.45}MnO_3$ in the absence of *B*. With decreasing *T*, the system successively exhibits the paramagnetic (PM) phase, the sinusoidal collinear antiferromagnetic (sc-AFM) order with Mn spins along the *b*-axis, the *bc*-CS phase, and the *ab*-CS phase. The specific heat $C(T)=(\langle H^2\rangle-\langle H\rangle^2)/Nk_BT^2$ and spin-helicity vector $h_\gamma(T)=\langle|\Sigma_i S_i\times S_{i+b}|\rangle/NS^2$ $(\gamma=a,b,c)$ are calculated to determine the transition points and spin structures, here *N* is the number of Mn ions, k_B is the Boltzmann constant, and the brackets denote thermal and configuration averaging. The spin and spin-helicity correlation functions in the momentum space, $\Phi_\gamma(k,T)=\Sigma_{ij}\langle S_{\gamma i}\cdot S_{\gamma j}\rangle\exp[ik\cdot(r_i-r_j)]/N^2$ and $\Psi_\gamma(k,T)=\Sigma_{ij}\langle h^b_{\gamma i}\cdot h^b_{\gamma j}\rangle\exp[ik\cdot(r_i-r_j)]/N^2$ for $\gamma=a,b,c$ are also calculated in order to characterize the spin structures.

The calculated phase diagram in the *B*-*T* plane with $B\|a$-axis is shown in Fig. 2(a), which reproduces the observed *P* flop from the *a*-axis to the *c*-axis, in associated with the flop of the spiral-spin plane from the *ab*-plane to the *bc*-plane. In the low field range ($B_a=3.0$ T), the simulated $C(T)$ curve shows three specific-heat peaks, indicating the successive three phase transitions with decreasing *T*, as shown in Fig. 2(b). The first one is the transition from the PM phase to the sc-AFM phase. When *T* falls down to the second transition point, spin-helicity vector $h_a(T)$ increases while $h_b(T)$ and $h_c(T)$ remain small, fingering a transition to the *bc*-CS order. At the third transition, $h_c(T)$ steeply increases, accompanied with the sudden drop of $h_a(T)$, as a sign of spin spiral flop from the *bc*-plane to the *ab*-plane. In addition, the third transition point shifts toward the low-*T* side as B_a increases, indicating that the spiral-plane gradually flops from the *bc*-plane to the *ab*-plane at low *T*. As B_a increases up to 5 T and above, the system exhibits only two transitions at low *T*. For instance, at $B_a=6$ T, $C(T)$ shows two peaks and $h_a(T)$ is small over the whole *T*-range, as shown in Fig. 2(c). This simply indicates that the *bc*-CS order component if any is completely suppressed and the *ab*-CS order occupies the whole *T*-range below the second transition point, in agreement with experiments. It is well known that for an isotropic AFM or spiral spin system, field *B* tends to align the spins in perpendicular to *B*. The flop of spiral spin order into the *bc*-plane from the *ab* plane under high B_a becomes physically reasonable. Surely, such spiral-plane flop must be accompanied with the reorientation of *P*.

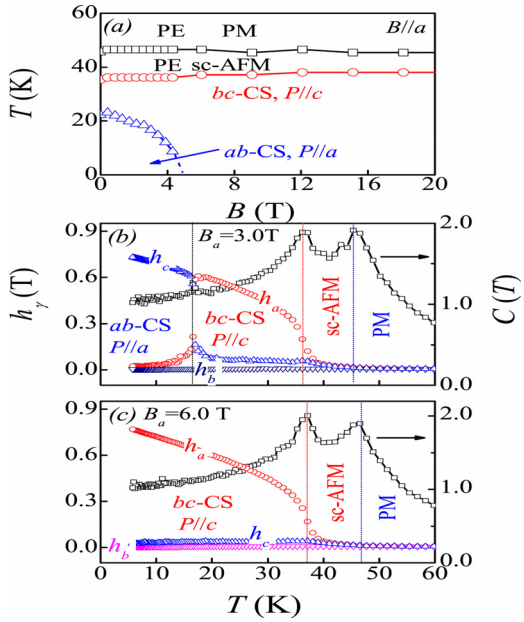

FIG. 2. (Color online) (a) Calculated B_a-*T* phase diagram of $Eu_{0.55}Y_{0.45}MnO_3$. Here, the high-temperature PM phase is denoted by PM, accompanied by the paraelectric phase PE, CS order denotes cycloidal spin order, sc-AFM stands for sinusoidal collinear antiferromagnetic order. Specific heat $C(T)$ and spin-helicity vector $h_\gamma(T)$ $(\gamma=a,b,c)$ as a function of *T* under various B_a: (b) $B_a=3.0$ T, and (c) $B_a=6.0$ T.

The effect of *B* on the multiferroicity revealed above also applies to the case with $B\|c$-axis (B_c). The calculated B_c-*T* phase diagram is displayed in Fig. 3(a). The magnetic field applied along the *c*-axis suppresses the *bc*-CS order while it enhances the *ab*-CS order, resulting in the flop of *P* from the *c*-axis to the *a*-axis. The *ab*-CS order overwhelms the *bc*-CS order at $B_c\sim3.0$ T, coinciding with experiments. For details, the calculated $C(T)$ and $h_\gamma(T)$ for $B_c=6.0$ T are shown in Fig. 3(b), indicating that the *ab*-plane spiral spin order is completely suppressed.

Subsequently, we look at the case of $B\|b$-axis (B_b). A prominent feature is that the magnetic phases in $Eu_{0.55}Y_{0.45}MnO_3$ show little dependence on B_b up to $B_b=7.0$ T, which is also reproduced in our simulation. At low field, the three magnetic transitions remain essentially unchanged and in fact no changes in the transition points (not shown here). One notes that for $RMnO_3$, the *ac*-CS order is unfavorable due to the fact that it cannot be stabilized by the DM interaction and the SIA. A low B_b cannot flip the spins into the *ac*-plane from the initial *ab*-plane and *bc*-plane, suggesting the robustness of the *ab*-CS or *bc*-CS orders. For high field case, as an example, we present the simulated $C(T)$ and $h_\gamma(T)$ at $B_b=9$ T in Fig. 3(c). The first and second transitions remain roughly unchanged while the third transition shifts toward the low-*T* side. In addition, below the second transition point, both $h_a(T)$ and $h_c(T)$ have large values, indicating the coexistence of the *bc*-CS order and the *ab*-CS

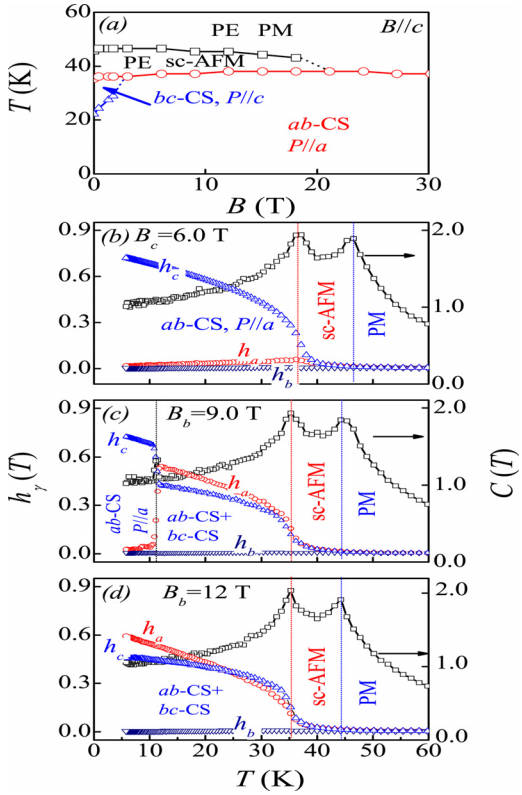

FIG. 3. (Color online) (a) Calculated B_c-T phase diagram. Specific heat $C(T)$ and spin-helicity vector $h_\gamma(T)$ as a function of T under: (b) B_c =1.3 T, (c) B_b=9.0 T, and (d) B_b=12 T.

order. In this case, the spins have both a-axis components and c-axis components. At the same time, the DM interaction with vectors on the in-plane Mn–O–Mn bonds stabilizes the ab-CS order while the DM interaction with vectors on the out-of-plane bonds stabilizes the bc-CS order. This leads to the simultaneous appearance of these two types of spiral spin orders. Around the third transition point, $h_a(T)$ suddenly drops to nearly zero, indicating the disappearance of the bc-CS order. As B_b increases up to 12 T, the system exhibits only two transitions, as shown in Fig. 3(d). The former is a transition from the PM phase into the sc-AFM phase, and the latter is a transition into a magnetic phase in which the ab-CS order and the bc-CS order coexist. According to the spin-current model, both P_a and P_c will be observed in the state with the coexisting ab-CS and bc-CS orders.

The Mochizuki–Furukawa model, proposed in the classical Heisenberg spin framework, shows surprisingly good consistency with experiments. In particular, our simulations reveal the coexistence of the ab-CS and bc-CS orders under high magnetic field along the b-axis, implying the coexistence of the a-axis and c-axis polarization components. In fact, the corresponding magnetic structures are also confirmed in our calculated spin-helicity correlations Ψ_γ. Figures 4(a) and 4(b) show the simulated $\Psi_\gamma(\gamma=a,c)$ under B_b=15 T at T=5 K. Both Ψ_a and Ψ_c have their peak locations at $k=(0,0,0)$, indicating the coexistence of the ab-CS and bc-CS orders. The simulated Φ_γ also characterize this spin structures. However, the predicted phase was not observed in earlier experiments in which the high field phase diagrams of $Eu_{1-x}Y_xMnO_3$(x=0 and 0.4) under B_b were studied in pulsed magnetic fields. This inconsistence between the theory and experiment may be due to the fact that the actual

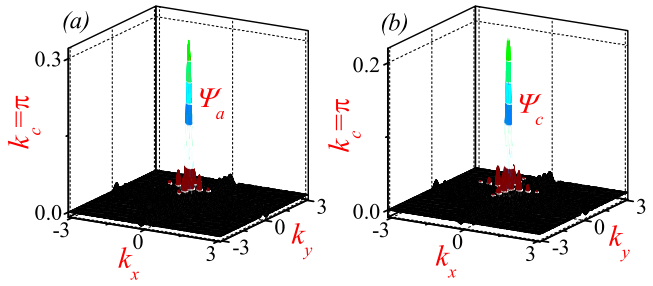

FIG. 4. (Color online) Calculated spin-helicity correlation functions (a) Ψ_a and (b) Ψ_c under B_b=15 T at T=5 K.

system is hard to be relaxed toward the equilibrium state at low T because of the high potential barrier between the equilibrium state and the quasi-static state under high B. Of course, this issue remains to be checked further.

This work was supported by the Natural Science Foundation of China (Grant Nos. 50832002, 51072061, 51031004, and 11004027), the National Key Projects for Basic Research of China (Grant No. 2011CB922101), and the China Postdoctoral Science Foundation (Grant No. 20100480768).

[1]M. Fiebig, J. Phys. D **38**, R123 (2005); W. Eerenstein, N. D. Mathur, and J. F. Scott, Nature (London) **442**, 759 (2006); Y. Tokura, J. Magn. Magn. Mater. **310**, 1145 (2007); S.-W. Cheong and M. Mostovoy, Nature Mater. **6**, 13 (2007); K. F. Wang, J.-M. Liu, and Z. F. Ren, Adv. Phys. **58**, 321 (2009).
[2]T. Kimura, T. Goto, H. Shintani, K. Ishizaka, T. Arima, and Y. Tokura, Nature (London) **426**, 55 (2003); T. Goto, T. Kimura, G. Lawes, A. P. Ramirez, and Y. Tokura, Phys. Rev. Lett. **92**, 257201 (2004).
[3]G. Lawes, A. B. Harris, T. Kimura, N. Rogado, R. J. Cava, A. Aharony, O. Entin-Wohlman, T. Yildirim, M. Kenzelmann, C. Broholm, and A. P. Ramirez, Phys. Rev. Lett. **95**, 087205 (2005).
[4]K. Taniguchi, N. Abe, T. Takenobu, Y. Iwasa, and T. Arima, Phys. Rev. Lett. **97**, 097203 (2006).
[5]Y. Yamasaki, S. Miyasaka, Y. Kaneko, J.-P. He, T. Arima, and T. Tokura, Phys. Rev. Lett. **96**, 207204 (2006).
[6]H. Katsura, N. Nagaosa, and A. V. Balatsky, Phys. Rev. Lett. **95**, 057205 (2005); M. Mostovoy, *ibid.* **96**, 067601 (2006); I. A. Sergienko and E. Dagotto, Phys. Rev. B **73**, 094434 (2006).
[7]T. Goto, Y. Yamasaki, H. Watanabe, T. Kimura, and Y. Tokura, Phys. Rev. B **72**, 220403(R) (2005); T. Kimura, Annu. Rev. Mater. Res. **37**, 387 (2007).
[8]S. Dong, R. Yu, S. Yunoki, J.-M. Liu, and E. Dagotto, Phys. Rev. B **78**, 155121 (2008).
[9]M. Mochizuki and N. Furukawa, J. Phys. Soc. Jpn. **78**, 053704 (2009); Phys. Rev. B **80**, 134416 (2009).
[10]M. Tokunaga, Y. Yamasaki, Y. Onose, M. Mochizuki, N. Furukawa, and Y. Tokura, Phys. Rev. Lett. **103**, 187202 (2009).
[11]M. Mochizuki and N. Furukawa, Phys. Rev. Lett. **105**, 187601 (2010).
[12]M. Mochizuki, N. Furukawa, and N. Nagaosa, Phys. Rev. Lett. **104**, 177206 (2010).
[13]M. Mochizuki and N. Nagaosa, Phys. Rev. Lett. **105**, 147202 (2010).
[14]M. Mochizuki, N. Furukawa, and N. Nagaosa, Phys. Rev. Lett. **105**, 037205 (2010).
[15]Y. Yamasaki, S. Miyasaka, T. Goto, H. Sagayama, T. Arima, and Y. Tokura, Phys. Rev. B **76**, 184418 (2007).
[16]H. Murakawa, Y. Onose, F. Kagawa, S. Ishiwata, Y. Kaneko, and Y. Tokura, Phys. Rev. Lett. **101**, 197207 (2008).
[17]S. Ishiwata, Y. Kaneko, Y. Tokunaga, Y. Taguchi, T. Arima, and Y. Tokura, Phys. Rev. B **81**, 100411(R) (2010).
[18]B. Dabrowski, S. Kolensnik, A. Baszczuk, O. Chmaissem, T. Maxwell, and J. Mais, J. Solid State Chem. **178**, 629 (2005).
[19]D. P. Landau and K. Binder, *A Guide to Monte Carlo Simulations in Statistical Physics* (Cambridge University Press, Cambridge, England, 2005).
[20]K. Hukushima and K. Nemoto, J. Phys. Soc. Jpn. **65**, 1604 (1996).
[21]M. H. Qin, X. Chen, and J.-M. Liu, Phys. Rev. B **80**, 224415 (2009).

Magnetic behaviors of classical spin model on the Shastry–Sutherland lattice: Monte Carlo simulation

M. H. Qin,[1] G. Q. Zhang,[2] K. F. Wang,[2] X. S. Gao,[1] and J.-M. Liu[1,2,3,a)]
[1]*School of Physics, South China Normal University, Guangzhou 510006, People's Republic of China*
[2]*Laboratory of Solid State Microstructures, Nanjing University, Nanjing 210093, People's Republic of China*
[3]*International Center for Materials Physics, Chinese Academy of Science, Shenyang 110016, People's Republic of China*

(Presented 15 November 2010; received 20 September 2010; accepted 1 November 2010; published online 18 March 2011)

We study the magnetic phase diagram of a classical Heisenberg spin model on the Shastry–Sutherland lattice using the Monte Carlo method. The simulated results indicate that the particular collinear phase region can be enlarged due to the implementation of easy-axis anisotropy, leading to the broadening of the magnetization plateau in the classical Heisenberg model. Also, the random exchange term is taken into account to study the effect of inhomogeneity on the steplike magnetization feature. It is indicated that the multi-step magnetic behaviors in the low temperature range remain observable when the inhomogeneity is in the appropriate range. © *2011 American Institute of Physics*. [doi:10.1063/1.3536664]

The so-called "frustrated" spin system is a system in which a spin configuration to fully satisfy the interactions between every pair of spins cannot be found.[1] During the last decades, frustrated spin systems have attracted widespread interest because very rich physics can appear in these systems. For example, amusing magnetization plateaus in the triangular spin-chain system $Ca_3Co_2O_6$[2,3] and Shastry–Sutherland (S–S) magnets have been observed.[4,5]

The S–S lattice, shown in Fig. 1, was introduced by Shastry and Sutherland as an example of a frustrated quantum mechanical antiferromagnetic (AFM) model with an exact ground state in as early as 1981.[6] Its experimental realization in $SrCu_2(BO_3)_2$ with Cu^{2+} ions carrying a quantum spin 1/2 and located on a two dimensional S–S lattice was identified in 1991.[7] The fascinating sequence of magnetization (M) plateaus at fractional values of the saturated magnetization (M_0) in $SrCu_2(BO_3)_2$ has been widely studied, both experimentally and theoretically.[8–12] On the other hand, rare earth tetraborides RB_4 with R = Tb, Dy, Ho, Tm, etc., as another representative of S–S magnets, are drawing more attention.[13–17] The rare earth moments in these compounds are located on a lattice, which is topologically equivalent to the S–S lattice. In contrast to $SrCu_2(BO_3)_2$, RB_4 presents a large total magnetic moment; thus, it can be considered a classical spin system. Similarly, RB_4 has a complex magnetic structure and exhibits puzzling magnetization plateaus at a low temperature. For example, magnetization plateaus at $M/M_0 = 1/7$, 1/8, 1/9, etc., have been reported at temperatures (T) below ~4K in TmB_4[16] and several theoretical works that explain this interesting phenomenon are available.

Experimental results indicate that TmB_4 is of strong easy-axis anisotropy caused by crystal field effects. Based on this property, the magnetization of the classical AFM Ising model on the S–S lattice was studied by Chang and Yang using the tensor renormalization-group approach.[18] A single magnetization plateau at $M/M_0 = 1/3$ is predicted in certain temperature range and coupling constant. Moliner *et al* investigated the magnetic properties of the classical Heisenberg model on the S–S lattice by using Monte Carlo simulations.[19] Magnetization pseudoplateaus around $M/M_0 = 1/3$ were observed for a range of magnetic coupling. However, the magnetization process for TmB_4 has not been completely understood until now. In the Heisenberg model, the easy-axis anisotropy is ignored while in the Ising limit, the anisotropy is emphasized. To some extent, the uniaxially anisotropic Heisenberg model seems to be a sound choice for the description of TmB_4. A systemic study of the impact of the anisotropy on the magnetic structure may be helpful to understand the experimental results. On the other hand, the inhomogeneity of frustrated spin systems may have a notable effect on the magnetic behaviors, as stated in earlier experimental and theoretical works.[20–22] For example, it has been

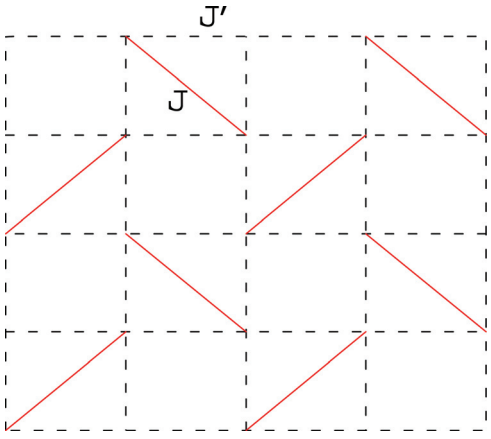

FIG. 1. (Color online) The Shastry–Sutherland lattice. J' bonds (black dashed line) are the exchange coupling along the edges of the squares, and J bonds (red solid lines) are the diagonal dimer couplings.

a)Author to whom correspondence should be addressed. Electronic mail: liujm@nju.edu.cn.

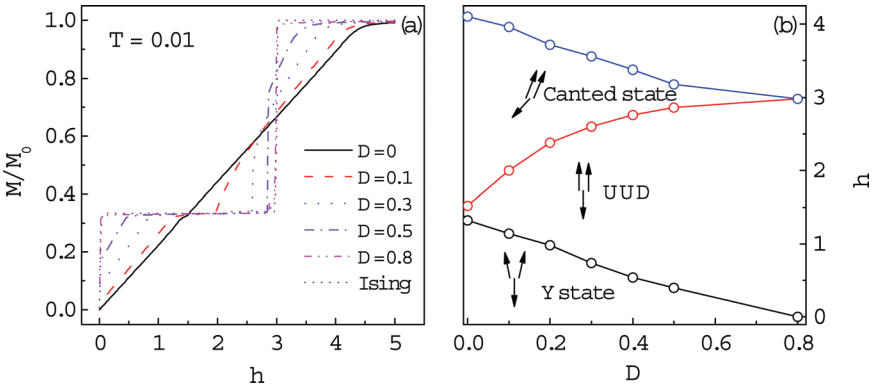

FIG. 2. (Color online) At $T=0.01$, (a) magnetization curves for different D and the Ising limit, (b) phase diagram of the classical Heisenberg model in the h-D plane.

proved in our earlier work that the distinct steplike magnetization behavior in $Ca_3Co_2O_6$ at low T range can be observed only when the inhomogeneity is in an appropriate range. This argument may also apply to S–S magnets.

In this work, the influence of the easy-axis anisotropy on the magnetization process in the classical Heisenberg model on the S–S lattice is investigated with the Monte Carlo method. It is indicated that the magnetization-step at $M/M_0=1/3$ is broadened due to the implementation of easy-axis anisotropy. The simulated results indicate that the multi-step magnetic behaviors at low T can be observed in a proper range of the inhomogeneity.

First, we study a classical Heisenberg model with easy-axis anisotropy on the S–S lattice. The Hamiltonian can be written as follows:

$$H=J'\sum_{edges} S_i\cdot S_j+J\sum_{diagonal} S_i\cdot S_j-h\sum_i S_i^z-D\sum_i (S_i^z)^2, \quad (1)$$

where the exchange coupling $J'=1/2$, $J=1$, S_i represents the Heisenberg spin with unit length on site i, h is the external magnetic field applied along the $+z$ axis, S_i^z denotes the z component of S_i, D is the uniaxial anisotropy constant (z axis as the easy axis), and the Boltzmann constant is set to unity. Here $J'/J=1/2$ is chosen for comparison with the earlier work.[18] It is noted that for $D=0$, the system is reduced to the isotropic Heisenberg model. For $D\to\infty$, it is the Ising model. The simulation is performed on an $L\times L$ ($L=24$) S–S lattice with period boundary conditions using the standard Metropolis algorithm.[23]

In Fig. 2(a), the simulated $M(h)$ curves at $T=0.01$ for different D are presented. The result of the Ising limit is also given for comparison. At $D=0$, the $M(h)$ curve exhibits a vague plateau at $M/M_0=1/3$, which is caused by the entropic selection of a particular collinear state in which each triangle contains two up-spins and one down-spin (UUD), as shown in Fig. 3(a). When D is increased, the magnetization step at $M/M_0=1/3$ is gradually broadened. When D increases to the value of 0.8, the system exhibits the magnetic behavior of the Ising model, as shown in Fig. 2(a). The phase diagram in the h-D plane at $T=0.01$ is shown in Fig. 2(b). The transition points in the diagram are estimated from the positions of the peaks in the susceptibility $\chi=dM/dh$, following the earlier work.[19] It is clearly shown that as D increases, both the Y state in the low-h region and the canted state in the high-h region gradually translate to the collinear UUD state. The enlargement of the range of the UUD state leads to the broadening of the magnetizationstep at $M/M_0=1/3$. In the Ising limit, the transition from the plateau at $M/M_0=1/3$ to the plateau at $M/M_0=1$ corresponds with the transition from the collinear UUD state to the ferromagnetic state. The down-spin may flip as the static magnetic energy increases to be comparable with the interaction energy. The critical field can be estimated to be $h=4J'+J=3$. This argument is verified in our simulated results.

The simulated $M(h)$ curves at different T under $D=0.3$ are shown in Fig. 3(b). The collinear UUD state is gradually destroyed due to the thermal fluctuations as the increase of T, leading to the melting of the magnetization-step at $M/M_0=1/3$. When T is raised to about 0.2, the $M_0/3$ plateau

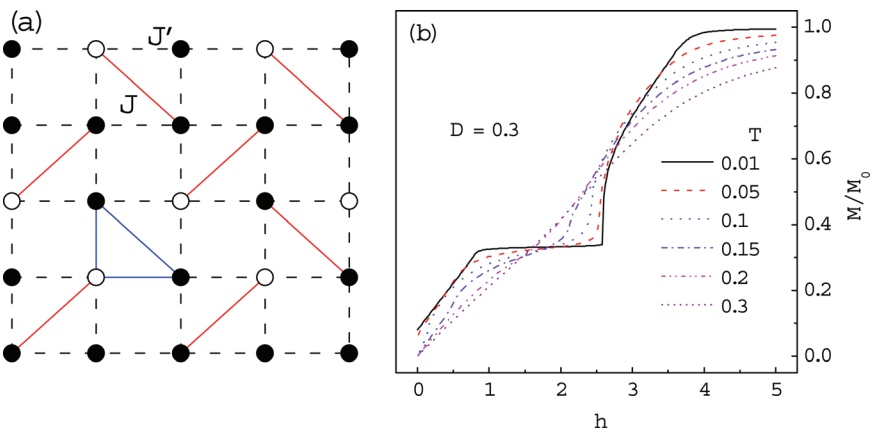

FIG. 3. (Color online) (a) Spin configuration for the UUD state. Each triangle contains two up-spins and one down-spin. One example of the triangle is shown with blue solid lines. The black solid circles represent up-spins and the white solid circles represent down-spins. (b) Magnetization curves for different T at $D=0.3$.

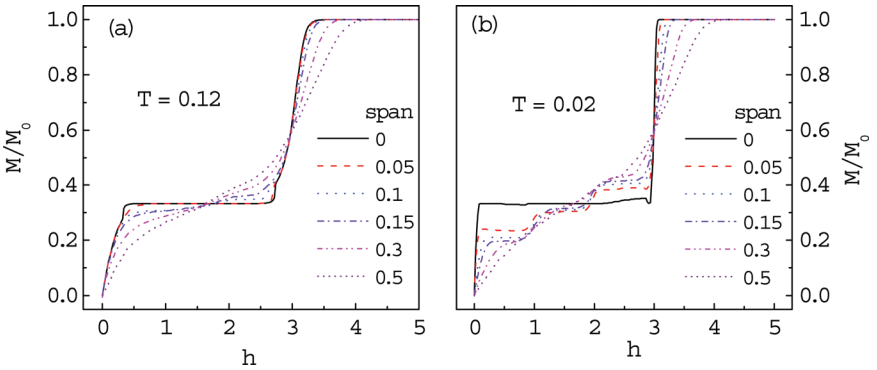

FIG. 4. (Color online) Magnetization curves for different *span* values at (a) $T=0.12$ and (b) $T=0.02$.

completely disappears and the system exhibits the paramagnetic behavior that M linearly increases with h.

In the Ising limit, the inhomogeneity of frustrated systems may have a notable effect on the magnetic behaviors. In this section, we study the role of the inhomogeneity of the classical Ising system on the S–S lattice with a random field method. The Hamiltonian can be expressed as

$$H = J' \sum_{edges} (1+\Delta_{i,j}) S_i \cdot S_j + J \sum_{diagonal} (1+\Delta_{i,j}) S_i \cdot S_j - h \sum_i S_i, \quad (2)$$

with

$$\Delta_{i,j} = span \cdot RAM_{i,j},$$

where S_i is the Ising spin with the value ± 1, $RAM_{i,j}$ is the random number in $[-1, 1]$, and *span* represents the magnitude of random exchange term, the values of J' and J are the same as those in Sec. II. The Monte Carlo simulation is performed on a 60×60 S–S lattice with period boundary conditions.

Figures 4(a) and 4(b), respectively, show the simulated $M(h)$ curves under different *spans* at $T=0.12$ and $T=0.02$. At $T=0.12$, the system without any random exchange term ($span=0$) exhibits the perfect $M_0/3$ plateau. The plateau gradually melts when the *span* is increased. When the *span* is increased to 0.3, the plateau disappears and a progressive-growth of M with increasing h is observed, as shown in Fig. 4(a). The single $M_0/3$ plateau under $span=0$ is stable even at $T=0.02$. However, the system with a small *span* (0.05) can exhibit an evident multi-step magnetic behavior. As the *span* increases, the M gaps between neighboring steps can be enhanced while the borders of the substeps are smoothed down. Below $h \approx 3$, the $M(h)$ curve shows three substeps occurring at about a regular field interval $\Delta h \approx 1$ under $span=0.15$. Similar behavior has been observed in the triangular Ising spin-chain system, as stated in our earlier work.[21,22] Eventually, these substeps are smeared out when the random exchange is very large ($span=0.5$).

The simulated results can be qualitatively explained from the point of spin configurations. At $span=0$, the UUD ordering is dominant below $h \approx 3$, leading to the single $M_0/3$ plateau. However, the random term enhances the fluctuations of the spin alignment, destroying the perfect UUD order and resulting in the local disordering. The existence of these spin patterns leads to the generation of the obvious substeps in the low T range. Finally, the disordering effect is prominent at $span=0.5$, leading to the disappearance of the substeps.

It is noted that the inhomogeneity of the S–S system has an important effect on the steplike magnetization feature in this work. However, a complete understanding of the magnetization process for S–S magnets remains to be an issue.

This work was supported by the Natural Science Foundation of China (50832002, 51031004, 10874075) and the National Key Projects for Basic Research of China (2011CB922101, 2009CB929501).

[1] H. T. Diep, *Frustrated Spin Systems* (World Scientific, Singapore, 2004).
[2] H. Kageyama, K. Yoshimura, K. Kosuge, M. Azuma, M. Takano, H. Mitamura, and T. Goto, J. Phys. Soc. Jpn. **66**, 3996 (1997).
[3] V. Hardy, M. R. Lees, O. A. Petrenko, D. M. K. Paul, D. Flahaut, S. Hebert, and A. Maignan, Phys. Rev. B **70**, 064424 (2004).
[4] H. Kageyama, K. Yoshimura, R. Stern, N. V. Mushnikov, K. Onizuka, M. Kato, K. Kosuge, C. P. Slichter, T. Goto, and Y. Ueda, Phys. Rev. Lett. **82**, 3168 (1999).
[5] K. Kodama, M. Takigawa, M. Horvatic, C. Berthier, H. Kageyama, Y. Ueda, S. Miyahara, F. Becca, and F. Mila, Science **298**, 395 (2002).
[6] B. S. Shastry and B. Sutherland, Physica B & C **108**, 1069 (1981).
[7] R. W. Smith and D. A. Keszler, J. Solid State Chem. **93**, 430 (1991).
[8] S. Miyahara and K. Ueda, J. Phys. Condens. Matter **15**, R327 (2003).
[9] A. Abendschein and S. Capponi, Phys. Rev. Lett. **101**, 227201 (2008).
[10] J. Dorier, K. P. Schmidt, and F. Mila, Phys. Rev. Lett. **101**, 250402 (2008).
[11] L. Isaev, G. Ortiz, and J. Dukelsky, Phys. Rev. Lett. **103**, 177201 (2009).
[12] J. Alicea, A. V. Chubukov, and O. A. Starykh, Phys. Rev. Lett. **102**, 137201 (2009).
[13] Z. Fisk, M. B. Maple, D. C. Johnston, and L. D. Woolf, Solid State Commun. **39**, 1189 (1981).
[14] R. Watanuki, G. Sato, K. Suzuki, M. Ishihara, T. Yanagisawa, Y. Nemoto, and T. Goto, J. Phys. Soc. Jpn. **74**, 2169 (2005).
[15] S. Michimura, A. Shigekawa, F. Iga, M. Sera, T. Takabatake, K. Ohoyama, and Y. Okabe, Physica B: Condensed Matter **378**, 596 (2006).
[16] K. Siemensmeyer, E. Wulf, H. J. Mikeska, K. Flachbart, S. Gabani, S. Matas, P. Priputen, A. Efdokimova, and N. Shitsevalova, Phys. Rev. Lett. **101**, 177201 (2008).
[17] S. Yoshii, T. Yamamoto, M. Hagiwara, S. Michimura, A. Shigekawa, F. Iga, T. Takabatake, and K. Kindo, Phys. Rev. Lett. **101**, 087202 (2008).
[18] M. C. Chang and M. F. Yang, Phys. Rev. B **79**, 104411 (2009).
[19] M. Moliner, D. C. Cabra, A. Honecker, P. Pujol, and F. Stauffer, Phys. Rev. B **79**, 144401 (2009).
[20] D. Flahaut, A. Maignan, S. Hebert, C. Martin, R. Retoux, and V. Hardy, Phys. Rev. B **70**, 094418 (2004).
[21] X. Y. Yao, S. Dong, and J.-M. Liu, Phys. Rev. B **73**, 212415 (2006).
[22] X. Y. Yao, S. Dong, H. Yu, and J.-M. Liu, Phys. Rev. B **74**, 134421 (2006).
[23] D. P. Landau and K. Binder, *A Guide to Monte Carlo Simulations in Statistical Physics* (Cambridge Univeristy Press, Cambridge, 2008).

AIP | Applied Physics Letters

Multiferroic phase competitions in perovskite manganite thin films

M. H. Qin, Y. M. Tao, M. Zeng, X. S. Gao, S. J. Wu et al.

Citation: Appl. Phys. Lett. **100**, 052410 (2012); doi: 10.1063/1.3682079
View online: http://dx.doi.org/10.1063/1.3682079
View Table of Contents: http://apl.aip.org/resource/1/APPLAB/v100/i5
Published by the American Institute of Physics.

Multiferroic phase competitions in perovskite manganite thin films

M. H. Qin,[1] Y. M. Tao,[2] M. Zeng,[1] X. S. Gao,[1] S. J. Wu,[1] S. Dong,[3] and J.-M. Liu[2,4,a)]
[1]*Institute of Advanced Materials, School of Physics, South China Normal University, Guangzhou 510006, China*
[2]*Laboratory of Solid State Microstructures, Nanjing University, Nanjing 210093, China*
[3]*Department of Physics, Southeast University, Nanjing 211189, China*
[4]*International Center for Materials Physics, Chinese Academy of Science, Shenyang 110016, China*

(Received 13 September 2011; accepted 15 January 2012; published online 3 February 2012)

Based on the Mochizuki-Furukawa model, the cycloidal spin structures of orthorhombic $R\mathrm{MnO_3}$ manganite thin films on various magnetic substrates are simulated using Monte Carlo method. It is revealed that the long range cycloidal spin order can be modulated by the film thickness and substrate spin structure. In particular, the ferromagnetic and antiferromagnetic spin orders of the substrate in different orientations have different pinning effects on the cycloidal spin order of the thin film. The simulated results are discussed in terms of the competition between the single-ion anisotropy and spin-orbit coupling. © *2012 American Institute of Physics*. [doi:10.1063/1.3682079]

Multiferroicity is attracting continuous attentions due to the interesting physics and potential applications.[1–4] Especially, type-II multiferroics, such as cycloidal magnets, orthorhombic manganites $R\mathrm{MnO_3}$ (R = Tb, Dy, $\mathrm{Eu_{1-x}Y_x}$, etc.),[5–7] $\mathrm{Ni_3V_2O_8}$,[8] and $\mathrm{MnWO_4}$,[9] have been addressed due to the unusual fact that the ferroelectricity is generated by frustrated spin orders. The spin current theory and the inverse Dzyaloshinskii-Moriya (DM) interaction model were proposed in order to understand the underlying microscopic mechanism.[10–12] It is believed that the spin-orbit coupling for two adjacent spins S_i and S_j separated by vector r_{ij} can generate a local polarization $P_{ij} \propto -r_{ij} \times (S_i \times S_j)$. Thus, a macroscopic ferroelectric (FE) polarization P can be induced because spin-helicity vector h defined as $S_i \times S_j$ is associated with a ferroic alignment. Taking orthorhombic manganites $R\mathrm{MnO_3}$ as examples, polarization P along the a-axis is induced in the ab-plane cycloidal spin (ab-CS) phase with propagation vector Q along the b-axis, while it is induced along the c-axis in the bc-plane cycloidal spin (bc-CS) phase, as illustrated in Figs. 1(a) and 1(b). In addition, several theoretical works on the origin for the CS order and magnetoelectric (ME) coupling in $R\mathrm{MnO_3}$ are available.[13,14]

Recently, Mochizuki and Furukawa proposed a classical Heisenberg spin model (M-F model) which includes the superexchange interaction, the single-ion anisotropy (SIA), the DM interaction, and the cubic anisotropy, to study the phase diagrams of $R\mathrm{MnO_3}$.[14] The ab-CS state is stabilized by the SIA and the DM interaction with vectors on the in-plane Mn-O-Mn bonds, while the bc-CS state is stabilized by the DM interaction with vectors on the out-of-plane Mn-O-Mn bonds. The R-site ionic radius mainly controls the lattice distortion which tunes the SIA and the DM interaction, thus in turn determines the competition between the ab-CS phase and bc-CS phase. This leads to the flop of the cycloidal plane from the ab-plane to the bc-plane with decreasing R-ion radius. It has been demonstrated that this model can explain the complicated multiferroic behaviors.[15–20]

While the physics of multiferroics is being progressively understood, researches proceed in related device designs where multiferroic thin films are expected to play an important role.[21,22] Understanding of the phase competitions in multiferroic thin films certainly becomes interested not only from the point of view of the physics responsible for multiferroic spin orders in this specific geometry, but more for insight in the design of advanced devices. However, so far rare work along this line is available and one of the main issues is that measurement of polarization in those type-II multiferroic thin films remains unsuccessful, while relevant theoretical progress is under the way. In this work, we address the multiferroic behaviors of a model orthorhombic $R\mathrm{MnO_3}$ thin film deposited epitaxially on a substrate by theoretical simulation. For simplicity, we focus on the impact of

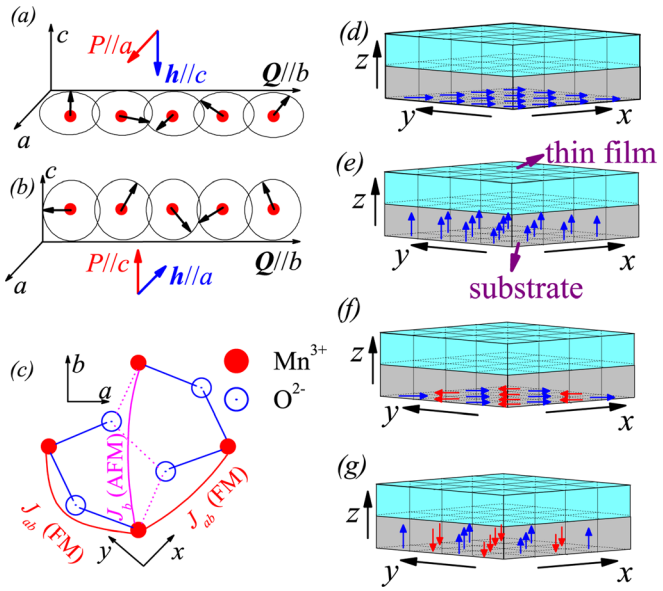

FIG. 1. (Color online) Induced electric polarization P and spin-helicity vector $h = \Sigma_{ij} S_i \times S_j$ in (a) the ab-CS and (b) bc-CS states. (c) Crystal structure (ab-plane) of orthorhombically distorted $R\mathrm{MnO_3}$. Sketch of thin film (top turquoise layer) grown on the magnetic substrate (bottom grey layer) in which all spins are fixed to the FM pattern with (d) $S_s//a$ and (e) $S_s//c$, and to the AFM pattern with (f) $S_s//a$ and (g) $S_s//c$.

a)Author to whom correspondence should be addressed. Electronic mail: liujm@nju.edu.cn.

thin film thickness and substrate magnetic structure, while the lattice mismatch between the substrate and thin films is ignored at this stage. For the magnetic structure of the substrate, we limit our discussion on three types of substrates: (1) without magnetism, (2) of simple ferromagnetic (FM) order, and (3) of antiferromagnetic (AFM) order. In the latter two cases, the spin alignments of the substrate along various orientations (spin moment $S_s = 2$) are fixed as shown in Figs. 1(d)–1(g), implying that the spin interaction in the substrate is no exception much stronger than that in the thin film so that the bottom layer of the thin film is pinned off.

In our simulation, the M-F model with Mn spin $S = 2$ on a cuboidal lattice is used.[14] The Hamiltonian can be written as $H = H_{ex} + H_{sia} + H_{DM} + H_{cub}$. The first term $H_{ex} = \Sigma_{\langle ij \rangle} J_{ij} \cdot (S_i \cdot S_j)$ is the spin exchange interactions with $J_{ab} = -0.8$ and $J_b = 0.8$ the coupling constants in the Mn-Mn bonds on the *ab*-plane (Fig. 1(c)), $J_c = 1.25$ the AFM exchange in the bonds along the *c*-(z-) axis. Here, the energy unit is meV. The second term is the SIA term $H_{sia} = D \cdot \Sigma_i S^i_{\zeta i} + E \cdot \Sigma_i (-1)^{ix+iy} \cdot (S^i_{\xi i} - S^i_{\eta i})$ with $D = 0.25$, $E = 0.30$, here, ξ_i, η_i, ζ_i are the tilted local axes attached to the *i*-th MnO_6 octahedron.[14] For their direction vectors, we use experimental data of $EuMnO_3$ for simplicity.[23] The third term H_{DM} denotes the DM interactions $H_{DM} = \Sigma_{\langle ij \rangle} d_{i,j} \cdot (S_i \times S_j)$, where factors $d_{i,j}$ are determined by five DM parameters, $(\alpha_{ab}, \beta_{ab}, \gamma_{ab}) = (0.10, 0.10, 0.14)$ and $(\alpha_c, \beta_c) = (0.30, 0.30)$. The last term $H_{cub} = A \cdot \Sigma_i (S^4_{xi} + S^4_{yi} + S^4_{zi})/S(S+1)$ represents the cubic anisotropy with coupling constant $A = 0.0162$.

The thin film is considered to be a three-dimensional (3D) half-infinite cuboidal lattice, e.g., infinite in the *x* and *y* directions, but finite in the *z* direction. The periodic boundary conditions are applied in the *x*- and *y*-axis directions, and the free boundary condition is applied onto the top layer along the *z* direction. The spins in the bottom layer are coupled with the spins of the substrate. Our simulation is performed on a $36 \times 36 \times L_z$ (unless stated elsewhere, $L_z = 6$ is chosen, and in fact the results for $L_z > 6$ show no much difference) cuboidal lattice using standard Metropolis algorithm and temperature exchange method.[24,25] Specific heat $C(T) = (\langle H^2 \rangle - \langle H \rangle^2)/Nk_BT^2$ and spin-helicity vector $h_\gamma(T) = \langle |\Sigma_i S_i \times S_{i+b}| \rangle / NS^2$ ($\gamma = a, b, c$) as a function of temperature (T) are calculated to determine the transition points and spin structure, here N is the number of Mn ions, k_B is the Boltzmann constant, and the brackets denote thermal and configuration averaging. It is expected that $h_c(h_a)$ has a large value for the *ab*-CS (*bc*-CS) order, while all of these three components of h_γ should be zero in the paramagnetic (PM) phase and sinusoidal collinear antiferromagnetic (sc-AFM) phase.

As a comparison, Fig. 2(a) shows the simulated $C(T)$ and $h_\gamma(T)$ for bulk case. The $C(T)$ curve shows three peaks, indicating successive three phase transitions with decreasing T. The first one is the transition from the PM phase to the sc-AFM phase at T_N. At the second transition point T_{bc}, $h_a(T)$ increases, indicating a transition of the sc-AFM phase to the *bc*-CS phase. When T falls down to the third transition point T_{ab}, $h_a(T)$ suddenly drops, accompanied with a steep increase of $h_c(T)$, indicating a transition from the *bc*-CS order to the *ab*-CS order.

Looking at the simulated data for the thin film on a non-magnetic substrate ($S_s = 0$) allows an investigation of the

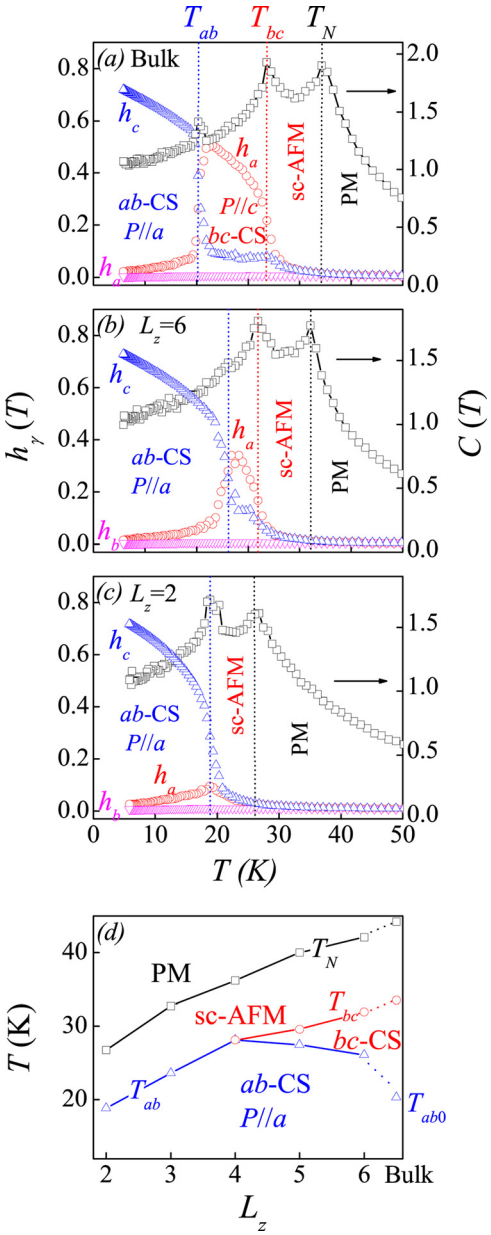

FIG. 2. (Color online) Specific heat $C(T)$ and spin-helicity vector $h_\gamma(T)$ ($\gamma = a, b, c$) as a function of T in (a) the bulk system, and in thin films with (b) $L_z = 6$, (c) $L_z = 2$. (d) The phase diagram in the (L_z, T) plane.

effect of the thin film thickness. The simulated results with $L_z = 6$ are shown in Fig. 2(b). Point T_N is slightly lower than that for the bulk case. What is interested is the enhanced T_{ab}, implying that the *bc*-CS order is suppressed in compensation with the promoted stability of the *ab*-CS order. This tendency continues upon further decreasing of L_z till the *bc*-CS phase is completely suppressed, leaving the *ab*-CS phase at low T side.

The disappearance of the *bc*-CS phase with decreasing thin film thickness is easily understood at the first glance. The DM interaction with vectors on the out-of-plane Mn-O-Mn bonds stabilizes the *bc*-CS order. In case of no DM interaction, the angles between the nearest two spins along the *c*-axis are $\phi_c = \pi$, due to the strong AFM coupling J_c. Inclusion of the DM interaction allows the angles to be alternatively modulated as $(\pi - \Delta\phi_c)$ and $(\pi + \Delta\phi_c)$ with $\Delta\phi_c > 0$. The energy gain from the DM interaction, due to

this modulation, is $\Delta E_{DM}/N = -\alpha_c S^2 |\cos\phi_c| \Delta\phi_c = -\alpha_c S^2 \Delta\phi_c$ with α_c the magnitude of the *a*-component of the DM vectors on the out-of-plane bonds. This energy gain is reduced with the film thickness since the spins on the up and bottom layers lack of this contribution, leading to the destabilization of the *bc*-CS phase.

On the other hand, the *ab*-CS order which is mainly stabilized by the SIA, less relevant with the DM interaction with vectors on the in-plane Mn-O-Mn bonds. As a result, the *ab*-CS phase is enhanced in energy with respect to the *bc*-CS phase. Both T_N and T_{bc} shift seriously downward with decreasing film thickness and as an extreme case with $L_z = 2$, shown in Fig. 2(c), T_{bc} disappears, leaving only the *ab*-CS phase at low-*T* side. What should be mentioned is that upon decreasing film thickness, T_{ab} first increases from the value (T_{ab0}) for the bulk case, and then decreases down to T_{ab0} at $L_z = 2$. This indicates that the sc-AFM order and *bc*-CS order are strongly suppressed, while the *ab*-CS order at low *T* remains quite robust. Because the *ab*-CS order is mainly determined by the *ab*-plane spin interaction, the present results are easily understood.

As a summary, we present the simulated phase diagram in the (L_z, *T*) plane of the spin structure in Fig. 2(d), from which the remarkable film-thickness dependence of the spin structure including the ferroelectric CS order is clearly shown. In fact, similar phenomenon was observed in earlier work in which the spiral spin structure in bulk $TbMnO_3$ can be intensively suppressed in epitaxially strained thin film form.[26]

Subsequently, one comes to look at the impact of the spin structure from the substrate. For a FM substrate with the spins aligning along either the *a*-axis or *c*-axis (in-plane or out-of-plane), Figs. 3(a) and 3(b) show the simulated results. It is clearly shown that the *ab*-CS order and *bc*-CS order are suppressed completely respectively for the in-plane and out-of-plane cases, while the sc-AFM order remains nearly unaffected.

To some extent, the effect of the FM substrate with $S_s//a$ ($S_s//c$) is similar to that of the applied magnetic filed $B//a$ ($B//c$) onto the bottom layer because of the strong AFM coupling J_c. Meanwhile, *B* tends to align the spins in perpendicular to *B* for a cycloidal spin system. As a result, the *bc*-CS (*ab*-CS) order is stabilized in the bottom layer, and in turn be extended to the whole film system to satisfy the energy relation for the case of the FM substrate with $S_s//a$ ($S_s//c$). In addition, it is noted that T_N for the two cases are almost identical, indicating that the transition from the PM phase to the sc-AFM order is mainly determined by the lattice size of the film.

At last, the effect of the AFM substrate on multiferroic properties is studied. It is indicated that the *ab*-CS order is enhanced for the case of the AFM substrate with $S_s//a$, as shown in Fig. 3(c). Being different from the FM substrate, the AFM one with $S_s//a$ tends to align the spins of the bottom layer in the *ab*-plane to satisfy the AFM coupling J_c. At the same time, the DM interaction with vectors on the in-plane bonds and the SIA stabilize the *ab*-CS order. This leads to the flop of the cycloidal plane from the *bc*-plane to the *ab*-plane. On the other hand, the AFM substrate with $S_s//c$ may enlarge the *T* region with the *bc*-CS order. This argument has been proved in our simulated results, as shown in Fig. 3(d). The transition from the *bc*-CS order to the *ab*-CS order in the pinning system occurs at a much lower *T* than that in non-pinning system (Fig. 2(b)), demonstrating that the *ab*-CS order is extensively suppressed for this case.

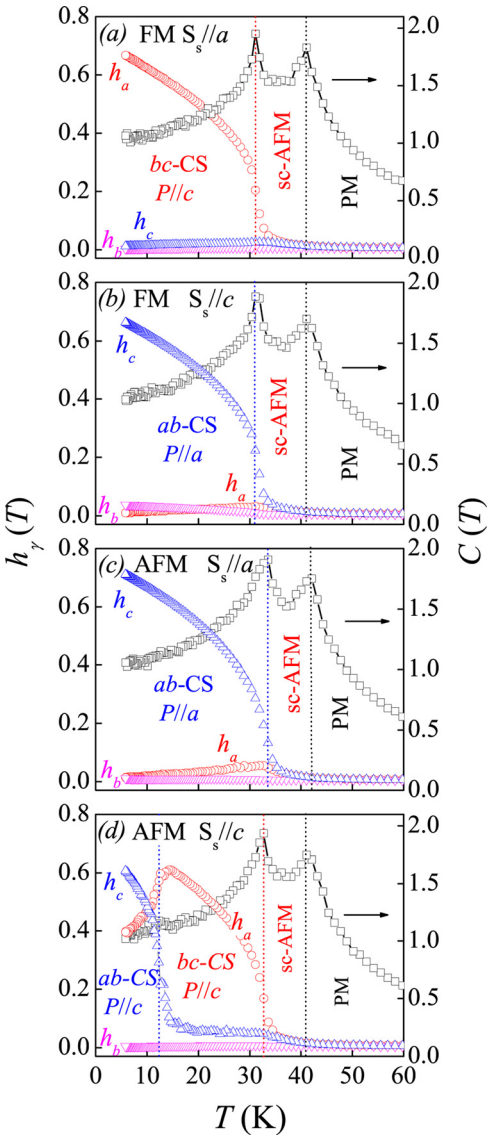

FIG. 3. (Color online) Specific heat $C(T)$ and spin-helicity vector $h_\gamma(T)$ ($\gamma = a, b, c$) as a function of *T* in thin film grown on the FM pinning substrate (a) with $S_s//a$, and (b) with $S_s//c$, and the AFM pinning substrate (a) with $S_s//a$, and (b) with $S_s//c$.

Up to now, there is an urgent need in studying multiferroic film to develop a better understanding of the evolution of ME properties in the special geometries. In this work, the multiferroic properties in orthorhombic manganites film are studied based on the M-F model. It is demonstrated that the long range cycloidal orders can be significantly modulated by the film thickness and substrate spin structure. In addition, our simulation indicates that the magnetic substrate may have a significantly pinning effect on the multiferroic behaviors in film systems. The simulated results are discussed from the energy landscape in details. Our simulation is helpful to understand the phase competitions, and provides useful information for practical applications of $RMnO_3$ film. Of course, the prediction given here deserves to be checked in further experiments.

This work was supported by the Natural Science Foundation of China (50832002, 51072061, and 51031004), the National Key Projects for Basic Researches of China (2009CB623303 and 2009CB929501), the China Postdoctoral Science Foundation (20100480768), and the Priority Academic Program Development of Jiangsu Higher Education Institutions, China.

[1]M. Fiebig, J. Phys. D **38**, R123 (2005).
[2]W. Eerenstein, N. D. Mathur, and J. F. Scott, Nature **442**, 759 (2006).
[3]S.-W. Cheong and M. Mostovoy, Nature Mater. **6**, 13 (2007).
[4]K. F. Wang, J.-M. Liu, and Z. F. Ren, Adv. Phys. **58**, 321 (2009).
[5]T. Kimura, T. Goto, H. Shintani, K. Ishizaka, T. Arima, and Y. Tokura, Nature **426**, 55 (2003).
[6]T. Goto, T. Kimura, G. Lawes, A. P. Ramirez, and Y. Tokura, Phys. Rev. Lett. **92**, 257201 (2004).
[7]J. Hemberger, F. Schrettle, A. Pimenov, P. Lunkenheimer, V. Y. Ivanov, A. A. Mukhin, A. M. Balbashov, and A. Loidl, Phys. Rev. B **75**, 035118 (2007).
[8]G. Lawes, A. B. Harris, T. Kimura, N. Rogado, R. J. Cava, A. Aharony, O. Entin-Wohlman, T. Yildirim, M. Kenzelmann, C. Broholm *et al*., Phys. Rev. Lett. **95**, 087205 (2005).
[9]K. Taniguchi, N. Abe, T. Takenobu, Y. Iwasa, and T. Arima, Phys. Rev. Lett. **97**, 097203 (2006).
[10]H. Katsura, N. Nagaosa, and A. V. Balatsky, Phys. Rev. Lett. **95**, 057205 (2005).
[11]M. Mostovoy, Phys. Rev. Lett. **96**, 067601 (2006).
[12]I. A. Sergienko and E. Dagotto, Phys. Rev. B **73**, 094434 (2006).
[13]S. Dong, R. Yu, S. Yunoki, J.-M. Liu, and E. Dagotto, Phys. Rev. B **78**, 155121 (2008).
[14]M. Mochizuki and N. Furukawa, Phys. Rev. B **80**, 134416 (2009).
[15]M. Mochizuki and N. Furukawa, Phys. Rev. Lett. **105**, 187601 (2010).
[16]M. Mochizuki, N. Furukawa, and N. Nagaosa, Phys. Rev. Lett. **104**, 177206 (2010).
[17]M. Mochizuki and N. Nagaosa, Phys. Rev. Lett. **105**, 147202 (2010).
[18]M. Mochizuki, N. Furukawa, and N. Nagaosa, Phys. Rev. Lett. **105**, 037205 (2010).
[19]M. H. Qin, Y. M. Tao, S. Dong, H. B. Zhao, X. S. Gao, and J.-M. Liu, Appl. Phys. Lett. **98**, 102510 (2011).
[20]Y. M. Tao, M. H. Qin, S. Dong, X. S. Gao, and J.-M. Liu, J. Appl. Phys. **109**, 113909 (2011).
[21]G. Lawes and G. Srinivasan, J. Phys. D: Appl. Phys. **44**, 243001 (2011).
[22]L. W. Martin, Y. H. Chu, and R. Ramesh, Mater. Sci. Eng. R **68**, 89 (2010).
[23]B. Dabrowski, S. Kolensnik, A. Baszczuk, O. Chmaissem, T. Maxwell, and J. Mais, J. Solid State Chem. **178**, 629 (2005).
[24]D. P. Landau and K. Binder, *A Guide to Monte Carlo Simulations in Statistical Physics* (Cambridge University Press, Cambridge, England, 2005).
[25]K. Hukushima and K. Nemoto, J. Phys. Soc. Jpn. **65**, 1604 (1996).
[26]C. J. M. Daumont, D. Mannix, S. Venkatesan, G. Catalan, D. Rubi, B. J. Kooi, J. Th. M. De Hosson, and B. Noheda, J. Phys.: Condens. Matter **21**, 182001 (2009).

Multiferroic properties in orthorhombic perovskite manganites: Monte Carlo simulation

M. H. Qin, Y. M. Tao, S. Dong, M. Zeng, S. J. Wu et al.

Citation: J. Appl. Phys. **111**, 053907 (2012); doi: 10.1063/1.3689162
View online: http://dx.doi.org/10.1063/1.3689162
View Table of Contents: http://jap.aip.org/resource/1/JAPIAU/v111/i5
Published by the American Institute of Physics.

Multiferroic properties in orthorhombic perovskite manganites: Monte Carlo simulation

M. H. Qin,[1,a)] Y. M. Tao,[2] S. Dong,[3] M. Zeng,[1] S. J. Wu,[1] H. B. Zhao,[1] X. S. Gao[1] and J.-M. Liu[2,4,a)]
[1]*Institute of Advanced Materials, School of Physics and Telecommunication Engineering, South China Normal University, Guangzhou 510006, China*
[2]*Laboratory of Solid State Microstructures, Nanjing University, Nanjing 210093, China*
[3]*Department of Physics, Southeast University, Nanjing 211189, China*
[4]*International Center for Materials Physics, Chinese Academy of Science, Shenyang 110016, China*

(Received 18 September 2011; accepted 24 January 2012; published online 2 March 2012)

In this work, a random field method (based on Mochizuki-Furukawa model) is used to study the effect of the *R*-site ionic disorder and inhomogeneity on the multiferroic behavior in orthorhombic manganites. It is shown that both the *R*-site ionic disorder and inhomogeneity can drive the reorientation of the plane in which cycloidal spin order takes place and actually lead to the flop of the spins from the *ab*-plane to the *bc*-plane. The simulated results can be understood as the consequence of the competition between exchange interactions and spin-orbit coupling. © *2012 American Institute of Physics*. [http://dx.doi.org/10.1063/1.3689162]

I. INTRODUCTION

In the past few years, multiferroics have been attracting continuous attentions due to their interesting physics and potential applications for new spintronic devices.[1–4] Especially, multiferroicity has been found in a series of cycloidal magnets such as $R\mathrm{MnO_3}$ (R = Tb, Dy, $\mathrm{Eu_{1-x}Y_x}$, etc.),[5–7] $\mathrm{Ni_3V_2O_8}$,[8] and $\mathrm{MnWO_4}$.[9] It is well established that the ferroelectric polarization (P) in these materials is induced by cycloidal magnetic orders through the inverse Dzyaloshinskii-Moriya (DM) interaction (alternatively the spin current model).[10–12] Based on the spin current scenario, adjacent two spins (S_i, S_j) can generate a local polarization as:

$$P_{ij} \propto -e_{ij} \times \left(S_i \times S_j\right), \tag{1}$$

with e_{ij} being the vector connecting the two sites. With decreasing *R*-site ionic radius in $R\mathrm{MnO_3}$, for instance, a transition from the *ab*-plane cycloidal spin (*ab*-CS) phase with the propagation vector $\boldsymbol{Q}$ along the *b*-axis to the *bc*-plane cycloidal spin (*bc*-CS) phase was observed at low temperature (T).[13] Thus, P is induced along the *a*-axis in the *ab*-CS phase, while it is along the *c*-axis in the *bc*-CS phase, as illustrated in Figs. 1(a) and 1(b).

In addition, the origin of multiferroic CS orders in $R\mathrm{MnO_3}$ has also been studied recently.[14,15] A microscopic spin model (Mochizuki-Furukawa model) which included the superexchange interaction, the single-ion anisotropy (SIA), the DM interaction, and the cubic anisotropy, was proposed and this model well reproduced the experimental phase diagrams of $R\mathrm{MnO_3}$.[15] It has been demonstrated that the *ab*-CS state is stabilized by the SIA and the DM interaction with vectors on the in-plane Mn-O-Mn bonds, while the *bc*-CS state is stabilized by the DM interaction with vectors on the out-of-plane Mn-O-Mn bonds. Moreover, several other experimental phenomena in $R\mathrm{MnO_3}$ have been successfully explained based on the same or similar models.[16–20] For example, the phase diagrams of $\mathrm{Eu_{1-x}Y_xMnO_3}$ under applied magnetic field B have been reproduced by Monte Carlo simulations of this model.[20]

Very recently, it has been experimentally demonstrated that the *R*-site substitution may have a significant impact on the multiferroic behaviors in $R\mathrm{MnO_3}$.[7] It is expected that the cation disorder may give rise to the spatially local fluctuations of the specific spin orders, thus probably lead to phase competitions among them. However, earlier models mainly focus on the effect of the average *R*-site ionic size, while the

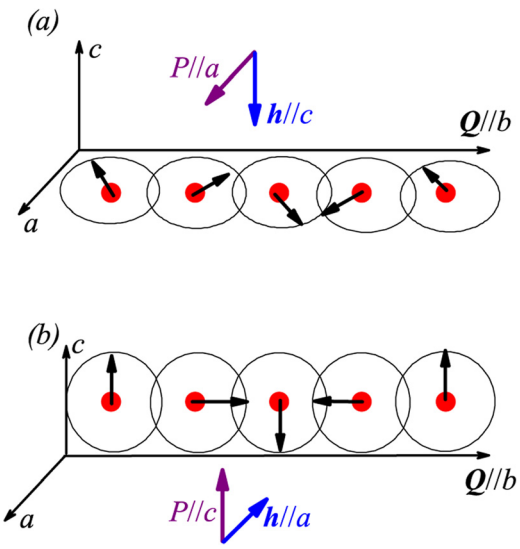

FIG. 1. (Color online) The induced electric polarization P and the spin-helicity vector $\boldsymbol{h} = \Sigma_{ij} S_i \times S_j$ in the (a) *ab*-cycloidal and (b) *bc*-cycloidal spin states.

a)Authors to whom correspondence should be addressed. Electronic mail: qinmh@scnu.edu.cn. (M. H.) and liujm@nju.edu.cn. (J. M.)

disorder effect caused by the substitution is usually ignored. Thus, a systematic study of the impact of local disorder on the multiferroic phase competitions in $R\mathrm{MnO_3}$ may be helpful to clarify the inherent physics. However, as far as we know, few works on this subject have been reported. In this work, a random field method based on the Mochizuki-Furukawa model will be used to study the impact of the *R*-site substitution on the multiferroic behaviors in $R\mathrm{MnO_3}$. The phase diagram obtained by Monte Carlo simulations shows that the long range cycloidal spin orders can be modulated by the *R*-site substitution. We also discuss the influence of the inhomogeneity in realistic materials.

The remainder of this paper is organized as follows: In Sec. II, the model and the simulation method will be described. Section III is attributed to the simulation results and discussion. At last, the conclusion is presented in Sec. IV.

II. MODEL AND METHOD

Following earlier works,[15] we study a classical Heisenberg model with Mn $S=2$ spins on a cuboidal lattice. The Hamiltonian can be written as:

$$H = H_{ex} + H_{sia} + H_{\mathrm{DM}} + H_{cub}. \tag{2}$$

Here the first term H_{ex} denotes the spin exchange interactions which can be given by:

$$H_{ex} = J_{ab}\sum_{\langle i,j\rangle}^{x,y} S_i \cdot S_j + J_b \sum_{\langle i,j\rangle}^{b} S_i \cdot S_j + J_c \sum_{\langle i,j\rangle}^{c} S_i \cdot S_j, \tag{3}$$

where J_{ab} is the ferromagnetic (FM) coupling between the nearest-neighbor (NN) Mn-Mn pairs along the *x*- and *y*-axes (pseudo-cubic notation), J_b is the antiferromagnetic (AFM) coupling between the next-nearest-neighbor Mn-Mn pairs along the *b*-axis (*Pbnm* notation), J_c is the AFM exchange between the NN Mn-Mn pairs along the *c*-axis. It is indicated that J_b is mainly controlled by the *R*-ionic radius and J_c is extensively affected by the nearest Mn-Mn bond length along the *c*-axis, while the SIA and DM interaction can hardly be affected by the cation disorder.[15] In our model, random exchanges are imposed to the Mn-Mn bonds along both the *b* axis and the *c* axis. In detail, the coupling between the nearest-neighbor spins (S_i, S_j) along the *b*-axis (*c*-axis) is changed to $J^b_{ij} = J_b(1 + span \cdot RAM_{i,j})$ ($J^c_{ij} = J_c(1 + span \cdot RAM_{i,j})$) with $RAM_{i,j}$ is the random number within [−1, 1], and *span* is the magnitude of the random exchange term which represents the intensity of the isovalent cation disorder (the intra-chain inhomogeneity) in $R\mathrm{MnO_3}$. Such an approach has been extensively accepted for random fields.[21,22] The second term is the SIA, which consists two parts as

$$H_{sia} = H^D_{sia} + H^E_{sia} = D\sum_i S^2_{\zeta i} + E\sum_i (-1)^{i_x+i_y}\left(S^2_{\xi i} - S^2_{\eta i}\right), \tag{4}$$

where ξ_i, η_i, ς_i are the tilted local axes attached to the *i*-th $\mathrm{MnO_6}$ octahedron. For their direction vectors, we use the experimental data of $\mathrm{EuMnO_3}$.[23] The third term H_{DM} represents the DM interactions which can be expressed as:

$$H_{\mathrm{DM}} = \sum_{\langle i,j\rangle} d_{i,j} \cdot \left(S_i \times S_j\right), \tag{5}$$

where the DM vectors $d_{i,j}$ are determined by five DM parameters, α_{ab}, β_{ab}, γ_{ab}, α_c, and β_c. The fourth term H_{cub} represents the cubic anisotropy and is given by:

$$H_{cub} = \frac{A}{S(S+1)}\sum_i \left(S^4_{xi} + S^4_{yi} + S^4_{zi}\right), \tag{6}$$

where *A* is the coupling constant in the Mn ion and was evaluated to be 0.0162 meV in the electron-spin resonance measurement.[24]

Our simulation is performed on a $36\times36\times6$ cuboidal lattice with periodic boundary conditions using the standard Metropolis algorithm and temperature exchange method.[25,26] The initial spin configuration is totally disordered. The temperature exchange method is performed after every 200 standard Monte Carlo steps. Typically, the initial 2×10^5 Monte Carlo steps are discarded for equilibrium consideration and another 2×10^5 Monte Carlo steps are retained for statistic averaging of the simulation. The values of these parameters for the simulation are listed in Table I. Rich spin ordered phases were identified in the homogenous system with the selected parameters, which may be helpful to develop a better understanding of the multiferroic phase competition in $R\mathrm{MnO_3}$. We calculate the specific heat $C(T)$ and spin-helicity vector $h_\gamma(T)$ ($\gamma = a, b, c$) to determine the transition points and the spin structures. $C(T)$ and $h_\gamma(T)$ are calculated by:

$$C(T) = \frac{1}{Nk_BT^2}\left(\langle H^2\rangle - \langle H\rangle^2\right), \tag{7}$$

$$h_\gamma(T) = \frac{1}{N}\left\langle\left|\sum_i S_i \times S_{i+b}\right|\right\rangle \Big/ S^2, \tag{8}$$

where *N* is the number of Mn ions, k_B is the Boltzmann constant, the brackets denote thermal and configuration averaging. It is expected that h_c has a large value for the *ab*-CS order, while h_a is an index for the *bc*-CS order, as shown in Figs. 1(a) and 1(b). All these three components of spin-helicity vector are strongly suppressed in the paramagnetic (PM) and sinusoidal collinear antiferromagnetic (sc-AFM) phases.

III. SIMULATION RESULTS AND DISCUSSION

With the random exchange field applied to J_b, the calculated phase diagram in the *span-T* parameter space is shown in Fig. 2(a). It is clearly shown that the *ab*-CS state is gradually suppressed with increasing *span*. For moderate *spans*

TABLE I. Parameters chosen for the simulation.

Parameter	Value	Parameter	Value
J_{ab} (meV)	−0.80	α_{ab}	0.10
J_b (meV)	0.80	β_{ab}	0.10
J_c (meV)	1.25	γ_{ab}	0.14
D (meV)	0.25	α_c	0.30
E (meV)	0.30	β_c	0.30
A (meV)	0.0162		

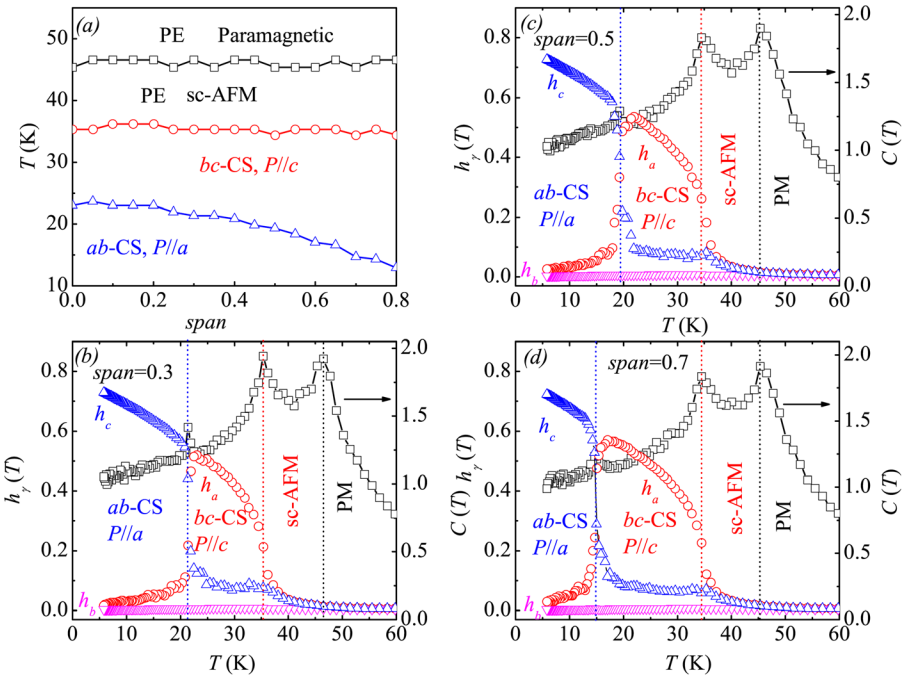

FIG. 2. (Color online) (a) Calculated *span-T* phase diagram with the random filed applied along the *b*-axis. The high-temperature paramagnetic phase is denoted by PM, which accompanied by the paraelectric phase PE. Specific heat $C(T)$ and spin-helicity vector $h_\gamma(T)$ ($\gamma = a, b, c$) as a function of T under various *span*: (b) *span* = 0.3, (c) *span* = 0.5, and (d) *span* = 0.7.

(e.g., *span* = 0.3, 0.5, 0.7), three specific-heat peaks are observed in the calculated $C(T)$ curves, indicating three successive phase transitions with decreasing temperature, as clearly shown in Fig. 2(b)–2(d). The first one is a transition from the PM phase to the sc-AFM phase. No P is observed in these two phases. When T falls down to the second transition point, $h_a(T)$ increases, while $h_b(T)$ and $h_c(T)$ remain small, indicating a phase transition into the *bc*-CS order. Below the third transition point, $h_c(T)$ increases fast, accompanied with a sudden drop of $h_a(T)$, clearly indicating a flop of the spin cycloidal-plane from the *bc*-plane to the *ab*-plane. The first and second transition points are almost independent on *span*, demonstrating that the fluctuation of the local *R*-site ionic size can hardly affect PM and sc-AFM phases. However, the third transition point shifts toward the low-T side as *span* increases, indicating a gradually suppression of the *ab*-CS order at low T.

In order to reveal the physics underlying our simulations, one may give a qualitative discussion from the energy landscape. It was indicated that the *ab*-CS state is stabilized by the SIA and the DM interaction with its vectors on the in-plane Mn-O-Mn bonds. Without the DM interaction, the spins along the *x*-axis and *y*-axis would rotate at uniform angles of ϕ_{ab} satisfies relation $\cos\phi_{ab} = J_{ab}/(2J_b)$ in the ground state. When the DM interaction is introduced, these angles are alternately modulated into $\phi_{ab} + \Delta\phi_{ab}$ and $\phi_{ab} - \Delta\phi_{ab}$ with $\Delta\phi_{ab} > 0$, in order to get an energy gain from the DM interaction. In this case, the *ab*-CS phase with propagation vector $|\boldsymbol{Q}| = \phi/\pi$ along the *b*-axis is stabilized at low T. However, when the random field is applied along the *b*-axis, there are competitions among local *ab*-CS orders with different rotation angles. Thus, the energy of the *ab*-CS phase is increased due to the competitions, leading to the destabilization of the *ab*-CS phase.

On the other hand, the energy of the *bc*-CS phase is irrespective of the value of J_b, as will be stated below. Without the DM interaction, the angles between the nearest two spins along the *c*-axis are $\phi_c = \pi$ due to the strong AFM coupling J_c. An inclusion of the DM interaction allows the angles to be alternatively modulated into π-$\Delta\phi_c$ and π+$\Delta\phi_c$ with $\Delta\phi_c > 0$. The energy gain from the DM interaction due to this modulation can be written as:

$$\Delta E_{DM}^{bc}/N = -\alpha_c S^2 |\cos\phi_c| \Delta\phi_c = -\alpha_c S^2 \Delta\phi_c, \qquad (9)$$

where α_c is the *a* component of DM vectors of the Mn-O-Mn bonds along the *c*-axis. Thus, it is demonstrated that the energy gain for the *bc*-CS phase is irrelevant of J_b. As a result, the *ab*-CS phase is suppressed while the *bc*-CS phase is enhanced when the random exchange field is applied to J_b, as clearly shown in our simulation results.

In addition, similar phenomenon has been observed when the random exchange field is applied along the *c*-axis. The calculated phase diagram in the *span-T* parameter space is shown in Fig. 3(a). The first and second transition points are almost unaffected by the consideration of the random exchange term, while the third transition point also shifts toward the low-T side as *span* increases [Fig. 3(b)–3(d)]. The simulation results may be understood from two different aspects. On one hand, from Eq. (9), one may note that the energy gain from the DM interaction ΔE_{DM}^{bc} in the *bc*-CS order is almost in proportion to $\Delta\varphi_c$ which is also influenced by J_c. When J_c is relatively weak, the state with $\varphi_c = \pi$ can be easily modulated by the DM interaction, leading to large $\Delta\varphi_c$ and ΔE_{DM}^{bc}. As a result, the *bc*-CS state is expected to be stabilized as J_c decreases. Our simulation result has also proved this point, which will be reported elsewhere. When the random exchange term on the Mn-Mn bonds along the *c*-axis is considered, the energy gain ΔE_{DM}^{bc} from the region with weak J_c is increased as *span* increases. On the other hand, the energy gain from the DM interaction in the *ab*-CS state is irrespective of J_c. Therefore, the *bc*-CS phase is

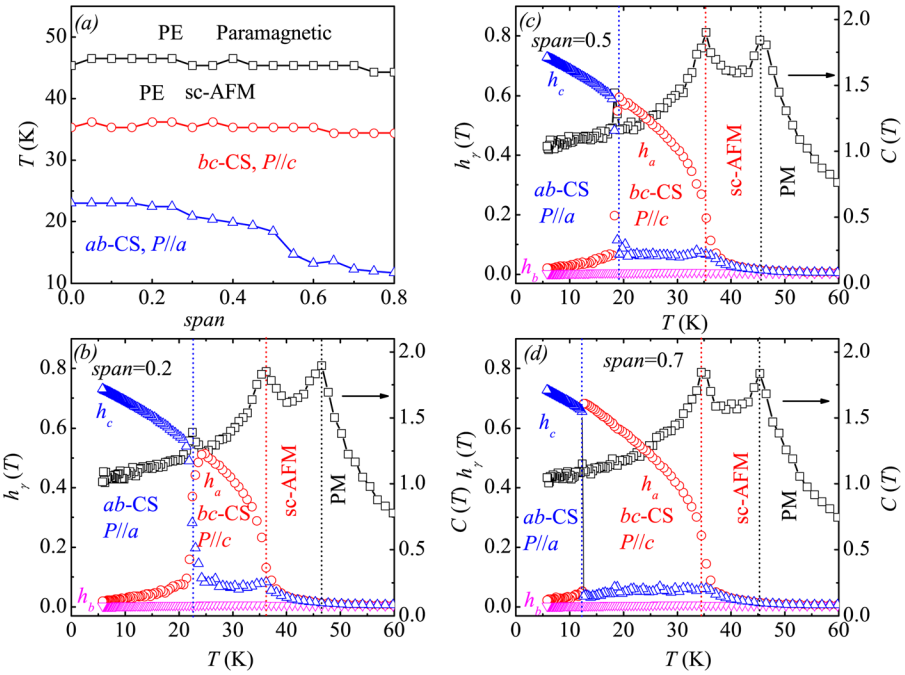

FIG. 3. (Color online) (a) Calculated *span-T* phase diagram with the random filed applied along the *c*-axis. Specific heat $C(T)$ and spin-helicity vector $h_\gamma(T)$ as a function of T under various *span*: (b) *span* = 0.2, (c) *span* = 0.5, and (d) *span* = 0.7.

enhanced while the *ab*-CS one is suppressed at low T with increasing *span*.

It was reported in earlier work that the multiferroic behaviors in orthorhombic manganites $R\mathrm{MnO_3}$ are mainly determined by the average *R*-site ionic size.[27] However, our simulations reveal that a flop of the spin-cycloid plane from the *ab*-plane to the *bc*-plane may be observed at low T in systems with the *R*-site ionic disorder or the intra-chain inhomogeneity. This issue remains to be checked further.

IV. CONCLUSION

So far, it is generally believed that the multiferroic behaviors are mainly determined by the average *R*-site ionic size in $R\mathrm{MnO_3}$. However, our results of Monte Carlo simulation clearly demonstrate that both the *R*-site ionic disorder and the inhomogeneity can drive the reorientation of the spin-cycloid plane. Namely, the *bc*-plane cycloidal spin phase is enhanced in energy with respect to the *ab*-plane cycloidal spin phase, leading to the flop of the spins from the *ab*-plane to the *bc*-plane. The simulated results can be understood as the consequence of the competition between the exchange interactions and spin-orbit coupling, and may be helpful to clarify the flop of the spin-cycloid plane observed in the perovskite manganites and other related systems.

ACKNOWLEDGMENTS

This work was supported by the National Key Projects for Basic Research of China (Grant No. 2011CB922101), the Natural Science Foundation of China (Grant Nos. 50832002, 11004027, and 10874075), China Postdoctoral Science Foundation funded project (Grant No. 20100480768), and the Priority Academic Program Development of Jiangsu Higher Education Institutions, China.

[1]M. Fiebig, J. Phys. D **38**, R123 (2005).
[2]W. Eerenstein, N. D. Mathur, and J. F. Scott, Nature **442**, 759 (2006).
[3]S.-W. Cheong and M. Mostovoy, Nat. Mater. **6**, 13 (2007).
[4]K. F. Wang, J.-M. Liu, and Z. F. Ren, Adv. Phys. **58**, 321 (2009).
[5]T. Kimura, T. Goto, H. Shintani, K. Ishizaka, T. Arima, and Y. Tokura, Nature **426**, 55 (2003).
[6]T. Goto, T. Kimura, G. Lawes, A. P. Ramirez, and Y. Tokura, Phys. Rev. Lett. **92**, 257201 (2004).
[7]J. Hemberger, F. Schrettle, A. Pimenov, P. Lunkenheimer, V. Y. Ivanov, A. A. Mukhin, A. M. Balbashov, and A. Loidl, Phys. Rev. B **75**, 035118 (2007).
[8]G. Lawes, A. B. Harris, T. Kimura, N. Rogado, R. J. Cava, A. Aharony, O. Entin-Wohlman, T. Yildirim, M. Kenzelmann, C. Broholm, and A. P. Ramirez, Phys. Rev. Lett. **95**, 087205 (2005).
[9]K. Taniguchi, N. Abe, T. Takenobu, Y. Iwasa, and T. Arima, Phys. Rev. Lett. **97**, 097203 (2006).
[10]H. Katsura, N. Nagaosa, and A. V. Balatsky, Phys. Rev. Lett. **95**, 057205 (2005).
[11]M. Mostovoy, Phys. Rev. Lett. **96**, 067601 (2006).
[12]I. A. Sergienko and E. Dagotto, Phys. Rev. B **73**, 094434 (2006).
[13]T. Goto, Y. Yamasaki, H. Watanabe, T. Kimura, and Y. Tokura, Phys. Rev. B **72**, 220403(R) (2005).
[14]S. Dong, R. Yu, S. Yunoki, J.-M. Liu, and E. Dagotto, Phys. Rev. B **78**, 155121 (2008).
[15]M. Mochizuki and N. Furukawa, Phys. Rev. B **80**, 134416 (2009).
[16]M. Mochizuki and N. Furukawa, Phys. Rev. Lett. **105**, 187601 (2010).
[17]M. Mochizuki, N. Furukawa, and N. Nagaosa, Phys. Rev. Lett. **104**, 177206 (2010).
[18]M. Mochizuki and N. Nagaosa, Phys. Rev. Lett. **105**, 147202 (2010).
[19]M. Mochizuki, N. Furukawa, and N. Nagaosa, Phys. Rev. Lett. **105**, 037205 (2010).
[20]M. H. Qin, Y. M. Tao, S. Dong, H. B. Zhao, X. S. Gao, and J.-M. Liu, Appl. Phys. Lett. **98**, 102510 (2011).
[21]H. Shinaoka, Y. Tomita, Y. Motome, Phys. Rev. Lett. **107**, 047204 (2011).
[22]X. Y. Yao, S. Dong, and J.-M. Liu, Phys. Rev. B **73**, 212415 (2006).
[23]B. Dabrowski, S. Kolensnik, A. Baszczuk, O. Chmaissem, T. Maxwell, and J. Mais, J. Solid State Chem. **178**, 629 (2005).
[24]H. J. Gerritsen and E. S. Sabisky, Phys. Rev. **132**, 1507 (1963).
[25] D. P. Landau and K. Binder, *A Guide to Monte Carlo Simulations in Statistical Physics* (Cambridge University Press, Cambridge, England, 2005).
[26]K. Hukushima and K. Nemoto, J. Phys. Soc. Jpn. **65**, 1604 (1996).
[27]T. Kimura, Annu. Rev. Mater. Res. **37**, 387 (2007).

Multi-step magnetization of the Ising model on a Shastry–Sutherland lattice: a Monte Carlo simulation

2012 J. Phys.: Condens. Matter 24 386003

(http://iopscience.iop.org/0953-8984/24/38/386003)

J. Phys.: Condens. Matter **24** (2012) 386003 (6pp) doi:10.1088/0953-8984/24/38/386003

Multi-step magnetization of the Ising model on a Shastry–Sutherland lattice: a Monte Carlo simulation

W C Huang[1], L Huo[1], G Tian[1], H R Qian[1], X S Gao[1], M H Qin[1] and J-M Liu[2,3]

[1] Institute for Advanced Materials, South China Academy of Advanced Photonics Engineering, South China Normal University, Guangzhou 510006, People's Republic of China
[2] Laboratory of Solid State Microstructures, Nanjing University, Nanjing 210093, People's Republic of China
[3] International Center for Materials Physics, Chinese Academy of Science, Shenyang 110016, People's Republic of China

E-mail: qinmh@scnu.edu.cn and liujm@nju.edu.cn

Received 24 May 2012, in final form 8 August 2012
Published 28 August 2012
Online at stacks.iop.org/JPhysCM/24/386003

Abstract
The magnetization behaviors and spin configurations of the classical Ising model on a Shastry–Sutherland lattice are investigated using Monte Carlo simulations, in order to understand the fascinating magnetization plateaus observed in TmB_4 and other rare-earth tetraborides. The simulations reproduce the 1/2 magnetization plateau by taking into account the dipole–dipole interaction. In addition, a narrow 2/3 magnetization step at low temperature is predicted in our simulation. The multi-step magnetization can be understood as the consequence of the competitions among the spin-exchange interaction, the dipole–dipole interaction, and the static magnetic energy.

(Some figures may appear in colour only in the online journal)

1. Introduction

Over the past decades, frustrated spin systems in which all local interactions between every spin pair cannot be satisfied simultaneously have attracted widespread interest because very rich physics can appear in these systems [1]. For instance, multi-step magnetization behaviors have been experimentally observed in quite a number of frustrated spin systems, such as triangular spin-chain system $Ca_3Co_2O_6$ [2, 3] and Shastry–Sutherland (S–S) magnets [4–7]. Various theoretical and experimental explorations have been devoted to these interesting phenomena [8–11]. So far, it is generally believed that the multi-step magnetization behaviors in $Ca_3Co_2O_6$ are caused by non-equilibrium magnetization dynamics [12, 13], while those in S–S magnets are far from well understood. We address such phenomena in S–S magnets in this work.

The S–S lattice as a frustrated quantum antiferromagnetic (AFM) model with an exact ground state was first introduced by Shastry and Sutherland in the 1980s [14]. The lattice can be described as a square lattice with AFM couplings J' between the nearest neighbors and additional AFM couplings J between the next-nearest neighbors in every second square, as clearly shown in figure 1. As early as 1991, $SrCu_2(BO_3)_2$ with Cu^{2+} ions carrying a quantum spin $S = 1/2$ and located in a two-dimensional (2d) S–S lattice was investigated [15], triggering an extensive exploration of quantum S–S magnets which exhibit a fascinating sequence of magnetization (M) plateaus at fractional values of the saturated magnetization (M_s) [16, 17]. On the other hand, quite a few rare-earth tetraborides RB_4 (R = Tb, Dy, Ho, Tm, etc) with the magnetic moments located on a lattice that is topologically equivalent to the S–S lattice have attracted various interests [6, 7, 18, 19]. Similar to $SrCu_2(BO_3)_2$, complex magnetic structures and associated physical phenomena in these RB_4 compounds in response to magnetic field (h) at low temperature (T) were identified. In particular, magnetization multi-plateaus at the fractional values of M_s such as $M/M_s = 1/2, 1/7, 1/9$, etc, were observed in TmB_4 [7].

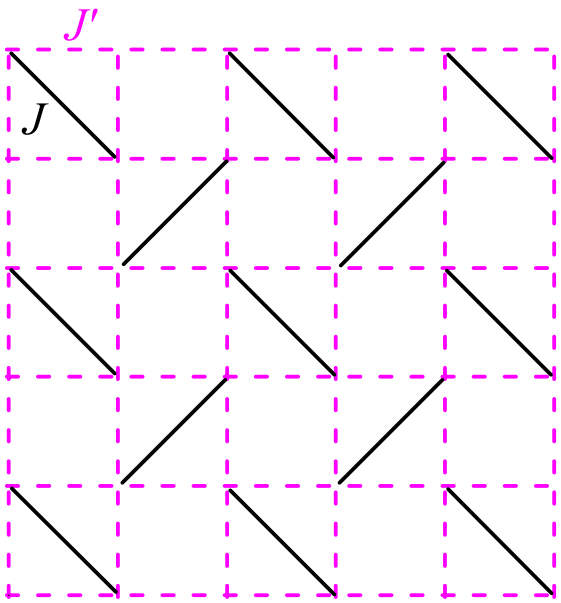

Figure 1. The Shastry–Sutherland lattice. J' bonds (dashed lines) are the exchange couplings along the edges of the squares and J bonds (solid lines) are the diagonal dimer couplings.

While a comprehensive understanding of the multi-step magnetization in $SrCu_2(BO_3)_2$ as a quantum magnet becomes challenging, TmB_4 presents a large total magnetic moment (the magnetic moment of Tm^{3+} is $\sim$6.0 μ_B), and thus can be considered as a classical spin system, making a theoretical approach easier. In addition, subjected to strong crystal field effects, TmB_4 exhibits strong easy-axis anisotropy and can be reasonably described by the classical Ising model rather than the Heisenberg one. Based on this fact, Cheng and Yang studied the magnetization process of the classical AFM Ising model on the S–S lattice using the tensor renormalization-group approach [20]. For a certain T range and coupling constants, only a single magnetization plateau at $M/M_s = 1/3$ resulting from a particular spin state in which each triangle contains two up-spins and one down-spin (UUD, see figure 2(a)) was predicted. Moreover, the spin-1/2 Ising-like XXZ model on the S–S lattice was also visited using the quantum Monte Carlo method, and the magnetization plateau at $M/M_s = 1/2$ was identified [21–23]. It was argued that quantum fluctuations and long-range interactions which may be considered to be the Ruderman–Kittel–Kasuya–Yosida (RKKY) interactions play an important role in the emergence of the $M/M_s = 1/2$ plateau, and a ferrimagnetic (FI) ground-state spin arrangement consisting of alternating AFM and ferromagnetic (FM) stripes was recognized, as depicted in figure 2(b). In addition, a model based on the coexistence of spin and electron subsystems was investigated to describe the magnetization processes in RB_4, and magnetization plateaus at $M/M_s = 1/2, 1/3, 1/5$, and $1/7$ were found [24]. It is

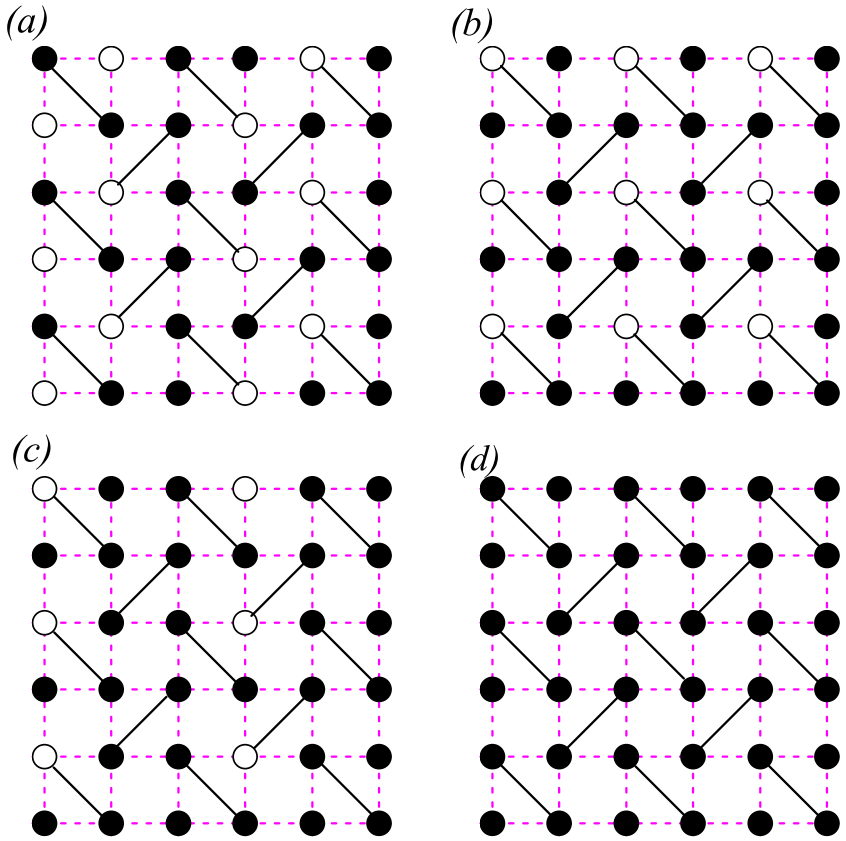

Figure 2. Spin configurations in the (a) UUD state, (b) FI state, (c) possible 2/3 plateau state, and (d) FM state. Solid and empty circles represent the up-spins and the down-spins, respectively.

believed that the interaction between the electron and spin subsystems may be responsible for the plateaus. This hints the substantial role of long-range interactions in determining the magnetization behaviors in these systems.

So far a complete understanding of the multi-step magnetization in TmB_4 remains open [25, 26]. For example, arguments concerning the origin of the experimentally observed 1/2 plateau in the high-h range have not yet reached an agreement. To some extent, an effective reduction of the neighboring spin interactions due to the spin frustration may enhance the relative importance of weak interactions. Besides the RKKY interaction, one such interaction is the long-range dipole–dipole (D–D) interaction, which is estimated to be on the same order of magnitude as the exchange coupling for rare-earth cations with considerable magnetic moments [27, 28]. When the D–D interaction is taken into account, spins in the system tend to be anti-parallel with each other, as will be stated later. Compared with the FM state (spin configuration is shown in figure 2(d)), the FI state with the plateau at $M/M_s = 1/2$ may be stabilized by the D–D interaction in a certain h region. In addition, a possible spin configuration with every AFM band separated by two FM stripes (figure 2(c)) may be stable when h is further increased, resulting in a magnetization plateau at $M/M_s = 2/3$.

Based on the above discussion on the possible spin configurations for the 1/2 and 2/3 magnetization plateaus, one may argue that the D–D interaction in the S–S magnets plays an important role in modulating the spin configuration. However, so far no work on this role of the D–D interaction has been available. In order to clarify this issue, we start with a classical Ising model on the 2d S–S lattice by including the D–D interaction, and then extensive simulations on the magnetization behavior are performed. The 1/2 plateau is indeed reproducible by including the D–D interaction, and the region for the FI state ($M/M_s = 1/2$) in the phase diagram can be significantly enlarged. Furthermore, the D–D interaction can also lead to a relatively narrow 2/3 plateau at low T.

2. Model and method

In the presence of a finite h, the Hamiltonian can be written as:

$$H = J' \sum_{\text{edges}} S_i \cdot S_j + J \sum_{\text{diagnol}} S_i \cdot S_j + g \sum_{\langle i,j \rangle} \left[\frac{S_i \cdot S_j}{\left| R_{ij}^3 \right|} - 3 \frac{\left(S_i \cdot R_{ij}\right)\left(S_j \cdot R_{ij}\right)}{\left| R_{ij}^5 \right|} \right] - h \sum_i S_i, \tag{1}$$

where the spin-exchange coupling $J' = 1/2, J = 1$, S_i is the Ising spin with unit length on site i, g is the dipolar factor, R_{ij} is the separation between sites i and j, and h is applied along the direction of up-spins ($+c$ axis). Since each Ising spin is along the c-axis, the second term in the D–D interaction can be safely ignored. In addition, a cut-off radius $R_{ij} = 6$ is chosen to save the CPU time, and it will be checked later that the choice of R_{ij} never affects our conclusion.

Our simulation is performed on an $L \times L$ (unless stated elsewhere, $L = 24$ is chosen) lattice with periodic boundary conditions using the standard Metropolis algorithm and the parallel tempering algorithm [29, 30]. Here, the parallel tempering algorithm is utilized in order to prevent the system from trapping in metastable free-energy minima caused by the frustration. We take an exchange sampling after every 10 standard Monte Carlo steps. Typically, the initial 2×10^4 Monte Carlo steps are discarded for equilibrium considerations and another 2×10^4 Monte Carlo steps are retained for statistic averaging of the simulation.

3. Simulation results and discussion

Figure 3(a) shows the calculated M as a function of g and h at $T = 0.02$. The magnetization curve for $g = 0$ clearly shows two steps. When h increases from zero, M rapidly reaches the first plateau at $M = M_s/3$ resulting from the UUD state, and then switches to M_s above $h \sim 3$. When g increases ($0 < g < 0.08$), a magnetization step at $M = 0$ is exhibited and gradually broadened. This plateau at $M = 0$ is caused by the collinear state (figure 3(c)), which is the same as the earlier report [20]. At the same time, the transition from the UUD state to the FM state shifts toward the high-h side, leading to the invariance of the plateau width at $M = M_s/3$ for $g < 0.08$. More interestingly, when g increases up to 0.08, a magnetization step at $M = M_s/2$ with the FI state is observed at a high-h range, which is consistent with experimental observation [7]. When g is further increased, the magnetization steps at $M = 0$ and $M = M_s/2$ are gradually broadened, while the step at $M = M_s/3$ is narrowed.

Figure 3(b) shows the simulated phase diagram in the g–h plane at $T = 0.02$, in which the transition points are estimated from the positions of the peaks in the susceptibility $\chi = \mathrm{d}M/\mathrm{d}h$, following earlier work [25]. In order to uncover the physics underlying our simulation, one may give a qualitative discussion from the energy landscape. At $g = 0$, the UUD state is stabilized by the magnetic energy when h is applied. As h further increases, the down-spins may flip as the static magnetic energy increases to be comparable with the interaction energy. The critical field can be estimated to be $h = 4J' + J = 3$, which is verified in our simulation. As stated earlier, spins in the system tend to be anti-parallel with each other when the D–D interaction is taken into account. Compared with the UUD state, the collinear state is stabilized by the D–D interaction. Thus, a higher h should be applied to convert the system from the collinear state to the UUD state as g increases, leading to the broadening of the magnetization step at $M = 0$. A similar behavior in the phase transition from the UUD state to the FM state can also be noticed, i.e. the transition shifts toward the high-h side as g increases ($0 < g < 0.08$), as clearly shown in figure 3(b). However, in the small g region ($g < 0.08$), the magnetic energy plays a significant role in modulating the step-M behavior, and the intermediate magnetization step at $M = M_s/2$ cannot be stabilized. On the other hand, in the large-g region ($g > 0.08$) in which the D–D interaction becomes more dominant, the magnetization

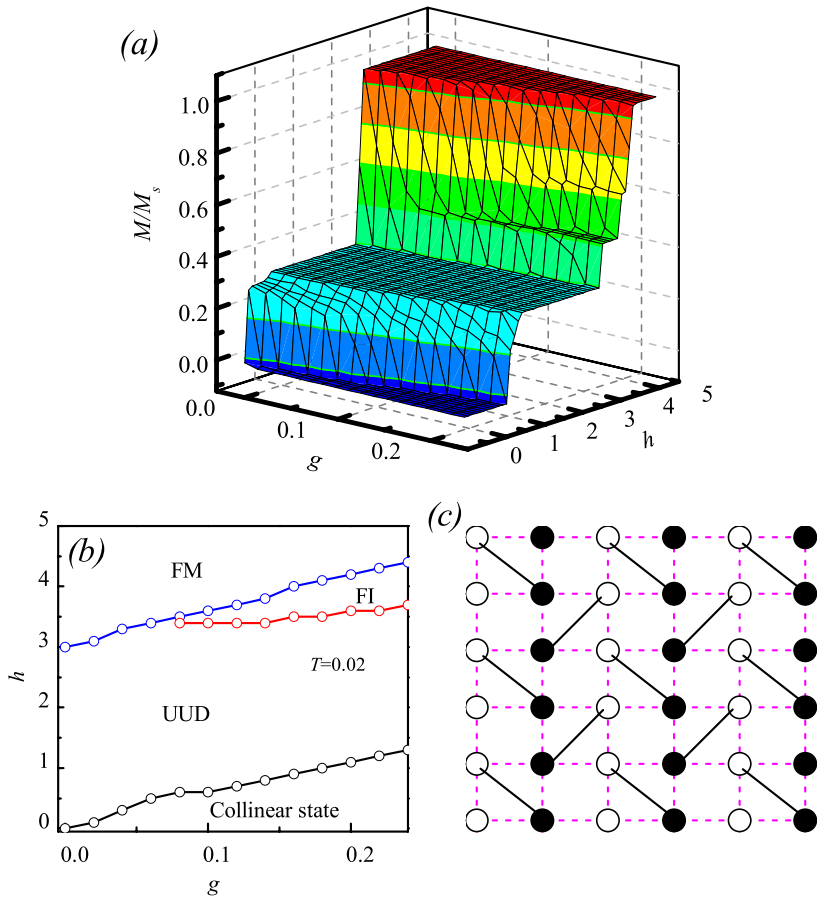

Figure 3. (a) Magnetization M versus dipolar factor g and magnetic field h. The parameters are $L = 24$, $T = 0.02$ and $R_{ij} = 6$. (b) Phase diagram of the magnetization plateau in the h–g plane. (c) Spin configuration for the collinear state with the plateau at $M = 0$. Solid and empty circles represent the up-spins and the down-spins, respectively.

step at $M = M_s/2$ is observed and is gradually enlarged with increasing g.

To identify the origin of the FI state with the 1/2 plateau, we respectively calculate the h-dependence of spin-exchange energy H_{ex}, D–D interaction H_{DD}, Zeeman energy H_{zee}, and the total energy H at $T = 0.02$ for $g = 0.2$ (see figure 4(a)). In order to help one to understand the results, the corresponding magnetization curve is also shown in figure 4(b). The enhancement of the FI state with increasing g may be understood from two different aspects. On one hand, within a certain h range, the energy loss from the D–D interaction and spin-exchange interaction due to the phase transition from the UUD state to the FI state is smaller than the energy gain from the Zeeman energy, leading to the stabilization of the FI state. In addition, the energy loss from the D–D interaction due to this transition is very small and increases slowly with increasing g, thus the transition from the UUD state to the FI state occurs at a relatively stable h, as shown with the red circles in figure 3(b). On the other hand, the energy loss from the D–D interaction due to the phase transition from the FI state to the FM state is large and increases quickly as g increases. So, a larger h will be needed to flip down-spins in the FI state with increasing g. As a result, when g is further increased from $g = 0.08$, the region of the FI state with the plateau at $M = M_s/2$ is enlarged, while that of the FM state with the plateau at $M = M_s$ is narrowed.

In addition, the effect of T is also studied in our simulation, and the corresponding results are shown in figure 5. Figure 5(a) shows the calculated M as a function of T and h for $g = 0.2$. At low T ($T < 0.02$), a narrow magnetization plateau at $M = 2M_s/3$ is observed in addition to the previously discussed plateaus at $M = 0, M_s/3, M_s/2$ and M_s. The spin configuration with the plateau at $M = 2M_s/3$ is confirmed in our work to be the same as that shown in figure 2(c). The related physical mechanism responsible for this phenomenon may be similar to that for the emergence of the plateau at $M = M_s/2$ in a certain h range. However, the $2M_s/3$ plateau is so unstable that it quickly disappears when T increases slightly, as shown in figure 5(b). In addition, the FI state is gradually destroyed due to the thermal fluctuations, leading to the melting of the magnetization step at $M = M_s/2$. When T is raised to about 0.15, the $M_s/2$ plateau completely disappears. On the other hand, the steps at $M = 0$ and $M_s/3$ are relatively stable, and are clearly visible even at $T = 0.4$. However, when T rises from 0.15, the borders between the steps become more and more indistinct, as shown in figure 5(a). One may note that the perfect collinear state and UUD state may be partially destroyed near the critical

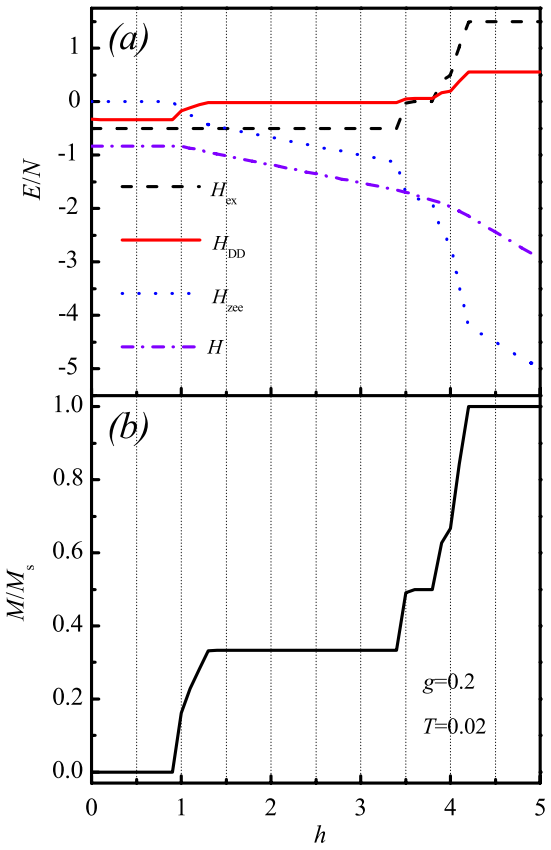

Figure 4. The calculated (a) H_{ex}, H_{DD}, H_{zee}, H, and (b) magnetization M/M_s as a function of h at $T = 0.02$ for $g = 0.2$.

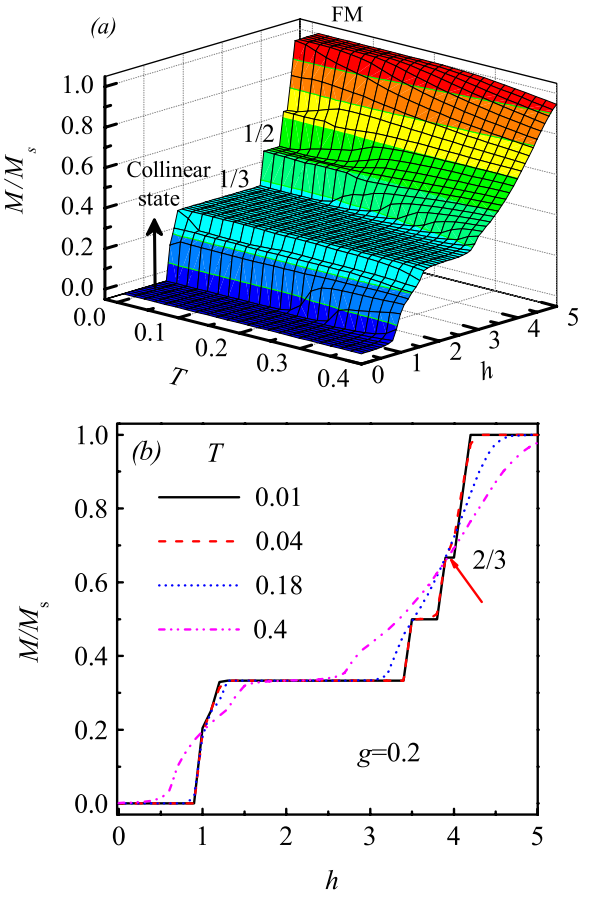

Figure 5. (a) Magnetization M/M_s versus temperature T and magnetic field h for $g = 0.2$. (b) Magnetization curves for different T for $g = 0.2$.

field at high T ($T > 0.15$), leading to the smoothness of the magnetization curves.

Up to now, the present work reveals that frustrated spin systems such as TmB_4 offer a very complicated spin configuration which is very sensitive to weak interactions, including the D–D interaction which is usually ignored in earlier work. The magnetization plateau at $M = M_s/2$ at low T as reported in experiments is reproduced in our simulation when the D–D interaction is taken into account. In addition, a narrow step at $M = 2M_s/3$ is predicted in our simulation, which remains to be checked further. Although not all the experimental results in TmB_4 can be explained based on the classical Ising model, the present study has taken an important step toward a complete understanding of the magnetization process of this system.

In order to verify the reliability of our simulation, the dependence of the step-like magnetization feature on the cut-off radius R_{ij} and the lattice size L has also been investigated, and the simulated results are presented in figure 6. Figure 6(a) shows the simulated magnetization curves for various R_{ij} ($R_{ij} = 4$, 6 and 8) at $T = 0.02$ for $g = 0.2$. The magnetization curve for $R_{ij} = 6$ perfectly coincides with that for $R_{ij} = 8$, indicating that the choice of R_{ij} in this work is reasonable enough. Finally, we check the finite-lattice-size effect in order to exclude the artificial facts due to the finite lattice size in our simulation. The simulated magnetization curves for different L ($L = 12$, 18, 24 and 30) are shown in figure 6(b). The simulated curves for various L are almost merged into one, demonstrating that the finite-size effect on the magnetization of the system is negligible and never affects our conclusion.

4. Conclusion

In conclusion, we have studied the magnetic behavior of the classical Ising model on the Shastry–Sutherland lattice by means of Monte Carlo simulation in order to understand the magnetic process in TmB_4. Our simulation successfully reproduces the magnetization plateau at $M = M_s/2$ observed in experiments when the D–D interaction is taken into account. In addition, a tiny plateau at $M = 2M_s/3$ is predicted in our work, which deserves to be checked further. The magnetic phase diagram can be understood from the competitions among the spin-exchange interaction, the D–D interaction and the static magnetic energy. It is indicated that even weak interactions available in realistic systems, such as the D–D interaction, may have a significant effect on the step-like magnetization feature. The present work may provide new insights into the understanding of the magnetization process for frustrated S–S magnets.

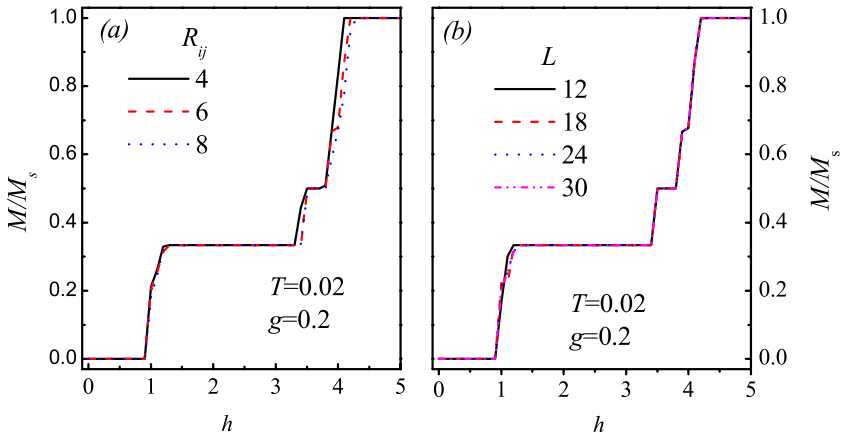

Figure 6. Magnetization curves for (a) different cut-off radius R_{ij} and (b) different lattice sizes L. The parameters are $T = 0.02$ and $g = 0.2$.

Acknowledgments

This work was supported by the National Key Projects for Basic Research of China (2011CB922101), the Natural Science Foundation of China (11204091, 11274094, 50832002, 51031004), China Postdoctoral Science Foundation funded project (20100480768), and the Priority Academic Program Development of Jiangsu Higher Education Institutions, China.

References

[1] Diep H T 2004 *Frustrated Spin Systems* (Singapore: World Scientific)
[2] Kageyama H, Yoshimura K, Kosuge K, Azuma M, Takano M, Mitamura H and Goto T 1997 *J. Phys. Soc. Japan* **66** 3996
[3] Maignan A, Michel C, Masset A C, Martin C and Raveau B 2000 *Eur. Phys. J.* B **15** 657
[4] Kageyama H, Yoshimura K, Stern R, Mushnikov N V, Onizuka K, Kato M, Kosuge K, Slichter C P, Goto T and Ueda Y 1999 *Phys. Rev. Lett.* **82** 3168
[5] Kodama K, Takigawa M, Horvatic M, Berthier C, Kageyama H, Ueda Y, Miyahara S, Becca F and Mila F 2002 *Science* **298** 395
[6] Yoshii S, Yamamoto T, Hagiwara M, Michimura S, Shigekawa A, Iga F, Takabatake T and Kindo K 2008 *Phys. Rev. Lett.* **101** 087202
[7] Siemensmeyer K, Wulf E, Mikeska H J, Flachbart K, Gabani S, Matas S, Priputen P, Efdokimova A and Shitsevalova N 2008 *Phys. Rev. Lett.* **101** 177201
[8] Kudasov Y B 2006 *Phys. Rev. Lett.* **96** 027212
[9] Yao X Y, Dong S and Liu J-M 2006 *Phys. Rev.* B **73** 212415
[10] Abendschein A and Capponi S 2008 *Phys. Rev. Lett.* **101** 227201
[11] Dorier J, Schmidt K P and Mila F 2008 *Phys. Rev. Lett.* **101** 250402
[12] Qin M H, Wang K F and Liu J-M 2009 *Phys. Rev.* B **79** 172405
[13] Kudasov Y B, Korshunov A S, Pavlov V N and Maslov D A 2008 *Phys. Rev.* B **78** 132407
[14] Shastry B S and Sutherland B 1981 *Physica* B + C **108** 1069
[15] Smith R W and Keszler D A 1991 *J. Solid State Chem.* **93** 430
[16] Alicea J, Chubukov A V and Starykh O A 2009 *Phys. Rev. Lett.* **102** 137201
[17] Isaev L, Ortiz G and Dukelsky J 2009 *Phys. Rev. Lett.* **103** 177201
[18] Watanuki R, Sato G, Suzuki K, Ishihara M, Yanagisawa T, Nemoto Y and Goto T 2005 *J. Phys. Soc. Japan* **74** 2169
[19] Michimura S, Shigekawa A, Iga F, Swra M, Takabatake T, Ohoyama K and Okabe Y 2006 *Physica* B **378** 596
[20] Chang M C and Yang M F 2009 *Phys. Rev.* B **79** 104411
[21] Meng Z Y and Wessel S 2008 *Phys. Rev.* B **78** 224416
[22] Suzuki T, Tomita Y and Kawashima N 2009 *Phys. Rev.* B **80** 180405
[23] Suzuki T, Tomita Y and Kawashima N 2010 *Phys. Rev.* B **82** 214404
[24] Farkasovsky P, Cencarikova H and Matas S 2010 *Phys. Rev.* B **82** 054409
[25] Moliner M, Cabra D C, Honecker A, Pujol P and Stauffer F 2009 *Phys. Rev.* B **79** 144401
[26] Qin M H, Zhang G Q, Wang K F, Gao X S and Liu J-M 2011 *J. Appl. Phys.* **109** 07E103
[27] Melko R G, Hertog B C and Gingras M J P 2001 *Phys. Rev. Lett.* **87** 067203
[28] Xie Y L, Lin L, Yan Z B, Wang K F and Liu J-M 2012 *J. Appl. Phys.* **111** 07E133
[29] Landau D P and Binder K 2008 *A Guide to Monte Carlo Simulations in Statistical Physics* (Cambridge: Cambridge University Press)
[30] Hukushima K and Nemoto K 1996 *J. Phys. Soc. Japan* **65** 1604

The competing spin orders and fractional magnetization plateaus of the classical Heisenberg model on Shastry-Sutherland lattice: Consequence of long-range interactions

L. Huo, W. C. Huang, Z. B. Yan, X. T. Jia, X. S. Gao et al.

Citation: J. Appl. Phys. **113**, 073908 (2013); doi: 10.1063/1.4792504
View online: http://dx.doi.org/10.1063/1.4792504
View Table of Contents: http://jap.aip.org/resource/1/JAPIAU/v113/i7
Published by the American Institute of Physics.

The competing spin orders and fractional magnetization plateaus of the classical Heisenberg model on Shastry-Sutherland lattice: Consequence of long-range interactions

L. Huo,[1] W. C. Huang,[1] Z. B. Yan,[2] X. T. Jia,[3] X. S. Gao,[1] M. H. Qin,[1,a)] and J.-M. Liu[2,b)]
[1]*Institute for Advanced Materials, South China Normal University, Guangzhou 510006, China*
[2]*Laboratory of Solid State Microstructures, Nanjing University, Nanjing 210093, China*
[3]*School of Physics and Chemistry, Henan Polytechnic University, Jiaozuo 454000, China*

(Received 14 November 2012; accepted 1 February 2013; published online 20 February 2013)

The competing spin orders and fractional magnetization plateaus of the classical Heisenberg model with long-range interactions on a Shastry-Sutherland lattice are investigated using Monte Carlo simulations, in order to understand the fascinating spin ordering sequence observed in TmB_4 and other rare-earth tetraborides. The simulation reproduces the experimental 1/2 magnetization plateau at low temperature by considering multifold long range interactions. It is found that more local long range interactions can be satisfied in the 1/2 plateau state than those in the 1/3 plateau state, leading to the stabilization of the extended 1/2 plateau. The phase boundaries in the magnetic field at zero temperature are determined, demonstrating the simulation results. When the energies of the Neel state and the collinear state are degenerated, the former state is more likely to be stabilized due to the competitions among the local collinear spin orders. The present work provides a comprehensive proof of the phase transitions to the Neel state at nonzero temperature, in complimentary to the earlier predictions for the Fe-based superconductors. © *2013 American Institute of Physics*. [http://dx.doi.org/10.1063/1.4792504]

I. INTRODUCTION

During the past decades, frustrated spin systems such as triangular spin-chain system $Ca_3Co_2O_6$ and Shastry-Sutherland (S-S) magnets have attracted widespread interest from both theoretical and experimental approaches due to the fact that fascinating multi-step magnetization behaviors can appear in these systems.[1–6] Up to now, the magnetization plateaus in the former system are generally believed to be caused by non-equilibrium dynamics,[7–9] while those in the latter systems are still under controversy.

The S-S lattice which was first introduced as an interesting example of a frustrated quantum spin system with an exact ground state as early as 1981, can be described as a square lattice with diagonal antiferromagnetic (AFM) coupling J_1 in every second square and AFM coupling J_2 along the edges of the squares, as depicted in Fig. 1(a).[10] Experimentally, $SrCu_2(BO_3)_2$ with Cu^{2+} ions carrying a quantum spin $S = 1/2$ and arranged in a two-dimensional (2d) S-S lattice has triggered an extensive exploration of quantum S-S magnets which exhibit an amazing sequence of magnetization (M) plateaus at fractional values of the saturated magnetization (M_s).[11] On the other hand, quite a few rare-earth tetraborides RB_4 (R = Tb, Dy, Ho, Tm, etc.) as another representative of the S-S magnets have been accorded more and more attentions.[5,6,12,13] Similar to $SrCu_2(BO_3)_2$, the complex magnetic structures and their associated physical phenomena in these RB_4 compounds under various magnetic fields (h) at low temperatures (T) were identified. For example, the magnetization plateaus at the fractional values of M_s such as $M/M_s = 1/2$, 1/7, and 1/9, were experimentally observed in TmB_4 and several theoretical attempts to understand this interesting phenomenon are available as well.

Unlike Cu^{2+}, Tm^{3+} presents a large total magnetic moment $\sim 6.0\,\mu_B$, and can be considered as a classical spin system. In addition, TmB_4 is of strong easy-axis anisotropy caused by strong crystal field effects. Based on this fact, the magnetization process of the classical AFM Ising model on the S-S lattice was studied using the tensor renormalization-group approach.[14] Under low h, either the collinear state [Fig. 2(a)] or the Neel state [Fig. 2(b)] is stabilized depending on the value of J_1/J_2. For a certain T range and coupling constants, only a single magnetization plateau at $M/M_s = 1/3$ resulting from a particular spin state in which each triangle contains two up-spins and one down-spin [the UUD state, see Fig. 2(c)] was predicted in an intermediate h range. At almost the same time, magnetization pseudoplateaus around $M/M_s = 1/3$ were predicted in a classical Heisenberg model on the S-S lattice.[15] Most recently, the ground states of the Ising model on the S-S lattice are investigated and the existence of a single 1/3 plateau has been rigorously proved.[16] Three different ground states with $M/M_s = 1/2$ have been found when the additional third-neighbor interaction is considered.

On the other hand, the quantum spin-1/2 Ising-like XXZ model with additional interactions [Fig. 1(b)] on the S-S lattice was visited using the quantum Monte Carlo method, and the experimentally observed magnetization plateau at $M/M_s = 1/2$ in the absence of the $M/M_s = 1/3$ plateau was reproduced.[17–19] It was indicated that quantum spin fluctuations and long-range interactions may play an important role

a)Electronic mail: qinmh@scnu.edu.cn.
b)Electronic mail: liujm@nju.edu.cn.

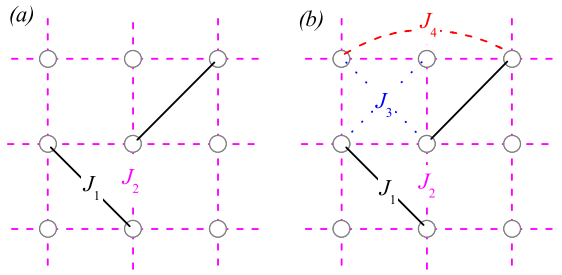

FIG. 1. Effective models on the Shastry-Sutherland lattice with (a) the diagonal coupling of J_1, and J_2 along the edges of the squares, (b) the additional interactions J_3 and J_4.

in the emergence of the $M/M_s = 1/2$ plateau, and a ferrimagnetic (FI) state spin arrangement consisting of alternative AFM and ferromagnetic (FM) stripes was recognized [Fig. 2(d)]. In our earlier work, the presence of the $M/M_s = 1/2$ plateau was also confirmed when the dipole-dipole interaction is taken into account in the classical Ising model on the S-S lattice.[20,21] Otherwise, a model based on the coexistence of the spin and the electron subsystems was investigated, and the latter subsystem and its interaction with the spin one were believed to be responsible for the plateaus in S-S magnets.[22]

So far, arguments concerning the origin of experimental $M/M_s = 1/2$ plateau have not yet reached a consensus. For frustrated spin systems, an effective reduction of the neighboring spin interactions due to the spin frustration may enhance the relative importance of weak interactions. This hints the substantial role of long-range interactions in determining the magnetization behaviors in these frustrated spin systems. For example, a weak FM coupling J_4 bond tends to align the connected spin pair parallel with each other, and may stabilize the $M/M_s = 1/2$ plateau. Similarly, more local AFM J_3 interactions are satisfied in the FI state than those in the UUD state, resulting in the stabilization of the $M/M_s = 1/2$ plateau with the increasing J_3. In fact, for a quantum spin system, it is confirmed that the FM J_4 and AFM J_3 couplings are essential to the stabilization of the $M/M_s = 1/2$ plateau.[18]

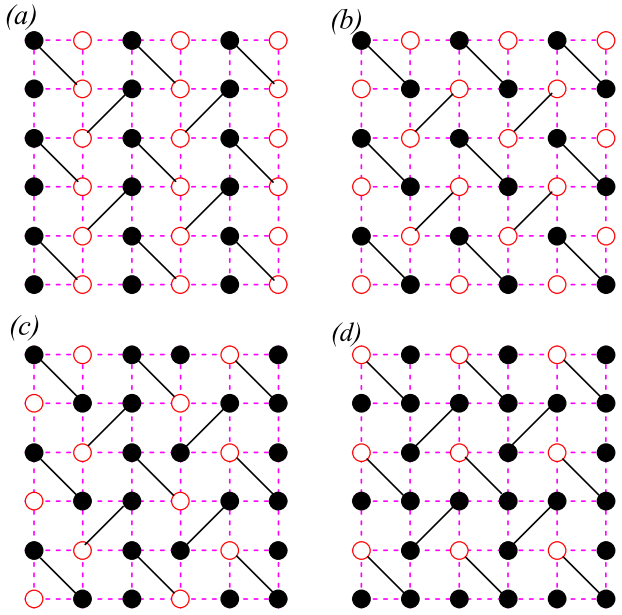

FIG. 2. Spin configurations in (a) the collinear state, (b) the Neel state, (c) the UUD state, and (d) the FI state. Solid and empty circles represent the up-spins and the down-spins, respectively.

Naturally, one may question whether the same mechanism still holds true for classical spin systems such as TmB_4. As a matter of fact, the investigation of the effect of further-neighbor interactions is suggested to eventually explain the plateaus in TmB_4 in earlier work.[16] On the other hand, the study of the nontrivial magnetic orders in these systems also plays an essential role in the sense of basic physical research. Most recently, the phase transition from the collinear state to the Neel state at finite T was reported in a frustrated AFM model on a square lattice, which is interested in explaining the antiferromagnetic behaviors associated with the Fe-based superconductors.[23] To some extent, this interesting phenomenon probably is observable for S-S magnets. However, as far as we know, few works on this subject have been reported.

In order to clarify this critical issue, we investigate the classical Heisenberg model with the easy-axis anisotropy and the long-range interactions on the S-S lattice. The main $M/M_s = 1/2$ plateau can be reproduced when the long-range interactions are included. The phase diagrams obtained by means of the Monte Carlo simulation indicate that both the J_3 and J_4 interactions have a significant effect on the modulation of the spin configurations. The simulated results at low T can be qualitatively interpreted from the spin structures of the ground states for the Ising limit. In addition, the Neel state is verified to be stable at low temperatures due to the competitions among the local collinear states, which strengthens the conclusion of Wang that the phase transition from the collinear state to the Neel state may occur at finite temperature in the Fe-based superconductors such as P-substituted LaFeAsO.[23]

The remainder of this paper is organized as follows: In Sec. II, the model and the simulation method will be presented and described. Section III is attributed to the simulation results and discussion of the simulation. The spin structures for the Ising limit at zero temperature will be discussed in Sec. IV, and the conclusion is presented in Sec. V.

II. MODEL AND METHOD

The easy-axis anisotropy is ignored in the Heisenberg model, which, on the other hand, is too much emphasized in the Ising limit. The uniaxially anisotropic Heisenberg model seems to be a sound choice for the description of TmB_4, as discussed earlier. In the presence of the long-range interactions and h, the Hamiltonian can be described as follows:

$$H = J_1 \sum_{diagonal} S_i \cdot S_j + J_2 \sum_{edges} S_i \cdot S_j + J_3 \sum_{\langle i,j \rangle} S_i \cdot S_j + J_4 \sum_{\langle i,j \rangle'} S_i \cdot S_j - h \sum_i S_i^z - D \sum_i (S_i^z)^2, \quad (1)$$

where the exchange couplings $J_1 = 1$, $J_2 = 1/2$, S_i represents the Heisenberg spin with unit length on site i, $\langle i, j \rangle$ and $\langle i, j \rangle'$, respectively, denote the summations over all pairs on the bonds with J_3 and J_4 couplings as shown in Fig. 1(b), h is

applied along the $+z$ axis, and S_i^z denotes the z component of S_i. Typically, the easy-axis anisotropy constant $D = 0.4$ is chosen in our simulation. In addition, $J_1/J_2 = 2$ is taken so that the collinear state and the Neel state are degenerated for zero J_3 which may help one to understand the phase competition between these two phases better.

Our simulation is performed on an $L \times L$ ($L = 24$) S-S lattice with period boundary conditions using the standard Metropolis algorithm and the parallel tempering algorithm.[24,25] Here, the parallel tempering algorithm is utilized in order to prevent the system from being trapped in the metastable free-energy minima caused by the frustration. We take an exchange sampling after every 10 standard Monte Carlo steps (MCs). The simulation is started from the FM state under high h, and the $M(h)$ curves are calculated upon h decreasing. Typically, the initial 2×10^5 MCs are discarded for equilibrium consideration and another 1×10^5 MCs are retained for statistic averaging of the simulation.

III. SIMULATION RESULTS AND DISCUSSION

In this study, we mainly concern the effect of the long-range interactions on the low-temperature magnetic behaviors of S-S magnets. The calculated M as a function of J_3 and h at $T = 0.01$ for $J_4 = 0$ is shown in Fig. 3(a). For small J_3 ($J_3 < 0.1$), M rapidly reaches the first plateau at $M = M_s/3$ resulting from the UUD state when h increases from zero, and then switches to M_s above $h \sim 3$. When J_3 further increases ($J_3 > 0.1$), the $M = M_s/3$ step splits into three steps, the $M = 0$ step, the $M = M_s/3$ step, and the $M = M_s/2$ step. The plateau at $M = 0$ is caused by the collinear state, and that at $M = M_s/2$ is caused by the FI state, as reported earlier. The magnetization steps at $M = 0$ and $M = M_s/2$ are gradually broadened, while the step at $M = M_s/3$ is narrowed with increasing J_3.

Fig. 3(b) shows the simulated phase diagram in the J_3-h plane at $T = 0.01$, in which the transition points are estimated from the positions of the peaks in the susceptibility $\chi = dM/dh$, following earlier work.[15] At $J_3 = 0$, the UUD state is stabilized by the magnetic energy when h is applied. The down-spins may flip when h is further increased to the critical field which can be estimated to be $h = 3$ for the Ising limit, as verified in our simulation. One may note that the spin pairs on the diagonal J_3 bonds tend to be anti-parallel with each other when AFM J_3 coupling is taken into account. Compared with the UUD state, the collinear state is stabilized by J_3 interaction. Thus, a higher h should be applied to convert the system from the collinear state to the UUD state as J_3 increases, leading to the broadening of the magnetization step at $M = 0$. To clearly identify the origins of the phase diagram, we, respectively, calculate the h-dependence of the spin-exchange energy H_1 from the J_1 coupling, H_2 from the J_2 coupling, H_3 from the J_3 coupling, the uniaxial anisotropy H_{an}, and the Zeeman energy H_{zee} at $T = 0.01$ for $J_3 = 0.3$ [see Fig. 3(c)]. The corresponding magnetization curve is also presented in Fig. 3(d) to help one to understand the results better. The enhancement of the FI state with the increasing J_3 can be understood from two parts. On one hand, within certain h range, the energy loss from H_1 and H_2 due to the phase transition from the UUD state to the FI state is smaller than the energy gain from H_3 and H_{zee}, leading to the stabilization of the FI state. In addition, the energy gain from H_3 due to this transition is increased with the increasing J_3, thus the transition shifts toward the small-h side as shown with the red circles in Fig. 3(b), leading to the gradually replacement of the 1/3 plateau by the 1/2 one. On the other hand, the energy loss from H_3 due to the phase transition from the FI state to the FM state increases as J_3 is increased. So, a larger h will be needed to flip down-spins in the FI state. As a result, when J_3 is increased from $J_3 = 0.1$, the regions of the FI state with the $M = M_s/2$ plateau and the collinear state with the $M = 0$ plateau are, respectively, enlarged, while that of the UUD state with the plateau at $M = M_s/3$ is narrowed.

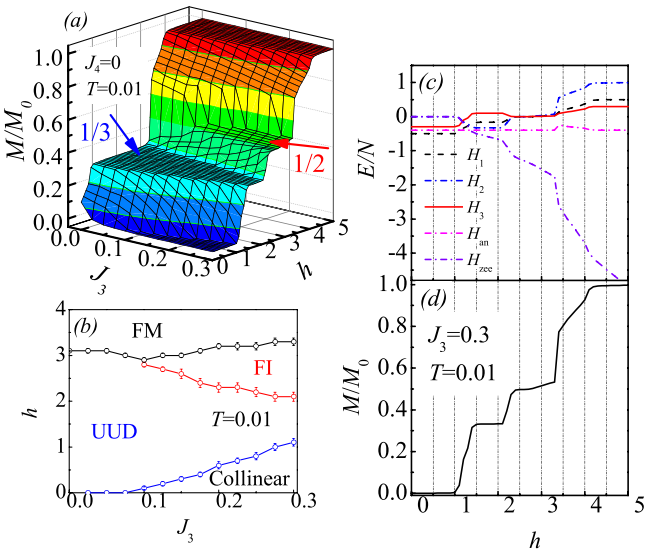

FIG. 3. (a) Magnetization M versus J_3 and magnetic field h. The parameters are $L = 24$, $T = 0.01$, and $J_4 = 0$. (b) Phase diagram of the magnetization plateau in the h-J_3 plane. The calculated (c) H_1, H_2, H_3, H_{an}, H_{zee} and (d) magnetization M/M_s as a function of h at $T = 0.01$ for $J_3 = 0.3$.

Similar phenomena can also be observed when a FM J_4 coupling is included in this system. Fig. 4(a) shows the calculated M as a function of J_4 and h at $T = 0.01$ for $J_3 = 0$. The $M = M_s/3$ step splits into three steps when J_4 is increased above -0.05. It is verified that the plateau at $M = 0$ is caused by the Neel state which will be discussed in detail in the next section. When J_4 is further increased to ~ -0.25, the 1/3 step is completely replaced by the $M = 0$ step and the $M = M_s/2$ step. In addition, the $M(h)$ curves for larger J_4 remain almost the same as that for $J_4 = -0.25$. The corresponding phase diagram is shown in Fig. 4(b), and can be clearly understood from the competitions among different energy terms. The energy H_4 from the J_4 coupling is significantly lost due to the transition from the Neel state to the UUD state as shown in Fig. 4(c), leading to the fact that the transition shifts toward the high-h side with the increasing J_4. At the same time, the energy gain from H_4 due to the transition from the UUD state to the FI state is increased, resulting in the enhancement of the FI state accompanied by the destabilization of the UUD state. When J_4 is increased to -0.25, the UUD state has been completely suppressed, leaving the stabilization of an extended $M = M_s/2$ plateau in the absence of

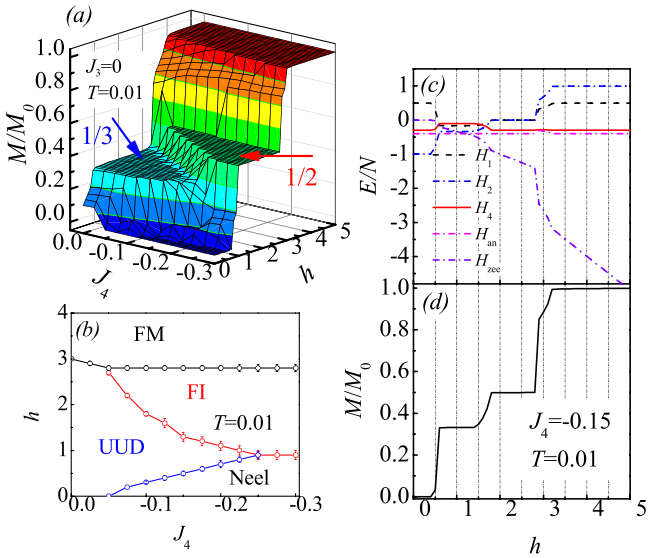

FIG. 4. (a) Magnetization M versus J_4 and magnetic field h. The parameters are $L=24$, $T=0.01$, and $J_3=0$. (b) Phase diagram of the magnetization plateau in the h-J_4 plane. The calculated (c) H_1, H_2, H_4, H_{an}, H_{zee} and (d) magnetization M/M_s as a function of h at $T=0.01$ for $J_4=-0.15$.

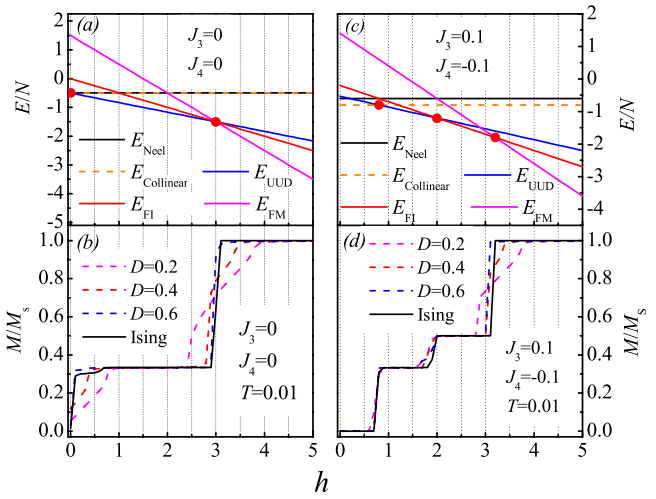

FIG. 5. The local energies as a function of h for the Ising limit for (a) $J_3=0$ and $J_4=0$ and (c) $J_3=0.1$ and $J_4=-0.1$. (b) and (d) are the correspondingly simulated magnetization curves at $T=0.01$.

the $M=M_s/3$ plateau. On the other hand, it is shown in Figs. 4(c) and 4(d) that H_4 maintains the same value for the Neel state, the FI state, and the FM state in which all local J_4 interactions are satisfied. So, the transition from the Neel state to the FI state and that from the FI state to the FM state, respectively, occur at stable h irrespective of J_4, as clearly shown in Fig. 4(b).

One may note that the perfect collinear state, the Neel state, the UUD state, and the FI state may be partially destroyed near the critical fields for the Heisenberg spin model even at T as low as 0.01, leading to the smoothness of the magnetization curves in our simulation. However, the present work reveals that classical S-S magnets such as TmB_4 exhibit complex spin structures which are very sensitive to weak long-range interactions. The experimentally observed magnetization plateau at $M=M_s/2$ can be reproduced when the AFM J_3 coupling or/and the FM J_4 coupling are taken into consideration. The plateau at $M=0$ stems from either the Neel state or the collinear state, depending on the choice of the exchange interaction coupling constants. To better understand the simulated results, the ground states at zero T for the Ising limit are also discussed based on a mean-field method, as will be found in Sec. IV.

IV. MAGNETIC ORDERS AT ZERO TEMPERATURE

In fact, the ground-state and the phase boundaries can be qualitatively determined by comparing the Ising energies at different spin configurations which are confirmed from the snapshot of spin configuration in Monte Carlo simulations. Excluding the anisotropy energy (constant here), the energy per site of the Neel state, the collinear state, the UUD state, the FI state, and the FM state can be, respectively, calculated as follows:

$$E_{\text{Neel}} = J_1/2 - 2\times J_2 + J_3 + 2\times J_4, \tag{2}$$

$$E_{\text{col}} = -J_1/2 - J_3 + 2\times J_4, \tag{3}$$

$$E_{\text{UUD}} = -J_1/6 - 2J_2/3 + J_3/3 + 2J_4/3 - h/3, \tag{4}$$

$$E_{\text{FI}} = 2\times J_4 - h/2, \tag{5}$$

$$E_{\text{FM}} = J_1/2 + 2\times J_2 + J_3 + 2\times J_4 - h. \tag{6}$$

Fig. 5(a) shows the calculated local energies as a function of h for these five states for the Ising limit under $J_3=0$ and $J_4=0$. It is clearly demonstrated that the energies of the UUD state, the FI state, and the FM state are degenerated at the saturation field which can be determined to be $h_c=4J_2+J_1=3$ by comparing E_{UUD} and E_{FM}. As a result, only the $M=M_s/3$ plateau is stabilized in certain h range $(0<h<3)$ as shown in Fig. 5(b) in which the corresponding magnetization curves for $D=0.2$, 0.4, 0.6 and the Ising limit at $T=0.01$ obtained from Monte Carlo simulation are presented. Most recently, it has been exactly proved that the UUD structure can be realized at a single point $(T, h)=(0, 3)$ for $D=0$.[26] The single UUD point is expanded into a finite region of the UUD phase when the anisotropy D is taken into account, leading to the broadening of the magnetization plateau at $M=M_s/3$. When D increases to the value of 0.6, the system exhibits the magnetic behavior of the Ising model, as shown in our simulation. The local energies for these five states under $J_3=0.1$ and $J_4=-0.1$ are presented in Fig. 5(c). The energy of the collinear state is lower than that of the Neel state when J_3 is included, which may be also noted from Eqs. (2) and (3). By comparing E_{col} and E_{UUD}, one can determine the boundary between the collinear state and the 1/3 plateau state, and the first critical field can be estimated to be $h_{c,1}=4J_3/3-4J_4/3$. The transition shifts toward the high-h side with increasing AFM J_3 or/and FM J_4. On the other hand, the degeneracy between the UUD state, the FI state, and the FM state can be significantly lifted when J_3 and J_4 are taken into account. When h is further increased, the FI state is stabilized and the second critical field can be estimated to be $h_{c,2}=-2J_3+8J_4+3$ by comparing the

energies in Eqs. (4) and (5). $h_{c,2}$ is intensively decreased when the AFM J_3 or/and the FM J_4 is/are increased. As a result, the main $M=M_s/3$ plateau is gradually replaced by the $M=0$ plateau and the $M=M_s/2$ one, as confirmed in our simulation [Fig. 5(d)]. In addition, the FM J_4 coupling is proved to be one of the most efficient ways to stabilize the $M=M_s/2$ plateau, as reported earlier.[18] When h is sufficiently strong, the system should be fully magnetized. Similarly, the upper critical field $h_{c,3}$ is calculated to be $h_{c,3}=2J_3+3$ by comparing E_{FI} and E_{FM}. So, $h_{c,3}$ is linearly increased with increasing J_3, which is irrelevant to J_4.

At last, we draw our eyes on the competition between the Neel state and the collinear state under small h. It is noted from Eqs. (2) and (3) that these two states are degenerated for zero J_3. However, only the perfect Neel state is stabilized for small h at low T, as confirmed in our simulation [Fig. 4(b)]. This phenomenon may be qualitatively understood from the competition between two kinds of collinear states with the spin configurations in which the same directed spins are horizontally/vertically arranged. These two states strongly compete with each other in the formation of the perfect collinear state. As a result, the Neel state in which the planar symmetry is still maintained is more likely to be stabilized. This argument is also verified in our simulation by the tracking of the spin configurations at different MCs. The simulation started from an arbitrary state is performed for the Ising limit at $J_3=0$ and $J_4=-0.15$, under zero h. The spin configuration at MCs = 5000 [Fig. 6(a)] indicates that the local collinear states can be quickly formed. As MCs increase, the competitions among these local collinear states leading to the enlargement of the region with the local Neel state, as shown in Figs. 6(b) and 6(c). Finally, the system reaches the equilibrium state in which the perfect Neel state dominates, as depicted in Fig. 6(d). Most recently, a possible phase transition from the collinear state to the Neel state is predicted in a 2d square lattice AFM spin model, which is interested in explaining the magnetic behaviors in the Fe-based superconductors.[23] The conclusion may be strengthened by the present work more or less.

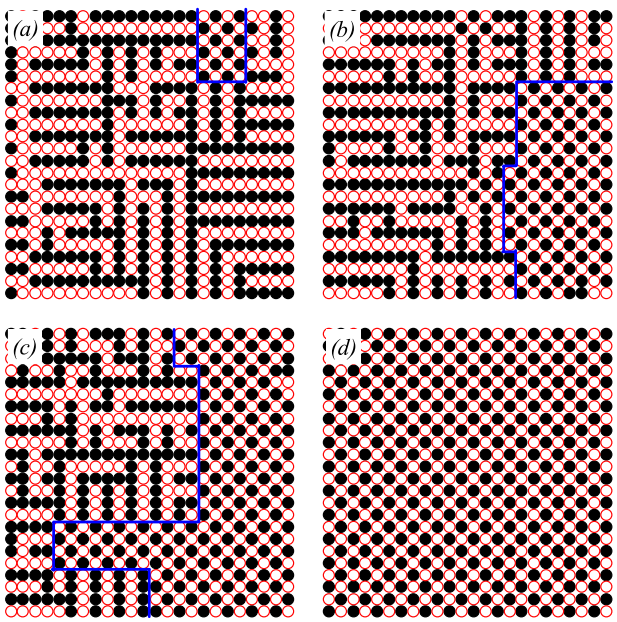

FIG. 6. Typical MC snapshot of the spin structure at $T=0.01$ for the Ising limit at (a) MCs = 5000, (b) MCs = 40 000, (c) MCs = 80 000, and (d) MCs = 120 000. The other parameters are $J_3=0$, $J_4=-0.15$, and $h=0$. Solid and empty circles represent the up-spins and the down-spins, respectively. The blue lines are guides to the eyes.

V. CONCLUSION

In this study, we have examined the low-temperature magnetic properties of a classical spin model with additional couplings on the Shastry-Sutherland lattice by means of Monte Carlo simulation. The 1/2 magnetization plateau as observed in TmB_4 and ErB_4 is successfully reproduced when the long-range interactions are taken into account. It is demonstrated that more local long-range interactions are satisfied in the 1/2 plateau state than those in the 1/3 plateau one, leading to the stabilization of the extended 1/2 plateau. The origins of these interesting magnetic orders are discussed in details, and are confirmed by the spin configuration of the plateau state at zero temperature. It is indicated that even weak long-range interactions may have a significant effect on the step-like magnetization feature for the classical S-S magnets. In addition, the competitions between the Neel state and the collinear state are discussed, and the former one is confirmed to be stabilized when the energies of these two states are degenerated. This simulated result provides evidence to the conclusion of the earlier work in which a phase transition to the Neel state is predicted in the Fe-based superconductors such as P-substituted LaFeAsO.

ACKNOWLEDGMENTS

This work was supported by the Natural Science Foundation of China (11204091, 11274094, 11234005), the National Key Projects for Basic Research of China (2011CB922101), China Postdoctoral Science Foundation funded Project (2012T50684, 20100480768, 2011M500088), and the Priority Academic Program Development of Jiangsu Higher Education Institutions, China.

[1]H. Kageyama, K. Yoshimura, K. Kosuge, M. Azuma, M. Takano, H. Mitamura, and T. Goto, J. Phys. Soc. Jpn. **66**, 3996 (1997).
[2]Y. B. Kudasov, Phys. Rev. Lett. **96**, 027212 (2006).
[3]H. Kageyama, K. Yoshimura, R. Stern, N. V. Mushnikov, K. Onizuka, M. Kato, K. Kosuge, C. P. Slichter, T. Goto, and Y. Ueda, Phys. Rev. Lett. **82**, 3168 (1999).
[4]K. Kodama, M. Takigawa, M. Horvatic, C. Berthier, H. Kageyama, Y. Ueda, S. Miyahara, F. Becca, and F. Mila, Science **298**, 395 (2002).
[5]S. Yoshii, T. Yamamoto, M. Hagiwara, S. Michimura, A. Shigekawa, F. Iga, T. Takabatake, and K. Kindo, Phys. Rev. Lett. **101**, 087202 (2008).
[6]K. Siemensmeyer, E. Wulf, H. J. Mikeska, K. Flachbart, S. Gabani, S. Matas, P. Priputen, A. Efdokimova, and N. Shitsevalova, Phys. Rev. Lett. **101**, 177201 (2008).
[7]X. Y. Yao, S. Dong, and J.-M. Liu, Phys. Rev. B **73**, 212415 (2006).
[8]Y. B. Kudasov, A. S. Korshunov, V. N. Pavlov, and D. A. Maslov, Phys. Rev. B **78**, 132407 (2008).
[9]M. H. Qin, K. F. Wang, and J.-M. Liu, Phys. Rev. B **79**, 172405 (2009).
[10]B. S. Shastry and B. Sutherland, Physica B & C **108**, 1069 (1981).
[11]R. W. Smith and D. A. Keszler, J. Solid State Chem. **93**, 430 (1991).
[12]R. Watanuki, G. Sato, K. Suzuki, M. Ishihara, T. Yanagisawa, Y. Nemoto, and T. Goto, J. Phys. Soc. Jpn. **74**, 2169 (2005).
[13]S. Michimura, A. Shigekawa, F. Iga, M. Swra, T. Takabatake, K. Ohoyama, and Y. Okabe, Physica B **378**, 596 (2006).

[14]M. C. Chang and M. F. Yang, Phys. Rev. B **79**, 104411 (2009).
[15]M. Moliner, D. C. Cabra, A. Honecker, P. Pujol, and F. Stauffer, Phys. Rev. B **79**, 144401 (2009).
[16]Y. I. Dublenych, Phys. Rev. Lett. **109**, 167202 (2012).
[17]Z. Y. Meng and S. Wessel, Phys. Rev. B **78**, 224416 (2008).
[18]T. Suzuki, Y. Tomita, and N. Kawashima, Phys. Rev. B **80**, 180405(R) (2009).
[19]T. Suzuki, Y. Tomita, N. Kawashima, and P. Sengupta, Phys. Rev. B **82**, 214404 (2010).
[20]W. C. Huang, L. Huo, G. Tian, H. R. Qian, X. S. Gao, M. H. Qin, and J.-M. Liu, J. Phys.: Condens. Matter **24**, 386003 (2012).
[21]M. H. Qin, G. Q. Zhang, K. F. Wang, X. S. Gao, and J.-M. Liu, J. Appl. Phys. **109**, 07E103 (2011).
[22]P. Farkasovsky, H. Cencarikova, and S. Matas, Phys. Rev. B **82**, 054409 (2010).
[23]H. Y. Wang, Phys. Rev. B **86**, 144411 (2012).
[24]D. P. Landau and K. Binder, *A Guide to Monte Carlo Simulations in Statistical Physics* (Cambridge University Press, Cambridge, England, 2008).
[25]K. Hukushima and K. Nemoto, J. Phys. Soc. Jpn. **65**, 1604 (1996).
[26]A. Grechnev, http://arxiv.org/abs/1212.2320.

A LETTERS JOURNAL EXPLORING THE FRONTIERS OF PHYSICS

OFFPRINT

Dynamic magnetization process in the frustrated Shastry-Sutherland system TmB_4

W. C. Huang, L. Huo, J. J. Feng, Z. B. Yan, X. T. Jia, X. S. Gao, M. H. Qin and J.-M. Liu

EPL, **102** (2013) 37005

A Letters Journal Exploring the Frontiers of Physics

May 2013

EPL, **102** (2013) 37005
doi: 10.1209/0295-5075/102/37005

www.epljournal.org

Dynamic magnetization process in the frustrated Shastry-Sutherland system TmB_4

W. C. Huang[1], L. Huo[1], J. J. Feng[1], Z. B. Yan[2], X. T. Jia[3], X. S. Gao[1], M. H. Qin[1(a)] and J.-M. Liu[2(b)]

[1] *Institute for Advanced Materials, South China Academy of Advanced Photonics Engineering, South China Normal University - Guangzhou 510006, China*
[2] *Laboratory of Solid State Microstructures, Nanjing University - Nanjing 210093, China*
[3] *School of Physics and Chemistry, Henan Polytechnic University - Jiaozuo 454000, China*

received 4 February 2013; accepted in final form 18 April 2013
published online 15 May 2013

PACS 75.10.Hk – Classical spin models
PACS 07.55.Db – Generation of magnetic fields; magnets
PACS 71.10.Hf – Non-Fermi-liquid ground states, electron phase diagrams and phase transitions in model systems

Abstract – The dynamic magnetization behaviors of the classical Ising model on the Shastry-Sutherland lattice with additional long-range interactions are investigated by means of the Glauber dynamics, in order to understand the fascinating magnetization plateaus and the hysteresis loop observed in TmB_4. With this algorithm, the experimental $1/n$ (n = 7, 9, 11) magnetization plateaus as well as the main 1/2 one can be reproduced at low temperatures. Furthermore, the hysteresis loop can also be well explained by the present theory. It is indicated that the formation of domain walls due to the non-equilibrium magnetization process may be responsible for the emergence of the fractional plateaus.

Introduction. – Geometrically frustrated spin systems which exhibit very rich magnetic properties have drawn considerable attentions during the last several decades [1]. For example, various experimental and theoretical explorations have been devoted to the emergence of multi-step magnetization (M) curves in frustrated systems such as the triangular spin-chain system $Ca_3Co_2O_6$ [2–5] and the Shastry-Sutherland (S-S) magnets [6–11]. So far, the step-like magnetization curves observed in $Ca_3Co_2O_6$ are generally believed to be caused by the non-equilibrium magnetization dynamics [12,13], while those in S-S systems are far from being fully understood and remains to be checked.

The S-S lattice [14] has attracted special attentions since its experimental realization in the compound $SrCu_2(BO_3)_2$ in which a fascinating sequence of magnetization plateaus at fractional values of the saturated magnetization (M_S) have been reported [15,16]. Most recently, similar magnetic behaviors have been identified in rare-earth tetraborides RB_4 (R = Tb, Dy, Ho, Tm, etc.) with the rare-earth moments located on a lattice which is topologically equivalent to the S-S lattice [8,9,17–20]. For instance, the fractional magnetization plateaus at $M/M_S = 1/2, 1/7, 1/9$ and $1/11, \ldots$ have been experimentally observed at temperature (T) below 4 K in TmB_4 [9]. In contrast to $SrCu_2(BO_3)_2$ with Cu^{2+} ions carrying a quantum spin 1/2, TmB_4 presents a large total magnetic moment ($\sim 6.0\,\mu_B$) and can be considered as a classical spin system, triggering an extensive theoretical investigation of classical spin models on the S-S lattice [21–28].

It is experimentally indicated that TmB_4 is of strong easy-axis anisotropy caused by crystal field effects. Based on this point, the magnetization process of the classical Ising model on the S-S lattice was investigated using the tensor renormalization group approach, and a single magnetization plateau at $M/M_S = 1/3$ was predicted at low T for certain coupling constants [21]. In fact, the ground states of the Ising model on the S-S lattice were investigated most recently and the existence of a single 1/3 plateau was rigorously proved [22,23]. The effect of further-neighbor interactions was suggested to eventually explain the magnetization plateaus in TmB_4, and three different ground states with $M/M_S = 1/2$ were recognized when the additional third-neighbor interaction was considered. On the other hand, the quantum spin-1/2

(a) E-mail: qinmh@scnu.edu.cn
(b) E-mail: liujm@nju.edu.cn

Ising-like XXZ model with additional interactions on the S-S lattice was studied using the quantum Monte Carlo method, and the plateau at $M/M_S = 1/2$ was identified [29–31]. It was believed that the emergence of the $M/M_S = 1/2$ plateau may be due to the quantum fluctuations and long-range interactions. In our earlier work, the presence of the $M/M_S = 1/2$ plateau was also confirmed when the additional long-range interactions were taken into account in the classical spin model [32].

So far, the main magnetization plateau at $M/M_S = 1/2$ and some of other small fractional plateaus in TmB_4 can be reproduced by the consideration of the long-range interactions for certain coupling constants. However, the origins of other small fractional plateaus are still under debate. Generally speaking, a frustrated spin system can be easily trapped into metastable states at low T and is hard to relax to the equilibrium state. The time available experimentally may not be sufficient for the spin rearrangement, even though the energy difference between plateaus may be very small. Thus, it is reasonable to assume that the spins in TmB_4 are easily trapped into a metastable state rather than into the equilibrium one at low T, which, to some extent, can be also favored by the obvious hysteresis loop observed in earlier experiments. Furthermore, the formation and the motion of domain walls due to the non-equilibrium magnetization process may play an important role in the emergence of the magnetization plateaus, which has been verified in the study of the triangular spin-chain compound $Ca_3Co_2O_6$ [13,33,34]. As a matter of fact, the $M/M_S = 1/8$ plateau has been predicted in the XXZ model on the S-S lattice for a short relaxation time, indicating that this plateau may arise from non-equilibrium state [31]. Thus, one may question if the non-equilibrium magnetization dynamics is also essential for the small fractional magnetization plateaus in TmB_4. A detailed discussion of this question is definitely crucial for the understanding of the fascinating magnetic properties in such a frustrated system. However, as far as we know, few works on this subject have been reported.

In order to make clear this question, we will study the magnetization dynamics of the classical Ising model on the S-S lattice with additional long-range interactions with the Glauber dynamics which has been successfully used in the study of the magnetic properties of $Ca_3Co_2O_6$ [13]. This algorithm allows us to investigate the dependence of the magnetization curves on temperature and magnetic-field (h) sweep rate. The experimental magnetization plateaus at small fractional values of $M/M_S = 1/7$, $1/9$, and $1/11$ followed by the main magnetization plateau at $M/M_S = 1/2$ can be reproduced at low T for certain magnetic-field sweep rates. In addition, the hysteresis loop observed in experiments can also be qualitatively explained in our simulation [9,19]. These results clearly demonstrate that the fascinating plateaus in TmB_4 magnetization curve may be closely related to the non-equilibrium magnetization dynamics. Our work provides a new insight into the study of the magnetization process for S-S magnets and other similar frustrated spin systems.

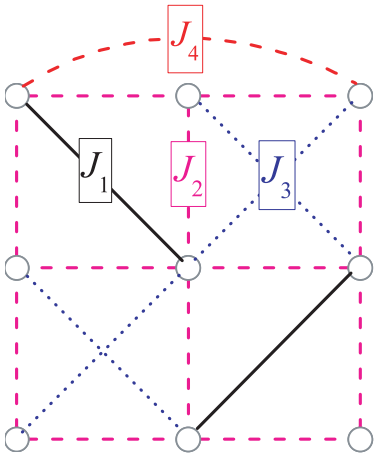

Fig. 1: (Color online) Effective model on the Shastry-Sutherland lattice with the diagonal coupling J_1 (black solid lines), J_2 along the edges of the squares (magenta dashed lines), the additional interactions J_3 (blue dashed lines) and J_4 (red dashed lines).

The remainder of this paper is organized as follows: In the second section, the model and the simulation method will be presented and described. The third section is attributed to the simulation results and discussion. At last, the conclusion is presented in the fourth section.

Model and method. – In the presence of the long-range interactions and h, the Hamiltonian can be described as follows:

$$H = J_1 \sum_{\langle i,j\rangle_1} S_i \cdot S_j + J_2 \sum_{\langle i,j\rangle_2} S_i \cdot S_j + J_3 \sum_{\langle i,j\rangle_3} S_i \cdot S_j + J_4 \sum_{\langle i,j\rangle_4} S_i \cdot S_j - h \sum_i S_i^z, \quad (1)$$

where $\langle i,j\rangle_1, \langle i,j\rangle_2, \langle i,j\rangle_3$, and $\langle i,j\rangle_4$ denote the summations over all pairs on the bonds with J_1, J_2, J_3 and J_4 couplings, respectively, as shown in fig. 1, S_i represents the Ising spin with unit length on site i, h is applied along the $+z$ axis and S_i^z denotes the z component of S_i. $J_1 = 1$ is the antiferromagnetic (AFM) coupling, the coupling ratio $J_2/J_1 = 1$ is expected from the crystal structure of TmB_4, similar with earlier estimation [30,31], the AFM $J_3 = 0.15J_1$ and the ferromagnetic (FM) $J_4 = -0.15J_1$ are estimated to qualitatively reproduce the experimental results. To investigate the magnetization dynamics of the spin system, the simulation is carried out by a single spin-flip rate in the Glauber form [13,34]. The spins are assumed to interact not only with the neighbors and external magnetic field but also with a heat reservoir, based on the Glauber theory [35]. The probability of a spin flip of the i-th spin per Monte Carlo step (MCs) can be described as

$$W_i = \frac{\alpha}{2}\left[1 - S_i \tanh\left(-\frac{D}{k_B T} + \frac{\mu h}{k_B T}\right)\right], \quad (2)$$

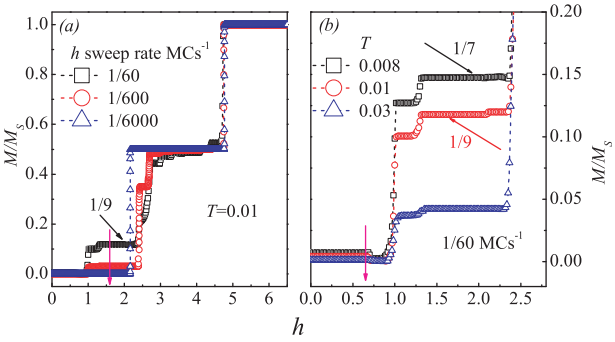

Fig. 2: (Color online) Magnetization curves for (a) different magnetic-field sweep rates at $T = 0.01$, and (b) enlargements of magnetization curves at different temperatures at a fixed sweep rate of $1/60\,\mathrm{MCs}^{-1}$.

with

$$D = J_1 \sum_{\langle i,j\rangle_1} S_j + J_2 \sum_{\langle i,j\rangle_2} S_j + J_3 \sum_{\langle i,j\rangle_3} S_j + J_4 \sum_{\langle i,j\rangle_4} S_j, \quad (3)$$

where $\alpha = 0.5\,\mathrm{MCs}^{-1}$ is the constant of the interaction of a spin with the heat reservoir, $k_B = 1$ is the Boltzmann constant, $\mu = 1$ is the magnetic moment of the Tm ion. In earlier work, the Glauber-type form of the spin-flip probability has been discussed in detail and successfully used in the frustrated spin-chain system $Ca_3Co_2O_6$ [13,34]. Similarly, a reasonable value $\alpha = 0.5\,\mathrm{MCs}^{-1}$ is used in our simulation to qualitatively coincide with the experimental results.

Our simulation is performed on an $L \times L$ ($L = 96$ is chosen unless stated otherwise) lattice with periodic boundary conditions. The simulation is started from the saturated magnetization state under high h, which is in the best accordance with the real case. Then the magnetization curves in the decreasing h at different sweep rates for various temperatures are studied to investigate the magnetization dynamics in detail. In addition, the sweep rate is defined by $1/m\,\mathrm{MCs}^{-1}$ which means that the $1/m$ of h unit is updated per MCs.

Simulation results and discussion. – Figure 2(a) shows the calculated M/M_S as a function of h for different magnetic-field sweep rates at a low temperature $T = 0.01$. Three steps can be observed for the lowest sweep rate of $1/6000\,\mathrm{MCs}^{-1}$. When h decreases down to $\sim$4.75, M reaches the plateau at $M/M_S = 1/2$, and then falls down to the step at $M = 0$ below $h \sim 2.2$. More interestingly, the step at $M = 0$ decomposes into two substeps (zero and nonzero) separated at $h \sim 1$ when the magnetic-field sweep rate is increased. The height of the nonzero substep increases with increasing sweep rate. When the magnetic-field sweep rate increases up to $1/60\,\mathrm{MCs}^{-1}$, the $M/M_S = 1/9$ plateau reported in experiments can be well reproduced in addition to the major magnetization plateaus at $M = 0$ and $M/M_S = 1/2$. Furthermore, the dynamic magnetization curves in response to T at the constant sweep rate of $1/60\,\mathrm{MCs}^{-1}$ are also investigated, and the simulated results are presented in fig. 2(b). It is clearly demonstrated that the nonzero substep is heightened as T decreases. When T falls down to 0.008, a magnetization step at $M/M_S = 1/7$ is observed at intermediate h range, which is consistent with experimental observation [9]. In addition, some additional narrow plateaus can also be noticeable in our simulation, which deserves to be checked in further experiments.

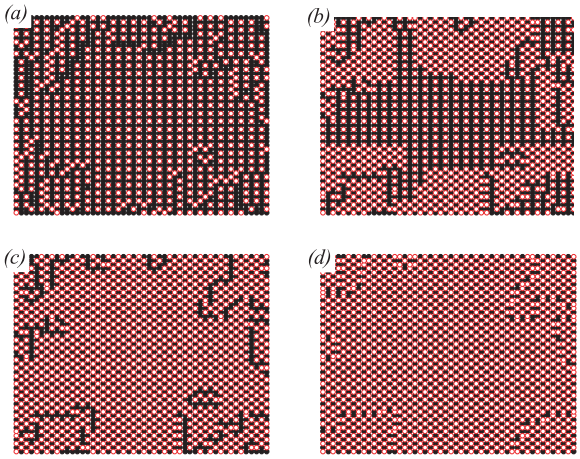

Fig. 3: (Color online) Spin configurations during the simulation at a magnetic-field sweep rate of $1/60\,\mathrm{MCs}^{-1}$ and $T = 0.01$ under (a) $h = 3.5$, (b) $h = 2.5$, (c) $h = 2.0$, (d) $h = 0$. The solid and empty squares represent the up-spins and the down-spins, respectively.

As stated earlier [32], the ferrimagnetic (FI) state spin arrangement consisting of alternative AFM and FM stripes is more favored than the FM state when h is decreased down to the first critical field, while the Neel state is likely stabilized below the following critical field. For the extremely slow sweep rate ($1/6000\,\mathrm{MCs}^{-1}$), the single-domain FI state with the plateau at $M/M_S = 1/2$ and the Neel state with the $M = 0$ plateau are, respectively, stabilized below these two critical fields, leading to the three-step magnetization curve which is similar to that obtained by the Monte Carlo simulation. To uncover the origin of the nonzero substep, the specimens of configurations for various plateaus under different h at the magnetic-field sweep rate of $1/60\,\mathrm{MCs}^{-1}$ are presented in fig. 3. It is clearly shown that the Neel state grows at a lot of nucleation centers when h falls down to the second critical field, resulting in the domain formation. A mixed state with the Neel order and domain walls constructed of polarized spin chains is responsible for the emergence of the $M/M_S = 1/9$ plateau in the magnetization curve, as shown in fig. 3(c). The domains become smaller with increasing magnetic-field sweep rate, leading to the heightening of the nonzero substep. When h is further decreased, the domain walls almost disappear (fig. 3(d)), and the magnetization plateau at $M = 0$ can be observed. On the other hand, the domain boundary mobility may

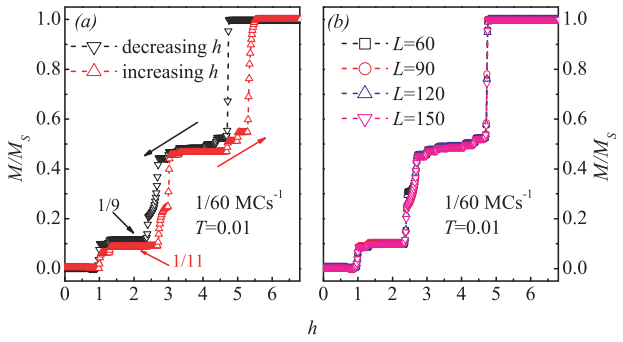

Fig. 4: (Color online) (a) Hysteresis loop at a sweep rate of $1/60\,\mathrm{MCs}^{-1}$ and $T = 0.01$. The red and the black symbols are the field-increasing branch and the field-decreasing branch, respectively. (b) Magnetization curves for different lattice sizes L at a sweep rate of $1/60\,\mathrm{MCs}^{-1}$ and $T = 0.01$.

be greatly decreased as T decreases. Thus, the domains become smaller with decreasing T, making the additional magnetization steps more apparent, as confirmed in our simulation (fig. 2(b)). It is noted that the temperature at which the experimental $M/M_{\mathrm{S}} = 1/7$ plateau is observed is higher than that of the $M/M_{\mathrm{S}} = 1/9$ one. The inconsistency between the present theory and the experiment may be due to the fact that the disorder effect caused by the inhomogeneity in realistic materials is completely ignored in our simulation. However, our work clearly indicates that the non-equilibrium magnetization dynamics may play an important role in the appearance of the fractional magnetization steps in TmB_4.

In addition, the hysteresis loop is also studied in our work, and the results can qualitatively reproduce the experimental observations [9,19]. Figure 4(a) shows the hysteresis loop at the magnetic-field sweep rate of $1/60\,\mathrm{MCs}^{-1}$ at $T = 0.01$. The nonzero substep emerges in both field-decreasing and field-increasing branches of the magnetization curve. The nonzero substep ($M/M_{\mathrm{S}} = 1/9$) in the field-decreasing branch is much higher than that ($M/M_{\mathrm{S}} = 1/11$) in the field-increasing branch, in a good agreement with the experimental report [9]. This phenomenon demonstrates that the domain structures can be strongly affected by the initial state at a high magnetic-field sweep rate. In fact, the spin configurations of the simulation reveal that the Neel domains for the nonzero substep in the field-increasing branch are generally larger than those in the field-decreasing branch, resulting in the emergence of the hysteresis loop. More interestingly, it is confirmed in our simulation that the value of plateau magnetization varies between different runs, similar with earlier experimental report [9]. The corresponding results are not shown here for brevity. Furthermore, it has been noticed in earlier experiment that the critical fields in the field-decreasing branch of the magnetization curve are respectively smaller than those in the field-increasing branch [19]. This magnetic behavior can also be well reproduced by the simulation.

As stated earlier, the time required for the spin rearrangement likely exceeds the time available experimentally. Thus, the non-equilibrium magnetization dynamics may be essential for the emergence of the fractional magnetization plateaus in TmB_4. This point has been confirmed in this work in which the non-equilibrium evolution is performed by means of the Glauber dynamics. The fractional magnetization plateaus and the hysteresis loop at low T reported in experiments can be reproduced in our simulation. Thus, our work may provide a new insight into the study of the magnetization process of TmB_4, although not all the experimental results can be excellently explained based on the present theory.

At last, the dependence of the step-like magnetization feature on the lattice size L has been investigated in order to exclude the artificial facts caused by the finite lattice size. Figure 4(b) shows the simulated magnetization curves for different L ($L = 60$, 96, 120 and 150) at $T = 0.01$ for the extremely fast magnetic-field sweep rate of $1/60\,\mathrm{MCs}^{-1}$. All the simulated curves for various L are almost merged into one, indicating that the finite-size effect on the magnetization of the system is almost negligible and never affects our conclusion.

Conclusion. – In summary, we have investigated the classical Shastry-Sutherland Ising model with long-range interactions employing a Glauber-type form of the spin-flip probability in order to understand the dynamic magnetization process in TmB_4. Besides the main $M/M_{\mathrm{S}} = 1/2$ plateau, other fractional magnetization plateaus at $M/M_{\mathrm{S}} = 1/n$ ($n = 7$, 9, 11) observed in experiments can be reproduced in our simulation of the model at low temperatures for certain magnetic-field sweep rates. In addition, the hysteresis loop can be also well explained in the present theory. It is indicated that the magnetization dynamics may be essential for the emergence of those fractional magnetization plateaus. Thus, the present work may provide a new insight into the understanding of the magnetization process for frustrated S-S magnets and other similar frustrated spin systems.

* * *

This work was supported by the Natural Science Foundation of China (11204091, 11274094, 11234005), the National Key Projects for Basic Research of China (2011CB922101), China Postdoctoral Science Foundation funded project (2012T50684, 20100480768, 2011M500088), and the Priority Academic Program Development of Jiangsu Higher Education Institutions, China.

REFERENCES

[1] Diep H. T., *Frustrated Spin Systems* (World Scientific, Singapore) 2004.

[2] Kageyama H., Yoshimura K., Kosuge K., Azuma M., Takano M., Mitamura H. and Goto T., *J. Phys. Soc. Jpn.*, **66** (1997) 3996.

[3] Maignan A., Michel C., Masset A. C., Martin C. and Raveau B., *Eur. Phys. J. B*, **15** (2000) 657.

[4] Kudasov Y. B., *Phys. Rev. Lett.*, **96** (2006) 027212.

[5] Yao X. Y., Dong S. and Liu J.-M., *Phys. Rev. B*, **73** (2006) 212415.

[6] Kageyama H., Yoshimura K., Stern R., Mushnikov N. V., Onizuka K., Kato M., Kosuge K., Slichter C. P., Goto T. and Ueda Y., *Phys. Rev. Lett.*, **82** (1999) 3168.

[7] Kodama K., Takigawa M., Horvatic M., Berthier C., Kageyama H., Ueda Y., Miyahara S., Becca F. and Mila F., *Science*, **298** (2002) 395.

[8] Yoshii S., Yamamoto T., Hagiwara M., Michimura S., Shigekawa A., Iga F., Takabatake T. and Kindo K., *Phys. Rev. Lett.*, **101** (2008) 087202.

[9] Siemensmeyer K., Wulf E., Mikeska H. J., Flachbart K., Gabani S., Matas S., Priputen P., Efdokimova A. and Shitsevalova N., *Phys. Rev. Lett.*, **101** (2008) 177201.

[10] Abendschein A. and Capponi S., *Phys. Rev. Lett.*, **101** (2008) 227201.

[11] Dorier J., Schmidt K. P. and Mila F., *Phys. Rev. Lett.*, **101** (2008) 250402.

[12] Qin M. H., Wang K. F. and Liu J.-M., *Phys. Rev. B*, **79** (2009) 172405.

[13] Kudasov Y. B., Korshunov A. S., Pavlov V. N. and Maslov D. A., *Phys. Rev. B*, **78** (2008) 132407.

[14] Shastry B. S. and Sutherland B., *Physica B+C*, **108** (1981) 1069.

[15] Smith R. W. and Keszler D. A., *J. Solid State Chem.*, **93** (1991) 430.

[16] Isaev L., Ortiz G. and Dukelsky J., *Phys. Rev. Lett.*, **103** (2009) 177201.

[17] Watanuki R., Sato G., Suzuki K., Ishihara M., Yanagisawa T., Nemoto Y. and Goto T., *J. Phys. Soc. Jpn.*, **74** (2005) 2169.

[18] Michimura S., Shigekawa A., Iga F., Swra M., Takabatake T., Ohoyama K. and Okabe Y., *Physica B*, **378** (2006) 596.

[19] Yoshii S., Yamamoto T., Hagiwara M., Shigekawa A., Michimura S., Iga F., Takabatake T. and Kindo K., *J. Phys.: Conf. Ser.*, **51** (2006) 59.

[20] Mat'aš S., Siemensmeyer K., Wheeler E., Wulf E., Beyer R., Hermannsdörfer Th., Ignatchik O., Uhlarz M., Flachbart K., Gabáni S., Priputen P., Efdokimova A., Shitsevalova N., *J. Phys.: Conf. Ser.*, **200** (2010) 032041.

[21] Chang M. C. and Yang M. F., *Phys. Rev. B*, **79** (2009) 104411.

[22] Dublenych Y. I., *Phys. Rev. Lett.*, **109** (2012) 167202.

[23] Dublenych Y. I., arXiv:1302.0377.

[24] Moliner M., Cabra D. C., Honecker A., Pujol P. and Stauffer F., *Phys. Rev. B*, **79** (2009) 144401.

[25] Grechnev A., *Phys. Rev. B*, **87** (2013) 144419.

[26] Farkasovsky P., Cencarikova H. and Matas S., *Phys. Rev. B*, **82** (2010) 054409.

[27] Qin M. H., Zhang G. Q., Wang K. F., Gao X. S. and Liu J.-M., *J. Appl. Phys.*, **109** (2011) 07E103.

[28] Huang W. C., Huo L., Tian G., Qian H. R., Gao X. S., Qin M. H. and Liu J.-M., *J. Phys.: Condens. Matter*, **24** (2012) 386003.

[29] Meng Z. Y. and Wessel S., *Phys. Rev. B*, **78** (2008) 224416.

[30] Suzuki T., Tomita Y. and Kawashima N., *Phys. Rev. B*, **80** (2009) 180405(R).

[31] Suzuki T., Tomita Y., Kawashima N. and Sengupta P., *Phys. Rev. B*, **82** (2010) 214404.

[32] Huo L., Huang W. C., Yan Z. B., Jia X. T., Gao X. S., Qin M. H. and Liu J.-M., *J. Appl. Phys.*, **113** (2013) 073908.

[33] Kudasov Y. B., Korshunov A. S., Pavlov V. N. and Maslov D. A., *J. Low Temp. Phys.*, **159** (2010) 76.

[34] Kudasov Y. B., Korshunov A. S., Pavlov V. N. and Maslov D. A., *Phys. Rev. B*, **83** (2011) 092404.

[35] Glauber R., *J. Math. Phys.*, **2** (1963) 294.

Journal of Magnetism and Magnetic Materials 340 (2013) 127–130

Contents lists available at SciVerse ScienceDirect

Journal of Magnetism and Magnetic Materials

journal homepage: www.elsevier.com/locate/jmmm

Phase diagram of ferromagnetic *XY* model with nematic coupling on a triangular lattice

K. Qi [a,b], M.H. Qin [a,*], X.T. Jia [c], J.-M. Liu [b,**]

[a] Laboratory for Advanced Materials, South China Normal University, Guangzhou 510006, China
[b] Laboratory of Solid State Microstructures, Nanjing University, Nanjing 210093, China
[c] School of Physics and Chemistry, Henan Polytechnic University, Jiaozuo 454000, China

ARTICLE INFO

Article history:
Received 11 December 2012
Available online 9 April 2013

Keywords:
XY model
Kosterlitz–Thouless transition
Monte Carlo simulation

ABSTRACT

The phase diagram of a ferromagnetic *XY* model with a nematic coupling (coupling strength x) on a triangular lattice is studied by means of Monte Carlo simulation. The algebraic-magnetic order associated with Kosterlitz–Thouless (KT) transition is observed over the whole x range. In the large x region, the phase transition from the algebraic-magnetic order to the algebraic-nematic order occurs at T_l. In addition, this phase transition can be scaled with the two-dimensional Ising critical exponents, demonstrating that the present system belongs to the universality class of Ising transition at T_l.

1. Introduction

The two dimensional (2D) *XY* model has been well investigated for several decades due to its application in magnetic systems with planar anisotropy, quantum liquids and superconductors. As early as in 1966, it was proved that the 2D *XY* model cannot sustain long-range order even with trivial thermal fluctuations [1]. Alternatively, the so-called algebraic-magnetic (aM) order with Kosterlitz–Thouless (KT) transition may ensue [2,3]. After that, lots of work about the *XY* model have been reported [4–18].

On the other hand, nontrivial orders such as chiral order and nematic order in magnets, are drawing more and more attentions due to their relevancy with real magnetic materials as well as the contribution to the development of statistical mechanics. For example, a phase with coexisting nematic and vector spin chirality orders has been observed in the antiferromagnetic *XY* model with a nematic (biquadratic) coupling on the triangular lattice [7]. Later on, the same phase is also reported in our earlier work where a frustrated *XY* model on the square lattice has been studied with the Monte Carlo method [8]. In fact, the ferromagnetic *XY* model with a nematic coupling on square lattice has been studied as early as in 1989 [5]. The variations of temperature and the nematic coupling strength lead to three phases: a high-temperature disordered phase and two low temperature phases, namely, aM phase and algebraic-nematic (aN) phase. At non-zero temperatures, spin waves destroy the long-range order of the ground state, leaving power-law decay of the spin correlations. The high-temperature phase is entered respectively via the transition associated with an integer vortex pair excitation in the aM phase and an half-integer vortex pairs one in the aN phase [9]. At the same time, it is stated that the phase transition from disordered phase to aN phase is driven by the domain wall in which the free energy is expected to decrease with increasing temperature.

In fact, the consideration of the nematic coupling terms is mostly due to the fact that they can be large for magnetic ions with large spin [19]. For example, it is identified that the nematic coupling and the ferromagnetic coupling between the nearest neighbors may play an important role in triangular lattice system $NiGa_2S_4$, as revealed most recently [20]. In this work, a ferromagnetic *XY* model with a nematic coupling (coupling strength x) on a triangular lattice is studied by means of Monte Carlo simulation. Besides its contribution to the development of statistical mechanics, the study may be helpful to understand the experimental phenomena observed in $NiGa_2S_4$. As far as we know, few works on such a system have been reported. It will be demonstrated that a general KT transition from the algebraically correlated phase to the paramagnetic phase occurs when temperature raises up to a critical value. For the region in which the nematic coupling is dominated, a transition from the aM phase to the aN phase occurs at the critical temperature T_l which is much lower than T_{KT}. In addition, the transition at T_l has the same universality of scaling as the two-dimensional (2D) Ising transition, which is similar to earlier report [5].

For a classical *XY* spin model on a triangular lattice, we consider the following Hamiltonian which includes the nematic coupling interaction:

$$H = -J_1 \sum_{[i,j]} \cos(\theta_{ij}) - J_2 \sum_{[i,j]} \cos(2\theta_{ij}), \quad (1)$$

* Corresponding author. Tel.: +86 13632457166.
** Corresponding author.
E-mail addresses: qinmh@scnu.edu.cn (M.H. Qin), liujm@nju.edu.cn (J.-M. Liu).

0304-8853/$ - see front matter © 2013 Elsevier B.V. All rights reserved.
http://dx.doi.org/10.1016/j.jmmm.2013.03.036

where θ_{ij} is the angle difference $\theta_i - \theta_j$ between the nearest neighbors [i,j]. $J_1 = 1 - x$ is the strength of the ferromagnetic coupling, and $J_2 = x$ is the nematic coupling strength. For definition of the energy parameters J_1 and J_2, the Boltzmann constant and the lattice constant are set to unity.

Unlike the model studied in Ref. [7], our model does not contain any chiral orders due to the lack of the frustration ingredient. In the large J_2/J_1 region where the nematic interaction is much stronger than the ferromagnetic one, the spins between the nearest neighbors prefer either parallel or antiparallel with each other at the equal probabilities at low temperature, forming the possible nematic order, same as the earlier report [5].

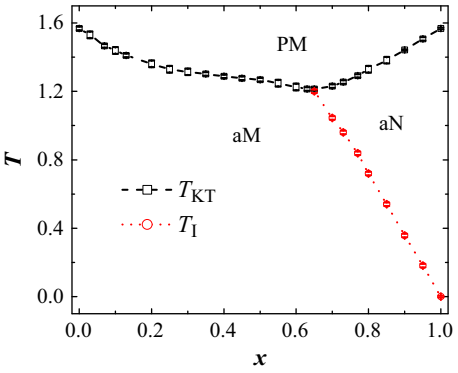

Fig. 1. Calculated phase diagram for the model in Eq. (1). The high-temperature paramagnetic phase is denoted by PM, the phases with algebraic correlations in magnetic and nematic order by aM and aN respectively. The statistical errors of all the symbols are given in the T direction.

The Monte Carlo simulation is performed on a 2D $L \times L$ ($L = 18$, 27, 36, 45, 54, and 72) triangular lattice with period boundary conditions using the standard Metropolis algorithm [21]. The initial spin configuration at high temperature (T) is totally disordered. Typically, the initial 3×10^5 Monte Carlo steps are discarded for the equilibrium consideration and another 2×10^5 Monte Carlo steps are retained for statistic averaging of the simulation.

The phase diagram in the x–T plane for the model stated in Eq. (1) is shown in Fig. 1. The two curves mark the boundaries between three different phases, which are the aM phase, aN phase and paramagnetic (PM) phase. An integer vortex-mediated KT transition marking the PM–aM boundary splits into a half-integer vortex-mediated KT transition which marks the PM–aN boundary, plus a transition which separates the aM order from the aN order. It is noticed that in the most cases the critical temperatures of the KT transition and Ising transition are relatively higher than the corresponding ones [5]. This phenomenon can be easily understood from the point that for the systems with the same ferromagnetic coupling, one with higher coordination number shows the higher critical temperature. It is noted that for triangular system one spin interacts with six nearest neighbors rather than four for square system. So, the algebraically correlated order in triangular system is so robust and its destruction needs relatively high temperature.

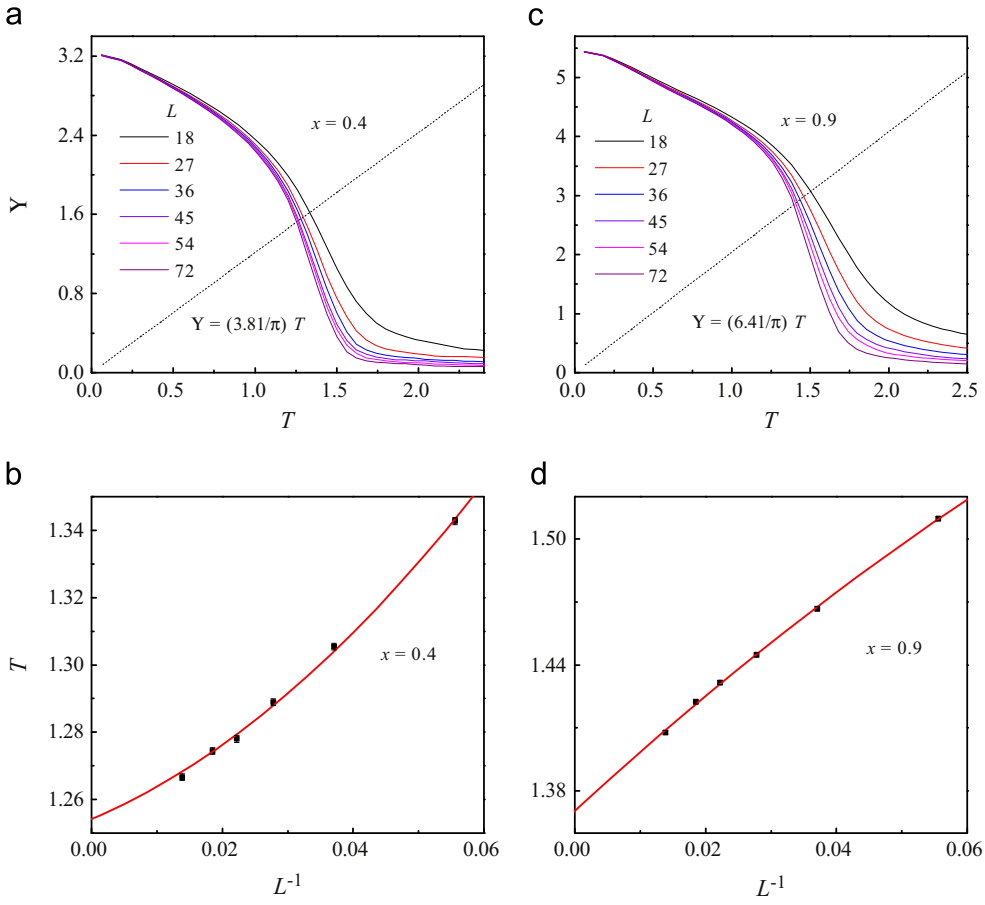

Fig. 2. Helicity modulus Y according to Eq. (2) for various sizes L (a) at $x = 0.4$ and (c) $x = 0.9$. The straight line is $(2/\pi)(\sqrt{3}/2)(1 + 3x)T$. The crossing temperatures of this line and Y for each L^{-1} are shown in (b) for $x = 0.4$ and (d) $x = 0.9$ with the extrapolation to $L^{-1} = 0$.

The determination of T_{KT} is made with the helicity modulus Y, also called the spin-wave stiffness [22,23]. Under this circumstance, Y can be defined by

$$Y = \frac{J_1}{2L^2}\left\langle \sum_{[i,j]} \cos\theta_{ij} \right\rangle + \frac{2J_2}{L^2}\left\langle \sum_{[i,j]} \cos 2\theta_{ij} \right\rangle - \frac{1}{TL^2}\left\langle \left(J_1 \sum_{[i,j]} x_{ij}\sin\theta_{ij} + 2J_2 \sum_{[i,j]} x_{ij}\sin 2\theta_{ij} \right)^2 \right\rangle \quad (2)$$

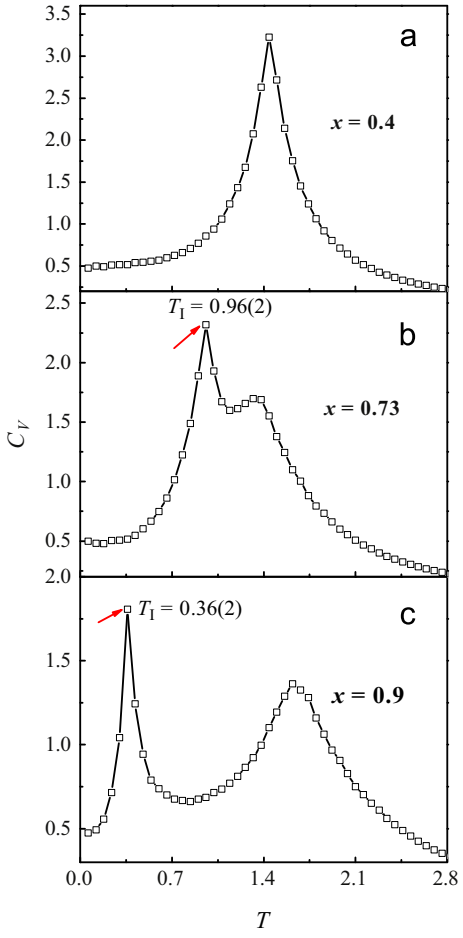

Fig. 3. Specific heat C as a function of T for $L=36$ at (a) $x=0.4$, (b) $x=0.73$ and (c) $x=0.9$.

Here $x_{ij}=x_i-x_j$ is the separation of two coordinate sites. For a given lattice size L, the critical temperature T_{KT} can be determined by the crossing of $Y(T)$ with the straight line $(2/\pi)(\sqrt{3}/2)(J_1+4J_2)T=(2/\pi)(\sqrt{3}/2)(1+3x)T$. The helicity modulus for $L=18$–72 at $x=0.4$ and 0.9 are shown in Fig. 2(a) and (c), and the corresponding crossing points are shown in Fig. 2(b) and (d) respectively. The extrapolations to $L\to\infty$ using the polynomial fits yield the estimated values of T_{KT} which is 1.254(5) for $x=0.4$ and 1.379(5) for $x=0.9$. This method is effective in giving a good estimate of T_{KT} and a more sophisticated method taking into account the logarithmic correction gives a similar result [24].

The critical temperature of the transition from the aM phase to the aN phase can be easily estimated from the low-temperature specific-heat peak, as stated in our earlier work [8]. Specific heat C as a function of T at $x=0.4$, $x=0.73$ and $x=0.9$ for $L=36$ are plotted in Fig. 3. It is indicated that the one single peak at small x separates to two independent peaks which gradually detach from each other with the increasing of x. In the low x region ($x<0.65$), no transition from the aM phase to the aN phase occurs, leaving the single peak in the C–T curves, as shown in Fig. 3(a). On the other hand, the low-temperature sharp peaks at 0.96(2) for $x=0.73$ and 0.36(2) for $x=0.9$ clearly mark the nematic phase transitions, as shown in Fig. 3(b) and (c).

In Fig. 4(a), we show a snapshot of the nematic order at $T=0.4$ for $x=0.95$. The spins become generally parallel or antiparallel with each other, forming the so-called nematic order. At last, the critical exponent of the nematic transition is estimated with the dependence of the specific heat peak upon the absolute value of the difference between the critical temperature and its neighbor ones, i.e., $C_{peak}\propto|T_c-T|^{-\alpha}$. In Fig. 4(b), we plot the specific heats under different temperatures around C_{peak} for $L=36$ at $x=0.9$. The linear fit gives $\alpha\approx0.02$ which is almost same as that of 2D Ising model, i.e., $\alpha=0$. Taking into account the simulation errors, it is reasonable to argue that the universality class of this phase transition is that of 2D Ising transition as reported in earlier works [5,7].

To sum up, the phase diagram of ferromagnetic XY model with nematic coupling (x) on a triangular lattice is studied in details with Monte Carlo method. The phase diagram exhibits three phases including the algebraic-magnetic phase, the algebraic-nematic phase and the paramagnetic phase. In the large region of x ($x\geq0.65$), an Ising transition from the aM phase to aN phase is observed in addition to the usual KT transition. This work is a complementary one to the study of 2D XY models, and may be helpful to understand the experimental phenomena observed in $NiGa_2S_4$.

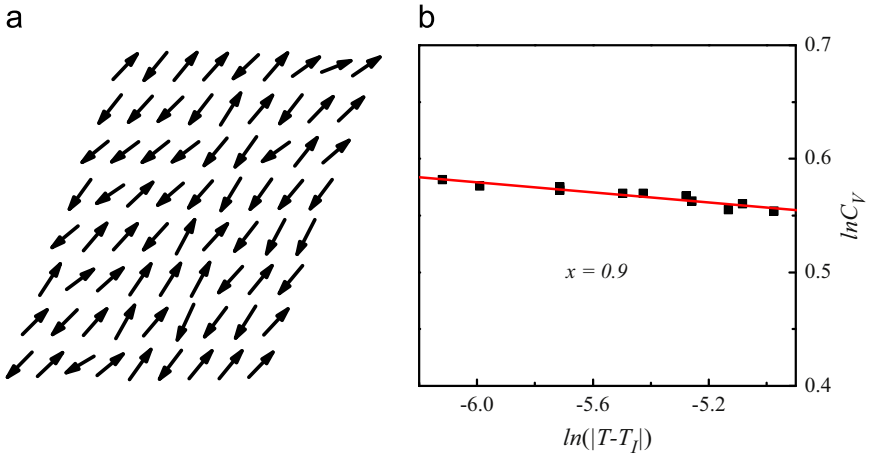

Fig. 4. (a) A snapshot of the nematic order at $T=0.4$ at $x=0.95$. (b) A scaling plot of specific heats under different T around critical temperature for lattice size $L=36$ at $x=0.9$.

Acknowledgment

This work was supported by the Natural Science Foundation of China (11204091, 11274094, and 11234005), the National Key Projects for Basic Research of China (2009CB623303), China Postdoctoral Science Foundation funded project (2012T50684 and 20100480768), and the Priority Academic Program Development of Jiangsu Higher Education Institutions, China.

References

[1] N.D. Mermin, H. Wagner, Physical Review Letters 17 (1966) 1133.
[2] J.M. Kosterlitz, D.J. Thouless, Journal of Physics C 6 (1973) 1181.
[3] D.P. Landau, Journal of Applied Physics 73 (1993) 6091.
[4] J.M. Kosterlitz, Journal of Physics C 7 (1974) 1046.
[5] D.B. Carpenter, J.T. Chalker, Journal of Physics: Condensed Matter 1 (1989) 4907.
[6] J. Villain, Journal of Physics C: Solid State Physics 10 (1977) 1717.
[7] J.H. Park, S. Onoda, N. Nagaosa, J.H. Han, Physical Review Letters 101 (2008) 167202.
[8] M.H. Qin, X. Chen, J.-M. Liu, Physical Review B 80 (2009) 224415.
[9] D.H. Lee, G. Grinstein, Physical Review Letters 55 (1985) 541.
[10] J. Tobochnik, G.V. Chester, Physical Review B 20 (1979) 3761.
[11] S. Teitel, C. Jayaprakash, Physical Review B 27 (1983) 598.
[12] J. Lee, E. Granato, J.M. Kosterlitz, Physical Review B 44 (1991) 4819.
[13] J. Villain, Journal of Physics C 10 (1977) 4793.
[14] S. Lee, K.C. Lee, Physical Review B 49 (1994) 15184.
[15] R. Gupta, J. DeLapp, G.G. Batrouni, G.C. Fox, C.F. Baillie, J. Apostolakis, Physical Review Letters 61 (1988) 1996.
[16] E. Granato, J.M. Kosterlitz, J. Lee, M.P. Nightingale, Physical Review Letters 66 (1991) 1090.
[17] P. Olsson, Physical Review Letters 75 (1995) 2758.
[18] S. Miyashita, H. Nishimori, A. Kuroda, M. Suzuki, Progress of Theoretical Physics 60 (1978) 1669.
[19] L.X. Hayden, T.A. Kaplan, S.D. Mahanti, Physical Review Letters 105 (2010) 047203.
[20] E.M. Stoudenmire, S. Trebst, L. Balents, Physical Review B 79 (2009) 214436.
[21] D.P. Landau, K. Binder, A Guide to Monte Carlo Simulations in Statistical Physics, Cambridge University Press, Cambridge, England, 2005.
[22] M.E. Fisher, M.N. Barber, D. Jasnow, Physical Review 0A 8 (1973) 1111.
[23] D.H. Lee, J.D. Joannopoulos, J.W. Negele, D.P. Landau, Physical Review B 33 (1986) 450.
[24] P. Minnhagen, B.J. Kim, S. Bernhardsson, G. Cristofano, Physical Review B 76 (2007) 224403.